Amphiphilic Block Copolymers: Synthesis, Self-assembly and Applications

Inauguraldissertation

Zur

Erlangung der Würde eines Doktors der Philosophie

Vorgelegt der

Philosophische-Naturwissenschaftlichen Fakultät

Der Universität Basel

Von

Dalin Wu

Aus

China

Basel 2015

UNI
BASEL

Genehmigt von der Philosophisch-Naturwissenschaftlichen Fakultät auf Antrag

von

Prof. Dr. Wolfgang Meier

Prof. Dr. Nico Bruns

Basel, den 09.12.2014

Prof. Dr. Jörg Schibler

The Dekan of Faculty

Acknowledgements

First, I would like to thank Prof. Wolfgang Meier for giving me the opportunity to do research for my PhD thesis at the University of Basel.

Also, I would like to thank Prof. Cornelia Palivan for her kind support and suggestions during my stay in Basel, especially for her patience when correcting manuscripts.

Furthermore, I would like to thank Prof. Nico Burns at the University of Fribourg for being an examiner.

In addition, I would like to thank all our former group members: Dr. Stefan Egli, Dr. Thomas Schuster, Dr. Olivier Casse, Dr. Etienne Cabane, Dr. Karolina Langowska, Dr. Dominik Dobrunz, and Dr. Ramona Enea Casse for their help when I started.

Of course, the present members are also thanked: Dr. Mariana Spulber, Dr. Viktoriia Postupalenko, Dr. Jason Duskey, Fabian Itel, Patric Baumann, Justyna Kowal, Juan Liu, Samuel Lörcher, Adriain Najer, Martin Nussbaumer, Pascal Richard, Gabriele Persy and Sven Kasper for their effort in my research projects and thesis writing.

This work would never be possible without the support outside our research group. Furthermore, I would like to thank Prof. Thomas Pfohl and Natalja Strelnikova (Physical Chemistry department, University of Basel), Dr. Mohamed Chami (C-CINA, Basel), Prof. Joerg Huwyler (Department of Pharmaceutical Sciences, University of Basel) and Mrs. Ursula Sanders and Mrs. Vesna Oliveri (ZMB).

I also would like to thank Mariana Spulber, Viktoriia Postupalenko, Karolina Langowska, Fabian Itel, Patric Baumann, Justyna Kowal, Samuel Lörcher, Adrain Najer, Martin Nussbaumer, Sven Kasper, the guys from the Chinese basketball team and football team in Basel and FC Scientific for spending a lot of their time with me and for being good friends in Basel.

Finally, I would like to thank my family in China and my wife Juan Liu for their support while I pursued my PhD in Basel. Of course, I would like to thank Chinese Government Schlolarship for financial support (09.2010-07.2014).

Abstract

Self-assembly of amphiphilic block copolymers in aqueous solution is one of the most important nanotechnological methods to prepare nanocarriers for different applications. Synthesis of new types of amphiphilic block copolymers with novel functionality and detailed characterization of self-assembly, influenced by self-assembly methods and different other parameters (molecular weight, hydrophilic to hydrophobic ratio), are important.

In this thesis, I present the influence of different parameters on the self-assembly nanostructures for the poly(dimethylsiloxane)-*block*-poly(2-methyl-2-oxazoline) (PDMS-*b*-PMOXA) amphiphilic block copolymers. In addition, in order to develop more functional amphiphilic block copolymers, another two types of copolymers, grafted poly(2-methyl-2-oxazoline)-graft(ss)-poly(ε-caprolactone) (PMOXA-graft(ss)-PCL) and linear poly(2-ethyl-2-oxazoline)-*block*-poly(ε-caprolactone)-ss-poly(L-lysine) (PEtOXA-*b*-PCL-ss-PLL), were designed and synthesized with reduction responsiveness, utilizing different polymerization techniques. The primary evaluation of these two new type amphiphilic block copolymers demonstrated that they are promising candidates as smart nanocarries for the application of drug delivery.

Contents

Abbreviations

ABPs	amphiphilic block copolymers
Ator	Atorvastatin calcium
ATRP	atom transfer radical polymerization
A_{zz}	hyperfine coupling constant
Boc	di-tert-butyl dicarbonate
^{13}C NMR	carbon nuclear magnetic resonance
CLRP	controlled/living radical polymerization
CLSM	confocal laser scanning microscopy
CMC	critical micelle concentration
CS	chondroitin sulfate
cryo-TEM	cryogenic transmission electron microscopy
D_3	hexamethylcyclotrisiloxane
DACHP	(1,2-diaminocyclohexane)platinum(II)
DCC	N,N'-Dicyclohexylcarbodiimid
DCM	dichloromethane
DIPEA	N,N-Diisopropylethylamine
DLS	dynamic light scattering
DMAP	4-Dimethylaminopyridine
DMF	dimethylformamide
DMSO	dimethyl sulfoxide
DNA	deoxyribonucleic acid
DOX	doxorubicin
DP	degree of polymerization
DTT	dithiothreitol
ELP	elastin-like polypeptide
EPR[1]	enhanced permeability and retention
EPR	electron paramagnetic resonance
FCS	fluorescence correlation spectroscopy
FT-IR	fourier transform infrared spectroscopy
G	Gauss

GSH	glutathione
GPC	gel permeation chromatography
HomoFRET	homo-fluorescence resonance energy transfer
^{1}H NMR	proton nuclear magnetic resonance
HBr	hydrogen bromide
K	Kelvin
KOH	potassium hydroxide
kDa	kilodalton
M	molar concentration
MeOH	methanol
M_n	number average molecule weight
M_w	weight average molecule weight
mg	milligram
mL	milliliter
mM	millimolar
NCA	α-Amino Acid *N*-Carboxyanhydride
NMP	nitroxide-mediated radical polymerization
ns	nanosecond
OmpF	outer membrane protein F
PAA	poly(acrylic acid)
PAD	poly(N-amidino) dodecyl acrylamide
PBS	phosphate buffered saline
PDI	polydispersity index
PCB	polycarboxybetaine methacrylate
PCL	poly(ε-caprolactone)
Pd/C	palladium on carbon
PDPA	poly(2-(diisopropylamino) ethyl methacrylate
PGA	penicillin G amidase
PEG	poly(ethylene glycol)
PLA	polylactid
PLLA	poly(L-lactide)
PLG*LAGr9	Pro-Leu-Gly-Leu-Ala-Gly-Arg-Arg-Arg-Arg-Arg-Arg-Arg-Arg-Arg

P(Glu)	poly-(L-glutamic acid):
Pt(dvs)	platinum(0)-1,3-divinyl-1,1,3,3-tetramethyldisiloxane complex
ppm	parts per million
RAFT	reversible addition-fragmentation chain transfer polymerization
ROP	ring-opening polymerization
RT	room temperature
R_g	radius of gyration
R_h	hydrodynamic radius
SAXS	small angle x-ray scattering
SCMF	self-consistent mean-field
SLS	static light scattering
TEM	transmission electron microscopy
TFA	trifluoroacetic acid
THF	tetrahydrofuran
Tris/HCl	tris(hydroxymethyl)aminomethane hydrochloride
T_g	glass transition temperature
VES	Vitamin E succinate
χ_{AB}	Flory-Huggins interaction parameter
µL	microliter
µm	micrometer
Å	angstrom
δ	chemical shift
ρ	$\frac{Rg}{Rh}$
7-ADCA	7-aminodesacetoxycephalosporanic acid
5-DSA	5-doxylstearic acid
16-DSA	16-doxylstearic acid
1,8-ANS	1-Anilinonaphthalene-8-sulfonic Acid

1. Introduction

1.1. Amphiphilic block copolymers (ABPs) synthesis techniques

1.1.1. Living polymerization

Living polymerization was first described by Szwarc in 1956, and represents one of the ultimate goals of synthetic polymer chemists. This requires that the number of produced polymer chains is equal to the number of initiator groups. Therefore, the polymerization will proceed until all monomers have been consumed and the polymer chain ends will remain active, such that further addition of monomers leads to continued polymerization.[1] Two key criteria are used to elucidate the "living" nature of a polymerization: i) the rate of initiation must exceed the rate of propagation, ii) no presence of termination caused by any reaction. The propagating species undergoes polymerization until full monomer conversion and then can continue to initiate the polymerization upon addition of more monomers.[2]

Because of the development of living polymerization, synthetic polymer chemists are now able to synthesize a wide variety of polymers with precise architectures that were previous inaccessible using non-living polymerization techniques. Generally, the living polymerization includes living ionic polymerization (living anionic or cationic polymerization) and living radical polymerization, depending on the property of the propagating center.

1.1.2. Living ionic (anionic and cationic) polymerization

ABPs with defined molecular structure and narrow polydispersity indexes (PDI) can be synthesized through living anionic and cationic polymerization techniques.[3] The main difference between anionic and cationic polymerization is the nature of the chain propagating center. If the propagating center is an anion, the polymerization is named anionic polymerization. Conversely, if the center is cationic, it is referred as cationic polymerization. For vinyl and acrylic monomers, the inductive and resonance characteristics of substituents decide if the monomers undergo cationic or anionic polymerization. For example, poly(styrene),[4] poly(methacrylate), and poly(methacrylamide)[5] can be synthesized through anionic polymerization while, poly(1, 3-dienes), poly(styrene), poly(*N*-vinyl carbazole) can be synthesized through cationic polymerization.[6] Comparing cationic and anionic polymerizations, anionic polymerization requires stricter polymerization conditions. For

example, high solvent purity and water- and oxygen-free polymerization conditions are required. ABPs can be synthesized in a controlled fashion to achieve PDIs of 1.2 using the living ionic polymerization technique.[7] Tomoya Higashihara et al. applied the anionic polymerization to synthesize ABPs, such as poly(4-vinyltriphenylamine)-*block*-poly(methyl methacrylate) (PVTPA-*b*-PMMA) and poly(styrene)-*block*-poly(4-vinyltriphenylamine)-*block*-poly(styrene) (PS-*b*-PVTPA-*b*-PS) with initiator *sec*-butyllithium. They synthesized ABPs with PDIs lower than 1.1. Also, not just vinyl and acrylic monomers can undergo anionic and cationic polymerization, but also some of the heterocyclic monomers, such as cyclic ethers, acetals and amides. In section of 1.1.3., anionic and cationic ring-opening polymerization will be thoroughly discussed.

1.1.3. Ring-opening polymerization (ROP)

Besides vinyl and acrylic monomers, monomers with heterocyclic structure can be polymerized by living polymerization, namely living ROP. Heterocyclic monomers, which are usually employed for the synthesis of various hydrophobic polymers, are ε-caprolactone (ε-CL),[8] glycolide,[9] D,L-lactide,[10] β-butyrolactone,[11] phosphoester[12]. The polymerization can be catalyzed by metal-alkoxides,[13] enzymes[14] and organic catalysts[15]. The typical polymerization mechanism catalyzed by metal-alkoxides for example Tin(II) 2-ethylhexanoate), is described in scheme 1. Most polymers synthesized from the above mentioned monomers are biocompatible and biodegradable.

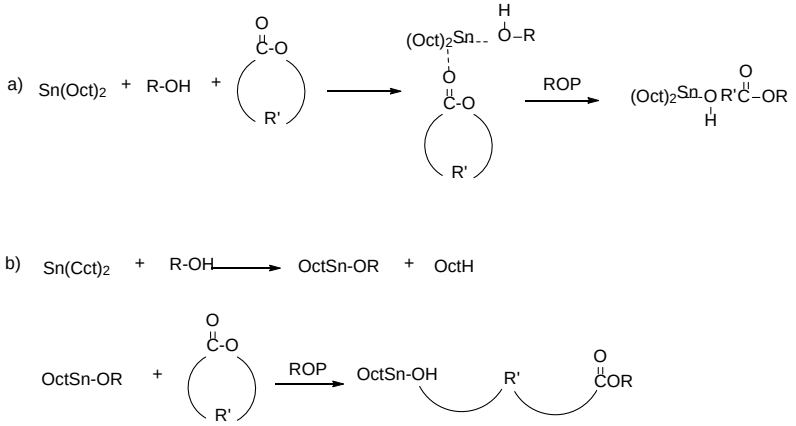

Scheme 1. The main ROP mechanism proposals with $Sn(Oct)_2$ as a catalyst, a) complexation of a monomer and alcohol prior to ROP and b) formation of a tin-alkoxide before ROP of heterocyclic structure monomer.[16]

Heterocyclic monomers, ethylene oxide and 2-methyl-2-oxazoline can also undergo ROP in order to obtain hydrophilic polymers, as poly(ethylene oxide) (PEO) and poly(2-methyl-2-oxazoline) (PMOXA). PEO and PMOXA can be synthesized by either anionic or cationic ROP. For example, PMOXA can be synthesized from 2-methyl-2-oxazoline through cationic ROP initiated by methyl trifluoromethanesulfonate in scheme 2.[17,18] Both PMOXA and PEO have high resistance to protein absorption and bacteria adhesion; therefore ABPs containing PMOXA and PEO blocks are especially designed and synthesized for medical applications.[19]

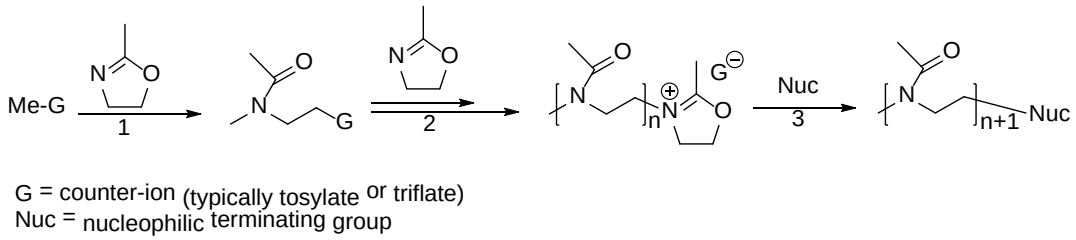

Scheme 2. Synthetic procedure of PMOXA through cationic ROP.

Interestingly, α-Amino Acid *N*-Carboxyanhydride (NCA) initiated by a primary or secondary amine through ROP can be applied to synthesize homopolypeptides.[20] However, the mechanism of ROP with NCA is not ionic polymerization. Homopolypeptides are a kind of advanced evolution biopolymers with striking secondary structures and with adjustable hydrophobicity and hydrophilicity controlled by selecting the suitable NCA (mechanism shown in Scheme 3).[20,21] By choosing the appropriate NCA, polymers containing domains comprised of structural and functional elements similar to those found within natural proteins (for example, α-helices, β-sheets, and containing desired polar and hydrophobic regions) can be obtained. It is quite challenging to control the structure of synthetic polymers and solid state peptides.[22, 23]

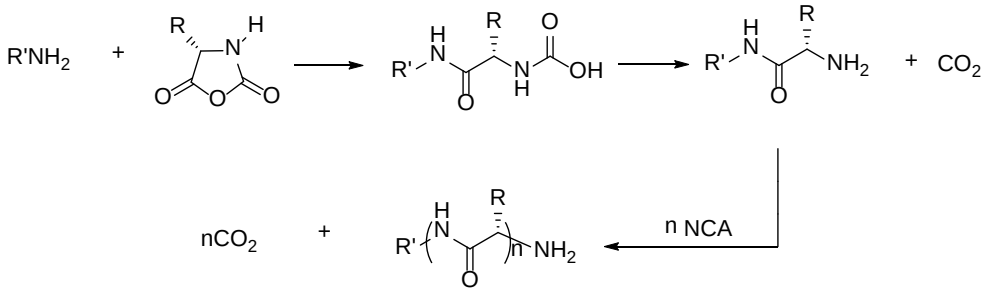

Scheme 3. Mechanism for NCA ROP initiated by nucleophilic amine.

1.1.4. Controlled/Living radical polymerization (CLRP)

Conventional free radical polymerization has an enormous industrial importance. Approximately 50% of all commercially available polymers are produced by radical polymerization, because it can be applied to a wide range of monomers (mainly vinyl, acrylic and methacrylic family monomers) under mild reaction conditions with wide temperature range (going from -80 °C to 250 °C).[24] However, the major drawback is that conventional free radical polymerization proceeds with very limited control, due to occurrence of biomolecules coupling and disproportionation termination and chain transfer reactions of propagating chains with polymer chains, initiators, monomers and solvent molecules during the polymerization, mainly caused by the high reactivity of radicals.[25] As a result, it is impossible to synthesize polymers with regular chemical structures and narrow PDIs. Along with conventional free radical polymerization, CLRP developed rapidly. CLRP maintains not only the advantages of conventional free radical polymerization, like a wide selection of monomers and mild reaction conditions, but also has its own advantages, such narrow PDIs of the synthesized polymers, preservation of functional groups, and possibility of synthesizing block copolymers with complicated structures.[26] Figure 1 illustrates the influence of CLRP and conventional radical polymerization for one monomer on the final molecular weights (M_n) and PDIs.

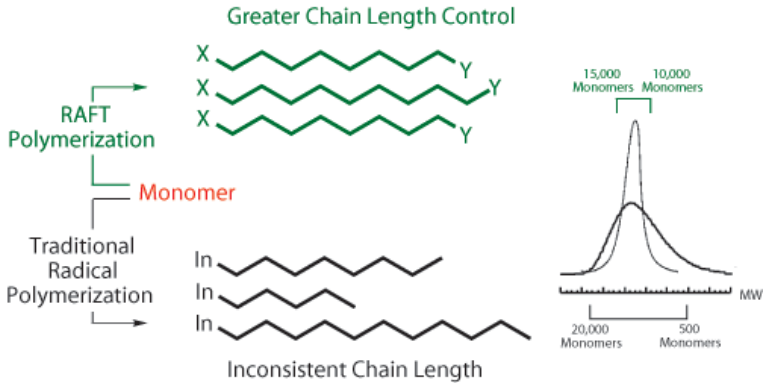

Figure 1. A general comparison of polymers synthesized by conventional radical polymerization and Reversible Addition-Fragmentation Chain Transfer Polymerization process. (http://www.sigmaaldrich.com/materials-science/polymer-science/raft-polymerization.html#sthash.PP5REwUp.dpuf)

The majority of CLRP systems developed to date proceed via one of two basic mechanisms: (i) The persistent radical effect and (ii) degenerative transfer.[25] Among the CLRP, Nitroxide-

Mediated Radical Polymerization (NMP), Atom Transfer Radical Polymerization (ATRP), and Reversible Addition-Fragmentation Chain Transfer Polymerization (RAFT) are most applied to synthesize polymers with a high degree of control.[27] The mechanism of NMP, ATRP and RAFT are depicted in Scheme 4.

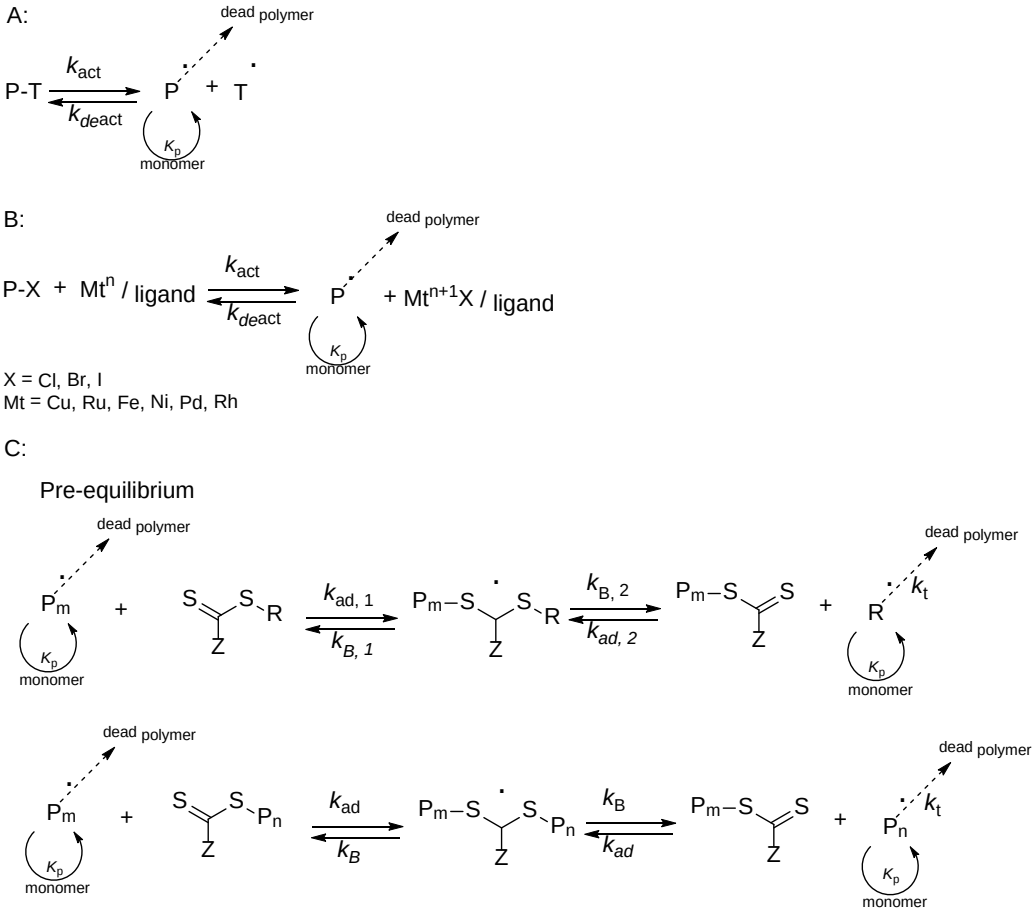

Scheme 4. Mechanism of the (A) NMP, (B) ATRP and (C) RAFT. k_{deact}: deactivation rate coefficient (M^{-1} s^{-1}), k_{act}: activation rate coefficient (s^{-1}), k_{ex}: degenerative chain transfer rate coefficient (M^{-1} s^{-1}), k_p: propagation rate coefficient (M^{-1} s^{-1}), k_t: termination rate coefficient (M^{-1} s^{-1}). [25]

The advanced development of CLRP has led to the synthesis of polymers with various chemical structures (linear, grafted, multi-armed, combed, networked and hyper branched structures).[28-30] CLRP has also contributed to the development of other researches based on polymers, for example the synthesis, self-assembly of ABPs, and applications thereof.[31, 32]

1.1.5. Other polymerization techniques

Beyond living ionic polymerization, ROP, and CLRP techniques, there are also several other types of polymerizations, such as polycondensation.[33] Polycondensation is a typical step-growth polymerization with loss of small molecules during the polymerization process, such as water and carbon dioxide (scheme 5).[34] In order to obtain high M_n polymers, controlling the same amount of reactants and elimination of newly formed small molecules are crucial. Recently, click chemistry has been applied in polycondensation. Suhrit Ghosh et al. used divinyl monomer (M1) and dithiol monomer (M2) to synthesize polymers basing thiol-ene click chemistry (Scheme 6).[35] Also, Krishna Dan et al. reported the synthesis of acid-labile ABPs with "thiol-ene click polycondensation" by introducing another hydrophiphilic polymer with a mono acrylate as ending group at the end point of polycondensation (Scheme 7).[36] In contrast to the mechanism shown in Scheme 5, no small molecules were formed during the "thiol-ene click polycondensation". Therefore, elimination of the newly formed small molecules during the "thiol-ene click polycondensation" is no longer required anymore.

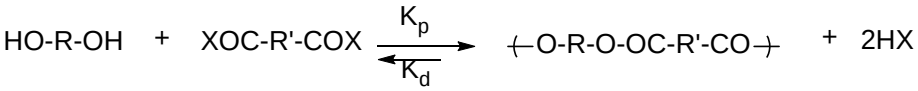

Scheme 5. Mechanism of polycondensation.

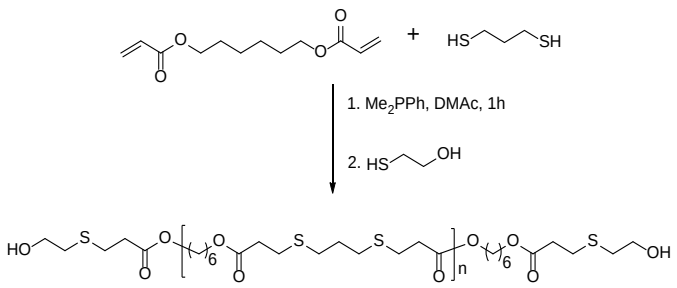

Scheme 6. Synthetic procedure of bi-functional polymers through "thiol-ene click polycondensation".[35]

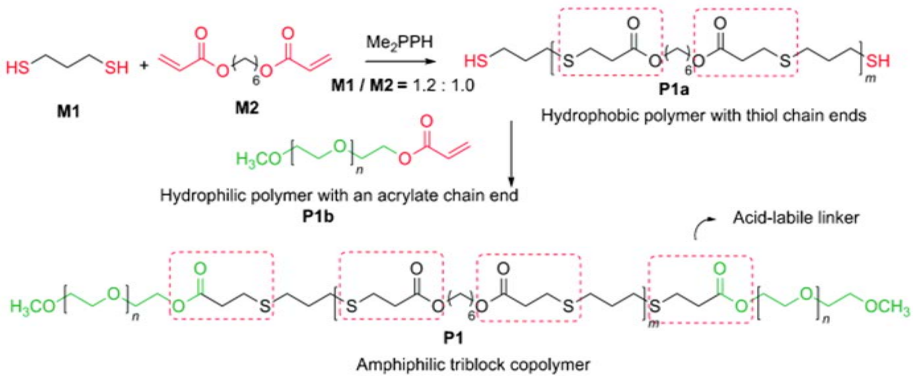

Scheme 7. One-pot synthesis of ABPs with "thiol-ene click polycondensation".[37]

With the development of various polymerization techniques, polymer chemists can specially design and synthesize different polymers with new chemical selective structures and interesting properties. For example, the introduction of polymer blocks or groups with pH-,[37] redox-,[38] light-,[39] thermal-,[40] enzyme-responsiveness[41] have allowed the synthesis of smart ABPs.

1.2. ABP self-assembly

An ABP is one type of polymer, which is constituted by hydrophobic and hydrophilic blocks connected through covalent bonds or by supermolecular interactions.[42, 43] ABPs can be linear, star, cyclic, combed or hyperbranched depending on the used synthetic strategy and monomers (Figure 2).[44, 45]

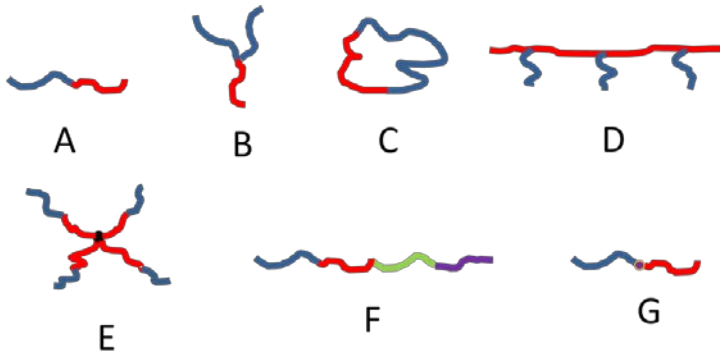

Figure 2. Possible ABPs architectures: A: linear AB diblock, B: star ABC triblock, C: cyclic AB block, D: comb AB block, E: miktoarm star block, F: multiblock, G: supermolecular AB diblock.

Because ABPs have similar structure with small molecule surfactants and lipids, the incompatibility between the molecular segments leads to local segregation or microphase separation in bulk,[46, 47] which means the microphases of each blocks are not lacated at

random but they may form a regular arrangement giving rise to a periodic structure.[48] The microphase separation of ABPs depends on three parameters: (i) the volume fraction of the A and B blocks (f_A and f_B, with $f_A + f_B = 1$), (ii) the total degree of polymerization (DP) ($N = N_A + N_B$), and (iii) the Flory-Huggins interaction parameter (χ_{AB}). The microphase separation structure phase diagram predicted according to the self-consistent mean-field (SCMF) theory and experimental phase portrait of polyisoprene-*block*-polystyrene of amphiphilic diblock copolymer are shown in Figure 3.[49] However, for the amphiphilic multiblock copolymers, understanding the microphase separation is even more complicated.

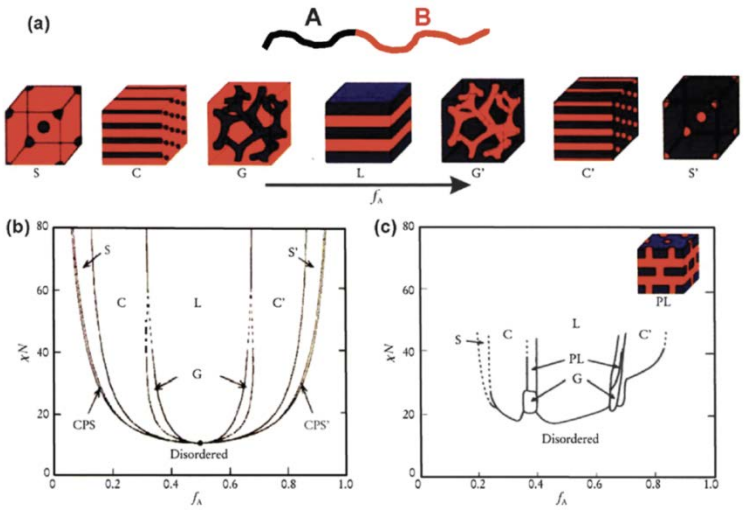

Figure 3. Equilibrium morphologies of amphiphilic diblock copolymers in bulk: S and S' = body-centered-cubic spheres, C and C' = hexagonally packed cylinders, G and G' = bicontinuous gyroids, and L = lamella. (b) Theoretical phase diagram of amphiphilic diblock copolymers predicted by the self-consistent mean-field theory, depending on volume fraction (f) of the blocks and the segregation parameter, χN, where χ is the Flory-Huggins segment-segment interaction energy and N is the degree of polymerization; CPS and CPS' = closely packed spheres. (c) Experimental phase portrait of polyisoprene-*block*-polystyrene copolymers, in which f_A represents the volume fraction of polyisoprene, PL = perforated lamellae.[49]

As just described ABPs can form various microphase separation structures in bulk, and in aqueous solution, they are also able to self-assemble into various nanostructures.[50, 51] The self-assembled nanostructures are with the hydrophilic blocks facing the aqueous environment, and the hydrophobic blocks orienting in the opposite direction to minimize the interaction with the aqueous environment. The final morphology of self-assembled

nanostructures are determined by several factors: i) the nature of constituted blocks (M_ns,[52] PDI[53, 54] and chemical composition);[55] ii) external conditions, including temperature,[56] pH,[57] salt concentration,[58] content of solution[59] and ABP concentration;[60] iii) preparation method; including film rehydration, cosolvent and electroformation.[61] Micelles, worm-like micelles, and vesicles are the three most common types of reported nanostructures (Figure 4).[47] In addition, some other special nanostructures were also reported, for example biocontinuous rods, lamellar structures, multilamellar vesicles and large compound micelles.[62, 63] The packing parameter, $p = v/a_0 l_c$ (Figure 4), determines the morphology of self-assembled ABPs, where v is the volume of the hydrophobic segment, a_0 is the contact area of the head group, and l_c is the length of the hydrophobic segment.[64] When $p < 1/3$, spheres are formed; when $1/3 < p < 1/2$, cylinders; when $1/2 < p < 1$, flexible lamellas or vesicles; finally, when $p = 1$, planar lamellas are obtained.[47, 50] The transition of morphologies can be attributed to two competing factors: interfacial energy between the two blocks and stretching. As microphase separation occurs, the two blocks separate from each other in such a way as to minimize interfacial area to lower the total interfacial energy. Phase separation induces chain stretching away from preferred coiled polymer chain conformation; the degree of stretching depends on the volume fraction of one block relative to that of the diblock. Figure 4 shows the well-known cone-column mechanism for morphological transitions.[65]

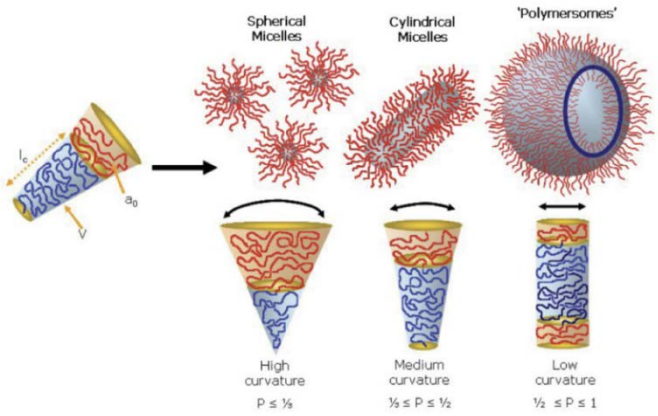

Figure 4. Self-assembled morphologies formed by ABPs in a block-selective solvent. The type of morphologies formed is due to the inherent curvature of the molecule which can be estimated through a calculation of its dimensionless packing parameter, p.[65]

Compared to lipids, ABPs have a higher M_n. Therefore, their self-assembled nanostructures, for example vesicles, exhibit stronger hydrophobic interactions and a higher membrane

thickness, affording them a higher mechanical resistance and a lower permeability than their lipid counterparts.[66, 67] In addition, as described above, by choosing the appropriate polymerization techniques and monomers, various functionalities can be endowed with the self-assembled nanostructures of ABPs.[38,41,68,69] That explains why the ABPs in general, and their self-assembled nanostructures attracted so much interest in the past years from the polymer community to pharmaceutical and medical application.

1.3. Responsive amphiphilic block copolymers (RABP)

RABP is a kind of ABPs with special functional motifs, which endow the ABPs and corresponding self-assemblies with unique functionality or responsibility.[70] The commonly appeared functionalities are pH-responsive groups, thermo-responsive groups, enzyme-responsive groups, light-responsive groups, redox-responsive groups and so on.[71, 72] Through pinpoint chemistry design, such smart groups or functionalities can be incorporated into side chains and tips of ABPs or as linkers between different blocks.[73] Noticeably, some of the RABP can have more than one functionality, for example, Hui Zou et al recently synthesized smart ABP poly(ε-carprolacton)-ss-poly(2-(N,N-dimethylamino)) (PCL-ss-PDEAEMA) with thermo- and redox- responsibility through ROP and ATRP techniques.[74]

1.3.1. RABPs with redox-responsibility

Most of the redox-responsive group which used in ABPs synthesis is disulfide group (-SS-). The disulfide bridge can be break by reduction agent with thiol groups through thiol-disulfide exchange reaction, for example glutathione (GSH). The reason why redox-responsive ABPs are popular is that: i) disulfide group can be conveniently incorporated into ABPs structure by using commercial disulfide-based monomers, ATRP and RAFT agents, functional linkers, and so on;[75] ii) the existence of a large difference in reducing potential between extracellular fluids and the intracellular environment (2-20 μM and 0.5-10 mM of glutathione respectively);[76] iii) the reaction between reducing agent and disulfide can happen in broad condition, including pH values and reaction solution (organic solvents and aqueous solution).[77]

1.4. Applications of ABPs and their self-assembled nanostructures

During the self-assembly process of ABP in aqueous solution, hydrophobic molecules (hydrophobic drugs,[78] porphyrin-based near infrad (NIR) supramolecular fluorophores[79] and

magnetic nanoparticles[80]) and hydrophilic molecules (proteins[81,82]), can be encapsulated into the hydrophobic and hydrophilic domain, respectively.[83] The procedure of encapsulating guest molecules is presented in Figure 5. By confining selected active molecules in enclosed structures, these nanosystems are promising candidates for targeted and triggered drug delivery system.[84,85,86] Polymersome as one of the most important self-assembled nanostructures of ABP can be possible to combine with proteins and enzymes to mimic organelles for therapeutic applications.[87] Interestingly, a membrane protein with two hydrophilic ends and a hydrophobic center, can be inserted into the hydrophobic domain of a polymersome to allow passive or active passage of substrates across the polymersome membrane, making it as a nanoreactor.[88] In nanoreactor, specific reactions can take place in a limited and confined apace.[89] The most interesting, after a nanoreactor is uptaken by cells, they can act as an artificial organelle inside of cells.[87] In addition, the self-assemblies surface can be modified by various targeting molecules (folic acid, antibodies and proteins) to accomplish selective targeting (Figure 6).[90]

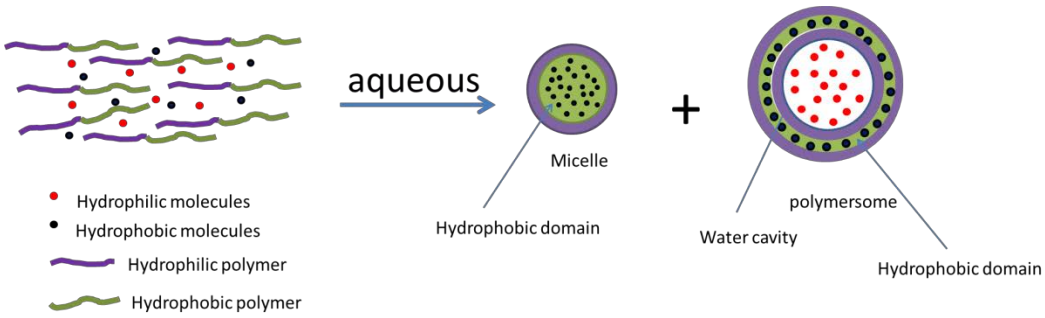

Figure 5. Guest molecules entrapment into the self-assemblies formed by ABPs.

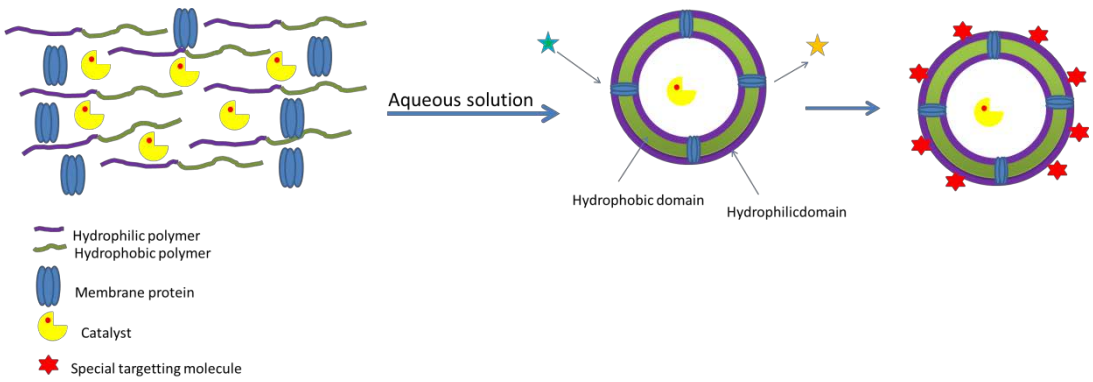

Figure 6. Encapsulation of enzymes into the self-assemblies, insertion of membrane proteins into hydrophobic membrane and surface modification with specific targeting molecules.

Because of the amphiphilicity of ABPs, and the ability of encapsulating hydrophobic and hydrophilic molecules in the ABPs self-assemblies, ABPs and their self-assemblies have been used in following application and research areas: macro-emulsifiers, diagnostics, cancer therapeutics (including anti-cancer drugs and genes delivery), infectious diseases treatments, and nanoreactors.[73, 88, 91-98]

1.4.1. Emulsifier

Because ABPs contain hydrophobic and hydrophilic blocks, they can be used as macro-emulsifiers (polymeric surfactants) to stabilize the hydrophobic droplets in aqueous solution (O/W), or water droplets in an organic solvent (W/O). Compared with the smaller molecular weight emulsifiers, ABPs have several advantages: i) higher stability than small molecule emulsifiers due to the higher M_n and longer molecular chains; ii) chemical and physical properties can be designed by varying the constituting monomers and advanced polymerization techniques. Mickael Chausson et al reported using of poly(caprolactone)-*block*-poly(ethylene oxide) (PCL-*b*-PEO) as the macro-emulsifier to stabilize nanoemulsions formed by hydrophobic PCL and Vitamin E acetate. Emulsification by nanoprecipitation process was successful when the PCL-*b*-PEO was added into the organic phase, especially for higher M_n of the PEO block (DP above 45). The stabilizing effect of PCL-*b*-PEO was similar to that reported for ethylene oxide/propylene oxide triblock copolmyers (Pluronic).[96] Poly(butadiene)-*block*-poly(ethylene glycol) (PBD-*b*-PEG) was a more effective macro-emulsifier to stabilize computed tomography (CT) blood pool contrast agents (Figure 7) when compared with the lipid-stabilized emulsions. Moreover, the blood circulation half-life time of a PBD-*b*-PEG stabilized emulsion is approximately 3 h and shows no toxicity in vivo.[99] The longer blood circulation half-life time can be attributed to higher M_n of PBS-*b*-PEO.

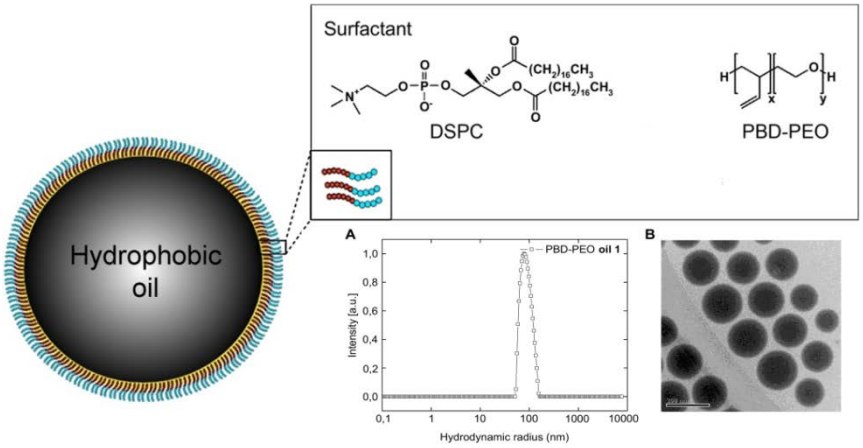

Figure 7. Schematic representation of a stabilized emulsion as a CT contrast agent showing lipid emulsifier and macro-emulsifier PBD-*b*-PEG. (A) The unweighted hydrophobic radius and distribution result from DLS and (B) Cryo-TEM of hydrophobic oil droplet.[99]

1.4.2. Medical application

ABP self-assembly structures have a wide range of biomedical applications ranging from drug delivery systems to artificial organelles. One of the most important medical applications of ABPs is anticancer therapy because of enhanced permeability and retention (EPR[1]) effect, defined by an enhanced uptake of loaded self-assemblies of ABPs with diameter lower than 200 nm by tumors.[97, 100] Moreover, low M_n compounds can enter into both normal and tumor tissues through the endothelia cell layer of blood capillaries by free diffusion-dependent equilibrium (Figure 8), while high M_n compounds (polymers, self-assembled nanostructures) cannot pass the endothelial cell barrier of normal tissue. Instead, they are uptaken into the tumors' leaky vasculature and remain there until taken up by the tumor cells. In normal tissue, the clearance of macromolecules and small size particles occur rapidly and steadily via the lymphatic system, whereas in tumor tissue the drainage system is defective. Macromolecules are retained in the tumor and accumulate high doses independent of the specific type of tumor.[101] This unique phenomenon in solid tumors, EPR[1] effect, is considered to be a landmark principle in tumor-targeting chemotherapy and become a promising paradigm for anticancer drug development. By encapsulating of anti-cancer drugs in the self-assemblies of ABPs, they will be transported preferential only to tumors decreasing in toxicity of anti-cancer drug to normal tissues.[102] That is why utilizing ABPs self-assembled nanostructures loading with anti-cancer drugs is one of the most promising cancer therapy alternatives.

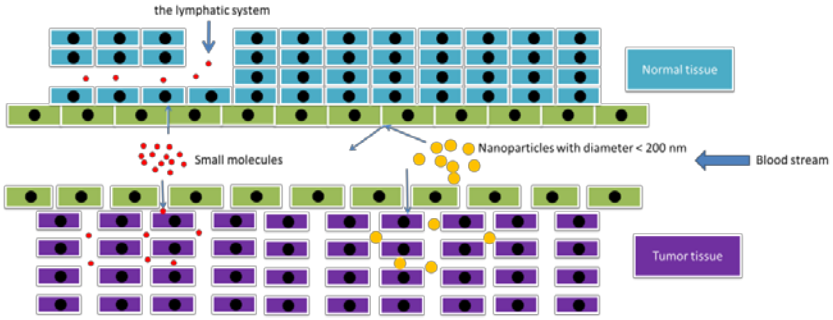

Figure 8. Schematic representation of EPR[1] effect to the small molecules and nanoparticles.[93]

Recently, stimuli-responsive self-assemblies of ABPs have been used for anti-cancer drug delivery.[70, 73, 97] Their fast development of these smart self-assemblies of ABPs is due to the presence of special stimuli-responsive functional groups as described above. [41, 93, 94,103,104,71, 105] Assaf J. Harnoy et al. synthesized an amphiphilic PEG-dendron, which self-assembled into micelles in aqueous solution. The end functional groups of the dendrons contain phenyl acetamide groups that are hydrophobic and can be cleaved by enzyme penicillin G amidase (PGA). When the micelles were exposed to PGA, the structures of micelles were destabilized and the encapsulated guest molecules were released (Figure 9).[106]

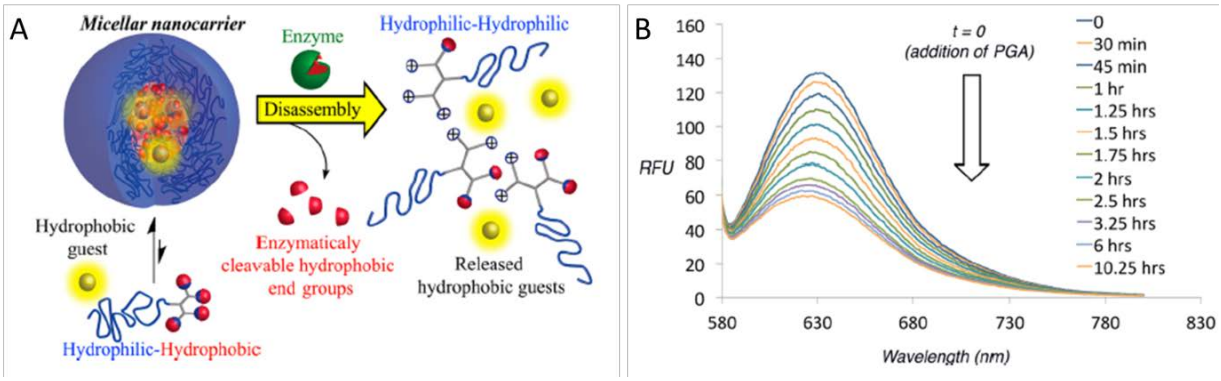

Figure 9. (A) Schematic representation of the encapsulation of hydrophobic compounds in the hydrophobic core of enzyme-responsive micelles. Upon enzymatic cleavage of the hydrophobic end groups, the micelles disassembled and the guest molecules were released. (B) Fluorescence spectra of Nile red (1.25 µM) in the presence of PEG-dendron (160 µM) as a function of time after the addition of PGA (0.14 µM). Fluorescence intensity decreased as Nile red was released into solution.[106]

ABPs are not only applied in anticancer therapy, but can be also used for treatment of various infectious diseases and in diagnostics. We reported that polymersomes formed from a mixture of PDMS-heparin block copolymers with poly(2-methyl-2-oxazoline)-*block*-poly(dimethylsiloxane)-*block*-poly(2-methyl2-oxazoline) (PMOXA-*b*-PDMS-*b*-PMOXA) can efficiently inhibit malaria parasites to attach to host cells and therefore to interrupt the life-cycle of the pathogen by invasion inhibition. The results showed that these nanomimics efficiently blocked the reinvasion of malaria parasites after their egress from host cells, and exhibited efficiency of more than two orders of magnitude higher than the soluble form of the heparin-receptor (Figure 10).

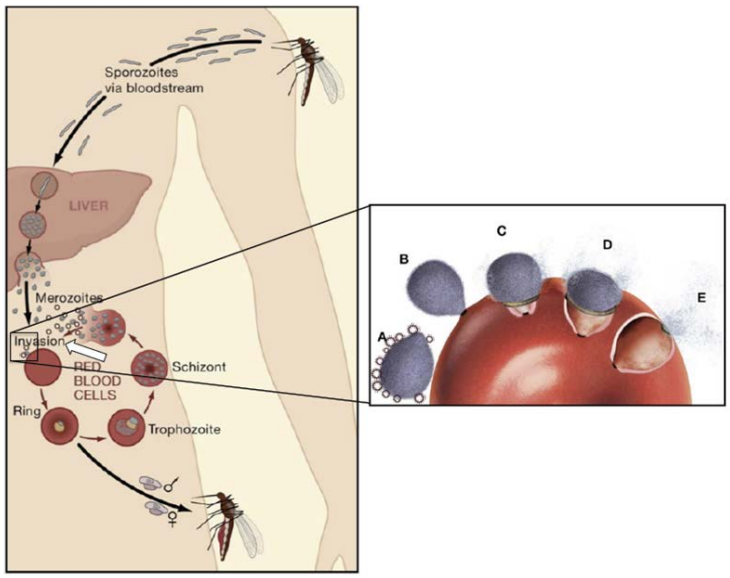

Figure 10. Schematic representation of the nanomimic concept. Left: life cycle of P. falciparum in the human host: an Anopheles mosquito injects sporozoites, which pass through Kupfer cells and invade hepatocytes, in which merozoites develop and are released into the blood stream to invade red blood cells (RBCs) after specific attachment to heparan sulphate.[107] In infected RBCs (iRBCs) merozoites develop through schizogeny releasing 16 - 32 daughter merozoites after 48 h, which subsequently invade new RBCs (asexual blood-stage). Right: schematic merozoite invasion into RBCs. An initial attachment through binding of the processed ligand $MSP1_{42}$ to heparan sulphate on RBCs.[107] Competing nanomimics (red circles) block fresh merozoites before they enter new RBCs (white arrow) (modified with permission from[108]).

Yiguang Wang et al. reported that ultra pH-responsive nano probes formed by self-assembly of ABP cRGDfK-poly(ethylene glycol)-*block*-poly(2-(diisopropyl amino)ethylmethacrylate) copolymer with conjugated near-infrared dye, Cy5.5 (cRGD-PEG-*b*-(PR-r-NIR) can be used as a diagnostics nanoreporter (Figure 11). At pH > 7.0, these nanostructures were stabilized by the hydrophobic interaction, and the homo-fluorescence resonance energy transfer (homoFRET) induced fluorescence of the dye was quenched (representing the “OFF” state). However, when the pH decreased < 7.0, the tertiary amine was protonated, and the hydrophobic domain of the nanostructures changed to hydrophilic resulting to increase the distance between fluorescent dye molecules. In this manner, the fluorescence of the dyes was not quenched (“ON” state). Because the pH is lower in tumor cells, these structures

showed no fluorescence while circulating in blood steam, but showed a high fluorescent signal in tumors after the nanoprobes were uptaken by the acidic cancer tissue.[109] It should be noted that ABPs used in medical application should be biocompatible and biodegradable. Table 1 listed some examples of ABPs which have been used for medical applications.

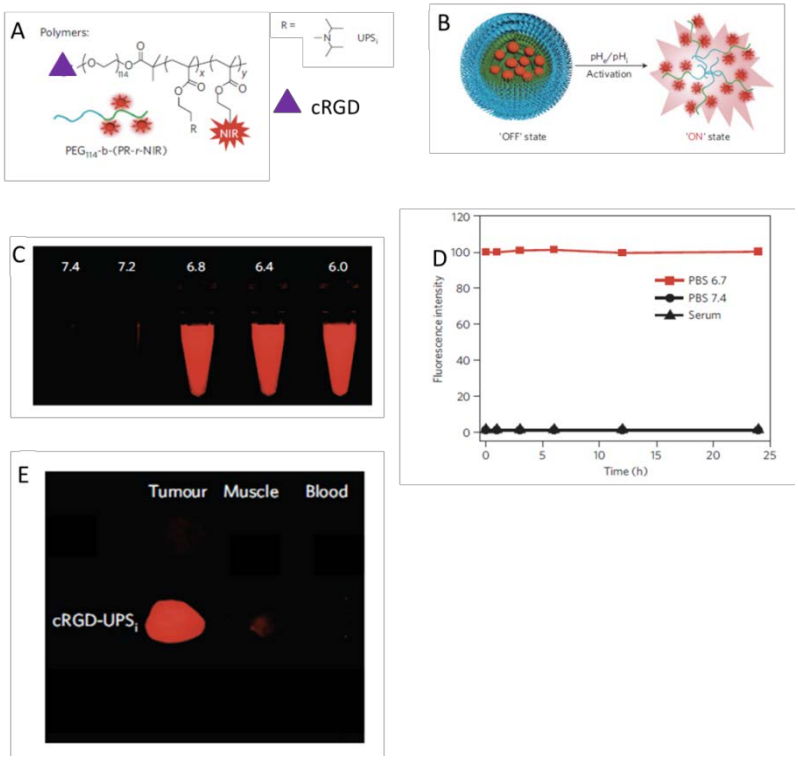

Figure 11. A. Chemical structure of ABPs used as the nanoprobes, UPS_i (chemical structure is shown in inset of Figure 11A) can be activated inside acidic endocytic organelles (pHi = 5.0-6.0). B. nanoprobes changing state from "OFF" to "ON". C. Normalized fluorescence intensity as a function of pH for UPSi nanoprobes, the nanoprobes can be activated as a result of micelle dissociation. D. UPS_i nanoprobes remain stable in fresh mouse serum over 24 h at 37 °C. E. Representative images of *ex vivo* tumours, muscles and blood at 6 h post-injection of nanoprobes.[109]

Table 1. Examples of ABPs used for medical applications (2013 and 2014).

ABPs	Active molecules	functionality	morphology of self-assemblies	Ref.
PEG-*b*-PLGA	DTX		Micelles	[110]
PEG-star-PCL	DOX.HCl	Redox-responsive	Micelles	[111]
PEG-*b*-PCL-*b*-PAA	DOX	pH-responsive	Vesicle	[112]
PCB-*b*-PDPA	DOX	pH-responsive	Nanoparticles	[113]
DL-ssAB	DOX	Redox-responsive	Micelles	[114]
mPEG-SS-VES	Ator	Redox-responsive	Micelles	[115]
PEG-XPLG*LAGr$_9$ X-PCL	siRNA		Micelles	[116]
PLLA-*b*-peptide-PLLA	fluorouracil	Enzymatic-responsive	Nanoparticles	[117]
ELP-*b*-PEG	1,8-ANS	pH-responsive	Nanoparticles	[118]
PEG-SS-PTMBPEC	DOX	pH-responsive and Redox-responsive	Micelles	[119]
PCL-*b*-P(OEGMA-co-MAEBA	CPT	pH-responsive and Redox-responsive	Micelles	[120]
PEG-*b*-PAD	Myoglobin	CO_2- responsive	Vesicle	[121]
PEO-*b*-P(DEA-*stat*-TMA)	DOX	pH and ultrasound responsive	Vesicle	[92]
Mal-PEG-*b*-P(Glu)	DACHPt		Micelles	[122]
PEG-PUSeSe-PEG	DOX	light responsive	Nanoparticles	[91]
PEG-*b*-PLA	SiQDs		Nanoparticles	[123]

1.4.3. Nanoreactors

Nanoreactors are new and exciting structures represented by vessels carrying out defined, chemical reactions in a confined nano-scale space.[89, 95] In order to be defined as a nanoreactors, the vessels must fulfill the following requirements: (i) efficient encapsulation of desired catalysts within their cavity; (ii) a physical stable membrane to protect the encapsulated catalysts; iii) polymer membrane with selective permeability allowing the

passage of certain reactants and products.[89] Due the higher M_n of ABPs, the self-assembled polymersomes with high mechanism stability membrane and several hundred nanometers diameters address the first two mentioned requirements. However, due to lack of permeability of hydrophobic polymer membrane for small molecules and ions,[98, 124-127] finding solutions to allow the passage of reactants and products is critical to create a nanoreactor. In order to induce permeability through polymer membranes, various methods have been used. For example, insertion of membrane proteins we describe above.[98, 128, 129, 95, 126]. Recently, Karolina Langowska et al. inserted outer membrane protein F (OmpF) into the membrane of PMOXA-*b*-PDMS-*b*-PMOXA self-assembled polymersome. The encapsulated penicillin acylase w Penicillin acylase inside of the polymersome can catalyze 7-aminodesacetoxycephalosporanic acid (7-ADCA) and phenylglycine methyl ester (PGME) to form antibiotic cephalexin. This nanoreactor system could synthesize antibiotics in the cavity of polymersomes, and the synthesized antibiotics can be transferred from inside through OmpF to outside inhibiting bacterial growth. The detailed design of antibiotic self-generating implants is presented in Figure 12.[89]

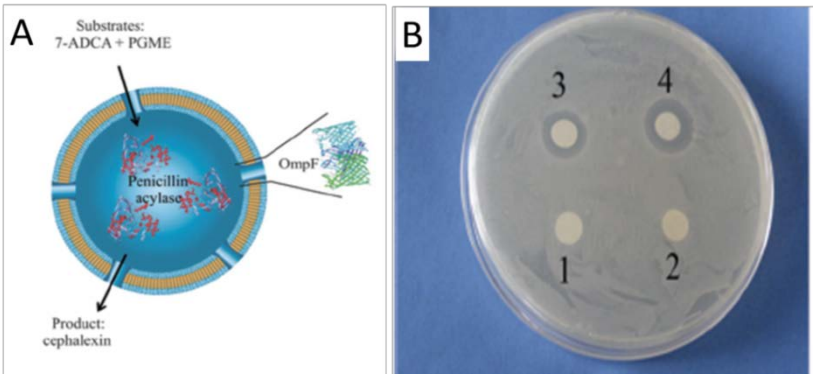

Figure 12. (A) Schematic representation of antibiotic nanoreactor producing cephalexin. (B) Picture of the MHB agar plate inoculated with bacteria. Inhibition areas: 1: control (not permeable polymersomes); 2: substrate solution; 3: nanoreactors prepared at RT; 4: nanoreactors prepared at 8 °C; after incubation for 24 h at 37 °C. No zones of inhibition were observed around control or substrate disks.[89]

Nanoreactors with selective permeability can be obtained by using a mixture of polyethylene glycol-*block*-polystyrene (PEG-*b*-PS) with poly(ethylene glycol)-*block*-poly(styrene boronic acid) (PEG-*b*-PSBA) as two types of different ABPs. By increasing the pH value, the solubility of the PSBA block in water increases when boronic acid is ionized to boronate, which makes

the copolymers of PEG-*b*-PSBA change from amphiphilic to hydrophilic allowing them to diffuse from the polymersome. Because the PS is a crystal polymer, the original space occupied by PSBA cannot be filled by the PS, and pores are formed in the membrane (Figure 13).[130] Interestingly, the chemical method can also be applied to create to pores on the membrane of polymersomes.[125] For example, UV-irradiation of 2-hydroxy-4-2-(hydroxyethoxy)-2-methylpropiophenone (PP-OH) added into the polymersome solution of PMOXA-*b*-PDMS-*b*-PMOXA, and poly(ethylene oxide)-*block*-poly(butadiene) (PEO-*b*-PBD), induced the increase of polymer membrane permeability to create nanoreactors (Figure 14).

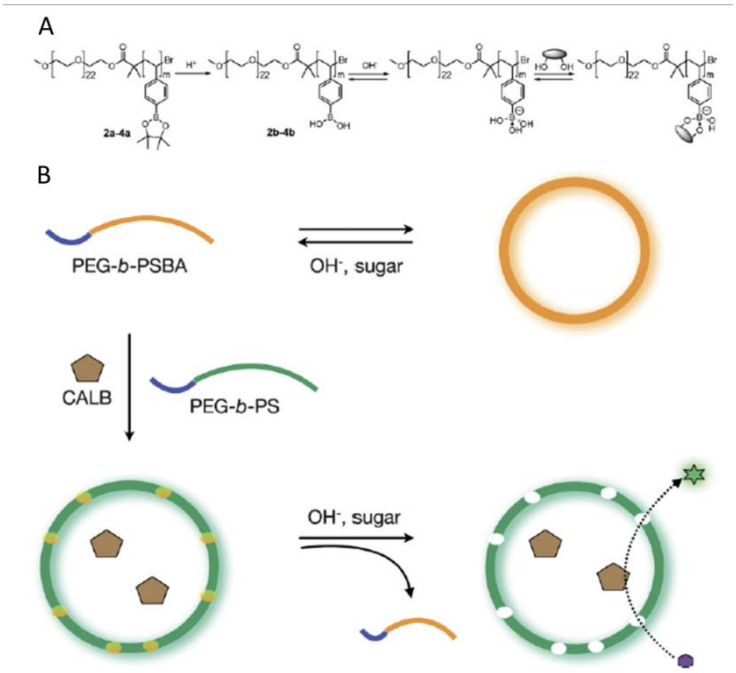

Figure 13. (A) Molecular structures of block copolymers, PEG-*b*-PSBA, and their equilibrium with sugar molecules in a basic aqueous phase. Complete ionization of boronic acid groups was assumed for simplicity. (B) Schematic representation of the formation of nanoreactors with a permeable membrane utilizing the sugar responsiveness of the block copolymers.[130]

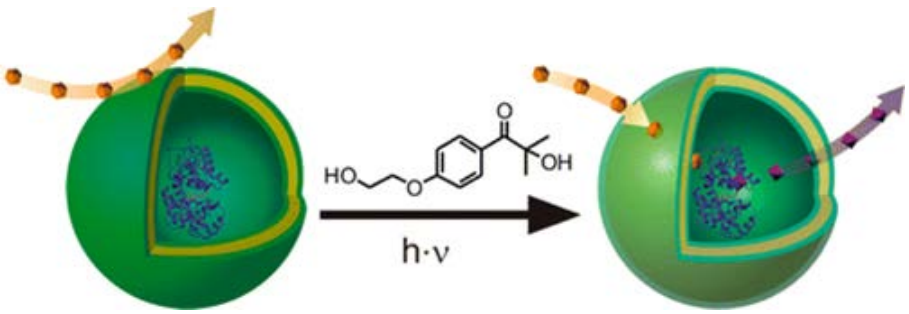

Figure 14. Schematic representation of nanoreactor produced by photoreaction of hydroxyalky phenone.[125]

1.5. Motivation and concept.

The influence of different parameters presented in the part of 1.2. on the self-assembled morphologies of ABPs have been reported by several papers using different ABPs. However, in depth and systematic analyses of various factors simultaneously affecting the self-assembly process is still needed. Due to the promising applications of ABPs in medical field, the development of new smart nanocarriers for drug and/or gene delivery is also interesting. In this respect, we aim to synthesize three different ABPs, poly(dimethylsiloxane)-*block*-poly(2-methyl-2-oxazoline) (PDMS-*b*-PMOXA), poly(2-methyl-2-oxazoline)-graft(ss)-poly(caprolactone) (PMOXA-graft(ss)-PCL) and poly(2-ethyl-2-oxazoline)-*block*-poly(caprolactone)-*block(ss)*-poly(L-lysine) (PEtOXA-*b*-PCL-ss-PLL), and investigate the different parameters that influence the self-assembly behaviors for the ABPs system of PDMS-*b*-PMOXA, and evaluate potential application for different medical applications of PMOXA-graft(ss)-PCL and PEtOXA-*b*-PCL-ss-PLL ABPs systems. The synthesized ABPs should fulfill the following requirements:

(i) They self-assemble nanostructures in aqueous solutions.

(ii) Reproducible synthesis employing the conventional polymerization techniques.

(iii) Biodegradability and biocompatibility.

(iv) Ability to entrap various selected drugs or plasmids inside the formed self-assembled structures.

In order to accomplish this aim, various diblock copolymers PDMS-*b*-PMOXA were synthesized through the anionic and cationic ROP techniques. That are designed specifically to facilitate the study of the effect of the M_n of both hydrophobic and hydrophilic blocks on the self-assembly behavior. The initial concentrations of copolymers, preparation methods for the supramolecular assemblies, and the contents of the aqueous solution are taken into account. Also, a new reduction responsive ABP with grafted polymer structure, PMOXA-graft(ss)-PCL, was synthesized through ROPs and a thiol-disulfide exchange reaction. The cell toxicity of ABPs and the anti-cancer profile of DOX loaded nanoparticles formed by ABPs were tested. In addition, in order to achieve the gene delivery, a third ABP with linear triblock structure, PEtOXA-*b*-PCL-ss-PLL was synthesized. Due to the negative charge of the DNA backbone, it can be complexed through charge interaction by the positive charge of the PLL block during the self-assembly of PEtOXA-*b*-PCL-ss-PLL. The overall performance of PEtOXA-*b*-PCL-ss-PLLs as gene delivery nanocarriers should be investigated in more depth.

2. Effect of molecular parameters on the architectures and membrane properties of 3D assemblies of amphiphilic copolymers

Dalin Wu, Mariana Spulber, Fabian Itel, Mohamed Chami, Thomas Pfohl, Cornelia G. Palivan*, and Wolfgang Meier*

The result have been published on the journal of Macromolecules

Macromolecules, 2014, 47 (15), pp 5060–5069

2.1. Introduction

ABPs represent one of the most promising self-assembling materials, because they form in dilute aqueous solutions a variety of supramolecular assemblies, such as polymersomes, free standing films, tubes, micelles, or hard spheres.[65] The architectures and properties of these synthetic supramolecular self-assemblies can be optimized by selecting a specific chemical structures of ABPs (chemical nature, block lengths, modulation of their hydrophilic-to-hydrophobic ratios), or by chemical modification functionalization.[50,131]

Interesting architectures in terms of possible novel applications of ABPs are polymeric vesicles or polymersomes, which are nanometer size compartments generated by self-assembly in dilute aqueous solution. They offer three different topological regions (membrane, external surface and inner cavity) that serve as appropriate locations for encapsulating active molecules, such as proteins, enzymes, mimics, genes, contrast agents, etc.[95, 132, 133] The hydrophobic membrane facilitates insertion of hydrophobic molecules, the external surface can be functionalized with specific molecules to support targeting approaches or immobilization on solid supports, whilst the inner cavity has the role of a confined space where hydrophilic active molecules can be encapsulated. A major advantage of polymersomes, which supports their application as drug delivery systems, is their dual role: they prevent leakage of encapsulated molecules from inner cavity, and protect them against exterior degradation agents.[134] A further step in the development of applications for polymersomes is to design nanoreactors by using their inner cavity as a confined space, in which reactions occur when catalytically active compounds are encapsulated.[98] To support nanoreactor functionality, the polymersome membrane has to allow an exchange of

substrates/products with the environment whilst preserving the spherical architecture of vesicles. Permeability of the membrane is achieved either by chemical modification,[125, 130] or by insertion of channel proteins.[98] To accomplish the insertion of membrane proteins in the hydrophobic shell of polymersomes, the ABPs should address at least three requirements: i) the hydrophobic blocks should be with quite flexibility without crystal structures (low glass transition temperature (Tg)); (ii) the thickness of the polymersome membrane should be in the same range of the membrane proteins. A large variety of nanoreactors have been produced by encapsulating proteins,[124] enzymes,[135] mimics[81] or combinations thereof that offer the possibility to mimic natural organelles inside of cells.[95]

In the present thesis, the synthesis of a library of ABPs poly(dimethylsiloxane)-*block*-poly(2-methyl-2-oxazoline) (PDMS-*b*-PMOXA), which are designed specifically to facilitate the study of the effect of the M_n of both hydrophobic and hydrophilic blocks on the self-assembly behaviors are described. The initial concentrations of copolymers, preparation methods for the supramolecular assemblies, and the contents of the aqueous solution are taken into account, and a combination of light scattering, TEM and cryo-TEM have been used to characterize the supramolecular assemblies. Due to the low Tg value (-123 °C), very low surface energy and physiological inertness of PDMS,[136] the self-assembled polymersome formed by PDMS-*b*-PMOXA will be the candidates for the insertion of membrane proteins to serve as nanoreactors and/or artificial organelles. In order to obtain greater insight into the organization of the hydrophilic and hydrophobic domains of the polymersomes, we have investigated the interaction of spin-probes with the polymer membranes of the polymersomes by electron paramagnetic resonance (EPR) to provide information on local flexibility and polarity of the polymer membranes. Such information is essential when planning the insertion of membrane proteins into polymersome membranes for nanoreactor development.

2.2. Results and discussion

2.2.1. Synthesis and characterization of PDMS-OH, PDMS-OTf and PDMS-*b*-PMOXA ABPs

PDMS-OH was obtained by hexamethylcyclotrisiloxane (D_3) through anionic ROP in presence of n-butyllithium (Scheme 8). The freshly dried and distilled D_3 was initially mixed with n-butyllithium in anhydrous cyclohexane to form the anionic initiator. Chain propagation

started after addition of freshly distilled THF which favors the presence of loose ion pairs and can further initiate the ROP of D_3. The anionic ROP of D_3 suffers from a backbiting reaction when the monomer concentration decreases more than 80% at room temperature. Because the backbiting reaction competes with the propagation,[137] the polymerization should be quenched to avoid the formation of cyclic PDMS molecules before the monomer concentration decreases by 80%. Cyclic PDMS molecules cannot further participate in the functionalization, so any free PDMS can affect the further synthesis and PDIs of the PDMS-*b*-PMOXA. Quenching was performed by reacting with chlorodimethylsilane, introducing the silane (SiH) group as the end functional group of linear PDMS (PDMS-SiH) (Figure 15-A). Next, hydrosilyzation between PDMS-SiH and 2-allyloxyethanol was performed in order to obtain PDMS-OH. When hydrosilyzation was carried out at 60 °C with 50 mM Pt(dvs) as catalyst, even after over 24 h, the peak of proton on end silane group (SiH) was still present in the ^{1}H NMR spectrum, indicating the incomplete hydrosilyzation reaction. After increasing the temperature to 110 °C, the complete modification by 2-allyloxyethanol was accomplished, where the peak of Si-H proton at 4.85 ppm disappeared completely. The appearance of new peaks at 3.86 ppm, 3.72 ppm and 3.60 ppm characteristic for the protons of 2-allyloxyethanol structure (Figure 15-B) proved that the PDMS-OH has been successfully synthesized. Three different PDMS-OH polymers with increasing DP: 16, 39 and 65 units were synthesized (Table 2).

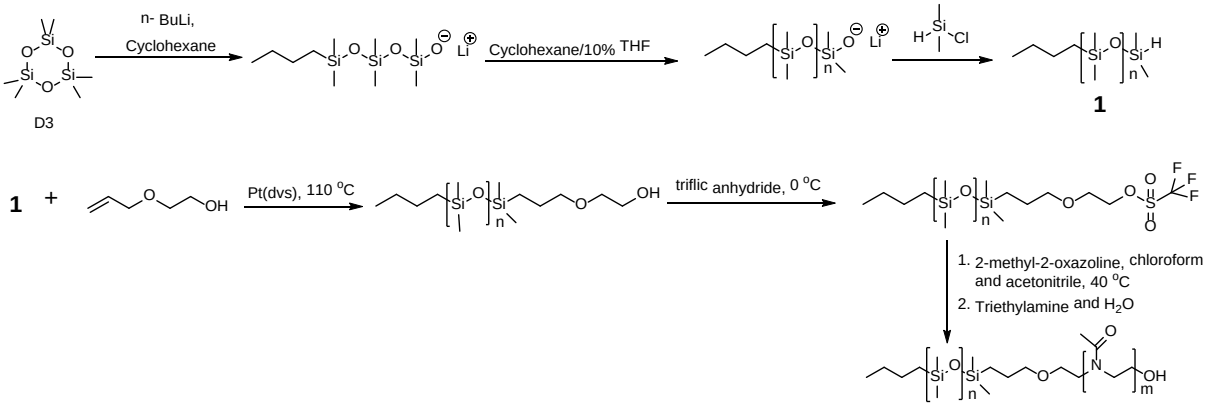

Scheme 8. Synthesis route of PDMS-OH, PDMS-OTf and PDMS-*b*-PMOXA ABPs.

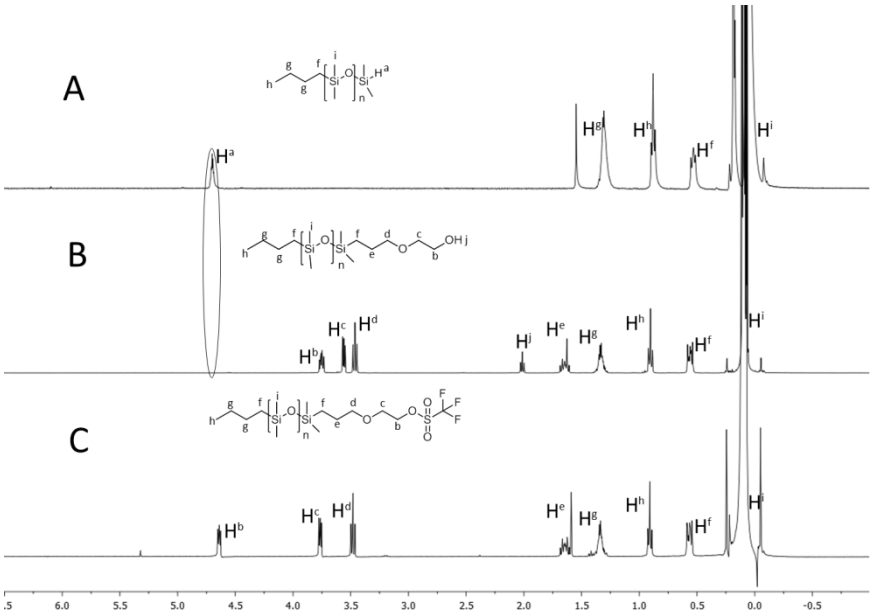

Figure 15. ^{1}H NMR spectrums of silane terminated PDMS-SiH, PDMS-OH and PDMS-OTf.

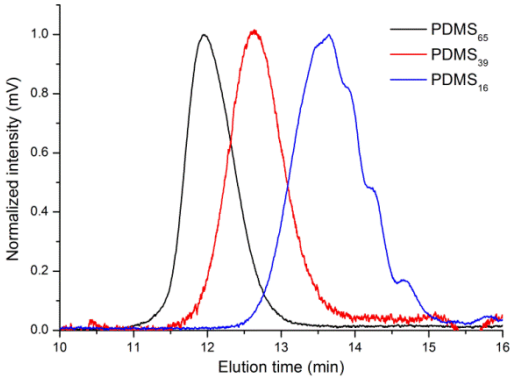

Figure 16. GPC curves of $PDMS_{65}$-OH, $PDMS_{39}$-OH and $PDMS_{16}$-OH with THF as the running phase.

The PDIs of these PDMS-OH polymers were 1.11, 1.08 and 1.12, respectively (Figure 16). Because water is a known quenching agent for the ROP of 2-methyl-2-oxazoline, the obtained PDMS-OH was dried by refluxing with toluene in a Soxleth apparatus containing 4Å molecular sieves overnight before further use. The dried PDMS-OH was reacted with trifluoromethanesulfonic anhydride to synthesize the PDMS-OTf macroinitiator. The chemical structure was characterized by ^{1}H NMR (Figure 15-C). After forming the triflate ester, the chemical peaks characteristic for protons on carbon b and c of PDMS-OH were completely shifted from 3.86 ppm and 3.71 ppm to 4.77 ppm and 3.94 ppm, respectively. This indicated that all the hydroxyl group of PDMS-OH were activated. The ROP of 2-methyl-2-oxazoline in acetonitrile initiated by triflate ester is a living cationic ROP.[138] However, the

acetonitrile was not a good solvent for the macroinitiator PDMS-OTf, so a mixture of chloroform and acetonitrile was used instead ($V_{chloroform}$: $V_{acetonitrile}$ = 7 : 3). The polymerization reaction kinetics was examined by ^{1}H NMR, and the result is shown in Figure 17. By increasing the polymerization time, the integrals of the protons on 2-methyl-2-oxazoline (δ = 4.20 ppm and δ = 3.76 ppm) decreased gradually, while those characteristic for poly(2-methyl-2-oxazoline) (PMOXA) (δ = 3.42 ppm and δ = 2.07 ppm) increased (Figure 17). The ROP of 2-methyl-2-oxazoline obeyed a first order kinetics as shown in Figure 18, which indicated that the lengths of the PMOXA blocks can be easily controlled by changing polymerization time.

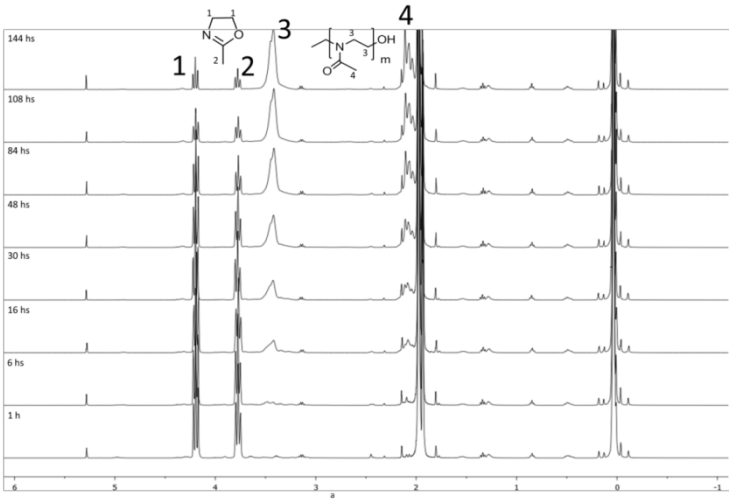

Figure 17. ^{1}H NMR spectrum of polymerization propagation of 2-methyl-2-oxazoline initiated by PDMS-OTf in different polymerization time.

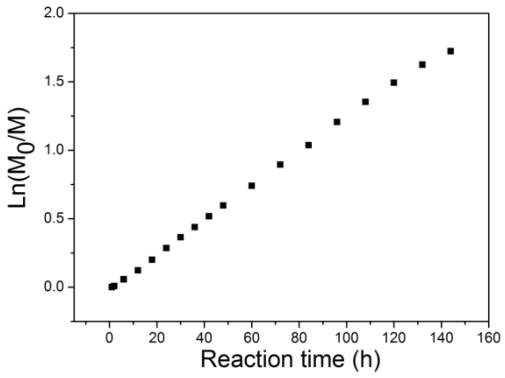

Figure 18. The kinetic of polymerization of 2-methyl-2-oxazoline initiated by PDMS-OTf in the chloroform and acetonitrile (V/V= 7:3) mixture solvents at 40 °C. (M_0: initial concentration of 2-methy-2-oxazoline; M: concentration of 2-methy-2-oxazoline in each reaction time).

We selected three hydrophobic PDMS-OH polymers with increasing DP: 16, 39 and 65. Variable hydrophilic PMOXA block with variable DP (ranging from 3 to 38 units) were coupled by living cationic ROP of 2-methyl-2-oxazoline. The library of $PDMS_x$-*b*-$PMOXA_y$ ABPs allowed the investigation of how to tune the formation of supramolecular assemblies with selected morphologies by varying the hydrophilic to hydrophobic block length ratio ($f_{PMOXA} = \frac{Mn\ of\ PMOXA}{Mn\ of\ PDMS}$) (Table 2).

Table 2. Molecular characteristics of PDMS-OH and PDMS-*b*-PMOXA ABPs.

Sample[a,b]	M_n [a] (KDa)	f_{PMOXA} [c]	f* [d]
A_{65}	5.00		
$A_{65}B_{10}$	5.88	16%	14%
$A_{65}B_{12}$	6.05	20%	16%
$A_{65}B_{14}$	6.18	24%	19%
$A_{65}B_{16}$	6.35	27%	21%
$A_{65}B_{19}$	6.59	31%	24%
$A_{65}B_{26}$	7.14	44%	31%
$A_{65}B_{32}$	7.68	53%	35%
$A_{65}B_{38}$	8.19	64%	39%
A_{39}	3.10		
$A_{39}B_{6}$	3.61	16%	14%
$A_{39}B_{7}$	3.69	19%	16%
$A_{39}B_{8}$	3.77	22%	18%
$A_{39}B_{9}$	3.85	24%	19%
$A_{39}B_{10}$	3.94	27%	20%
$A_{39}B_{11}$	4.02	30%	21%
$A_{39}B_{12}$	4.11	33%	23%
$A_{39}B_{13}$	4.19	35%	26%
$A_{39}B_{18}$	4.61	49%	33%
$A_{39}B_{22}$	4.95	60%	37%
A_{16}	1.40		
$A_{16}B_{2}$	1.57	12%	11%
$A_{16}B_{3}$	1.66	18%	15%

$A_{16}B_4$	1.74	24%	19%
$A_{16}B_5$	1.82	30%	23%
$A_{16}B_6$	1.91	36%	26%
$A_{16}B_7$	1.99	42%	23%
$A_{16}B_9$	2.16	54%	35%
$A_{16}B_{10}$	2.24	60%	38%

[a]DP determined by ^{1}H NMR; [b]A_xB_y represents PDMS$_x$-*b*-PMOXA$_y$; [c]Calculated from the equation $f_{PMOXA} = \frac{Mn\ of\ PMOXA}{Mn\ of\ PDMS}$; [d]Calculated from the equation $f^* = \frac{Mn\ of\ PMOXA}{Mn\ of\ block\ copolymer}$.

2.2.2. Preparation and characterization of self-assemblies of PDMS-*b*-PMOXA.

2.2.2.1. Critical micelle concentration (CMC) determination of PDMS-*b*-PMOXA.

ABPs can self-assemble into various nanostructures in aqueous solution with concentrations higher than the CMC. As one of the most important parameters, CMC values are first investigated for new ABPs. CMC values of PDMS$_{65}$-*b*-PMOXA$_{14}$ and PDMS$_{65}$-*b*-PMOXA$_{32}$ were determined by a surface tension technique with increasing ABPs concentration, ranging from $3*10^{-4}$ to $1*10^{-2}$ mg/mL. The determined CMC values are $1*10^{-3}$ mg/mL for PDMS$_{65}$-*b*-PMOXA$_{14}$ and $5.8*10^{-3}$ mg/mL for PDMS$_{65}$-*b*-PMOXA$_{32}$, respectively (Figure 19). The CMC value of PDMS$_{65}$-*b*-PMOXA$_{32}$ is 5.8 times higher than that of PDMS$_{65}$-*b*-PMOXA$_{14}$ due to a longer PMOXA block in PDMS$_{65}$-*b*-PMOXA$_{32}$ than in PDMS$_{65}$-*b*-PMOXA$_{14}$. These CMC values are in the same range as reported for other ABPs ($0.87*10^{-3}$ mg/mL for PEG-ss-PCL,[8] $8.9*10^{-3}$ mg/mL for PEO-*b*-HPLys,[139] and $17*10^{-3}$ mg/mL for PEO-ss-PHMssET [140])

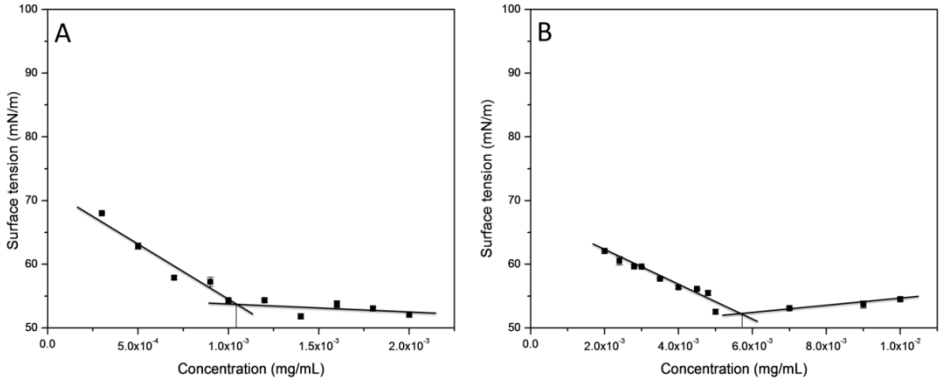

Figure 19. Surface tension experiments of (A) PDMS$_{65}$-*b*-PMOXA$_{14}$ and (B) PDMS$_{65}$-*b*-PMOXA$_{32}$ aqueous solution in different concentration.

2.2.2.2. Effect of preparation methods on the architectures of supramolecular assemblies of $PDMS_x$-*b*-$PMOXA_y$.

The method used for the preparation is one of the most important parameters that can influence the final architectures of self-assembled ABPs. Since the co-solvent, film rehydration, and electroformation methods are often used to prepare supramolecular assemblies of ABPs,[66,141] we investigated whether they affected the architecture of supramolecular assemblies of the model system $PDMS_{65}$-*b*-$PMOXA_{14}$. The film rehydration method involved dissolution of the copolymer (5 mg) in ethanol (2 mL) followed by slow evaporation of the solvent until a polymer film formed, which was then dried under high vacuum for another 2 h. Then, ddH_2O (1 mL) or buffer (1 mL) was added, and the mixture was stirred overnight at room temperature. The co-solvent method consisted of dissolution of copolymer (1 mg) in ethanol (50 µL), and adding it dropwise to 500 µL ddH_2O or 500 µL PBS, followed by dialysis against ddH_2O or PBS for 24 h with changes of ddH_2O or PBS three times. Giant unilamellar vesicles (GUVs) were prepared by the electroformation technique using the Nanion Vesicle Prep Pro setup (Nanion Technologies, Munich, Germany). 50 µL of the polymer solution (4 mg/mL in ethanol) were spread over an ITO-coated glass plate and evaporated in a vacuum chamber for at least one hour. With an O-ring, a chamber was formed around the polymer film, filled with 100 mM sucrose solution, and closed with a second ITO glass plate. GUVs were generated at 25 °C with a frequency of 3.0 Hz and amplitude of 2.5 V for three hours. For visualization, a few microliters of the GUV solution were stained with Bodipy 630/650, dropped into a microscopy chamber filled with 200 µL of buffer (20 mM Hepes, pH 7.4, 50 mM NaCl), and investigated at 20 °C using a confocal laser scanning microscope (Zeiss LSM 510-META/ConfoCor 2). Different assemblies were formed depending on the preparation method: the co-solvent method produced 20 nm diameter micelles (Figure 20A), whereas polymersomes with a 200 nm diameter were obtained by the film rehydration method (Figure 20B). The electroformation method induced the formation of giant polymersomes with diameters in the range 20 - 50 µm (Figure 20C).

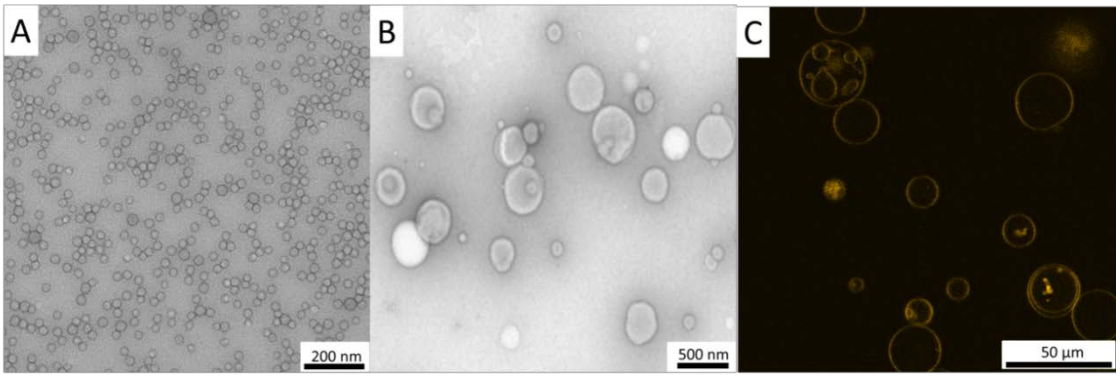

Figure 20. TEM micrographs of supramolecular assemblies of $PDMS_{65}$-*b*-$PMOXA_{14}$ produced by (A) co-solvent method, (B) film rehydration method and (C) LSM micrographs of supramolecular assemblies formed by electroformation technique.

2.2.2.3. Effect of initial copolymer concentration on the architecture of supramolecular assemblies of $PDMS_x$-*b*-$PMOXA_y$.

PDMS-*b*-PMOXA ABPs tend to form stable polymersomes by film rehydration and electroformation method. However, in order to further use them as nanoreactors, the electroformation method was not suitable, due to the very low utilization rate of copolymer to form the GUVs. As a result, we investigated the influence of the initial copolymer concentration from 0.1 mg/mL to 9 mg/mL on the supramolecular assembly architecture of $PDMS_{65}$-*b*-$PMOXA_{14}$ for this preparation method. The TEM results demonstrated that the initial concentration had no influence on the morphologies and diameters of the self-assemblies shown by DLS (Figure 21) and supported by TEM images (Figure 22).

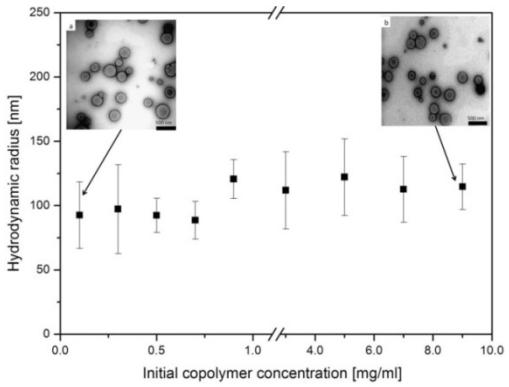

Figure 21. The influence of initial concentration of $PDMS_{65}$-*b*-$PMOXA_{14}$ on self-assembly behavior measured by DLS. Left and right insets show representative TEM for 0.1 and 9 mg/mL respectively.

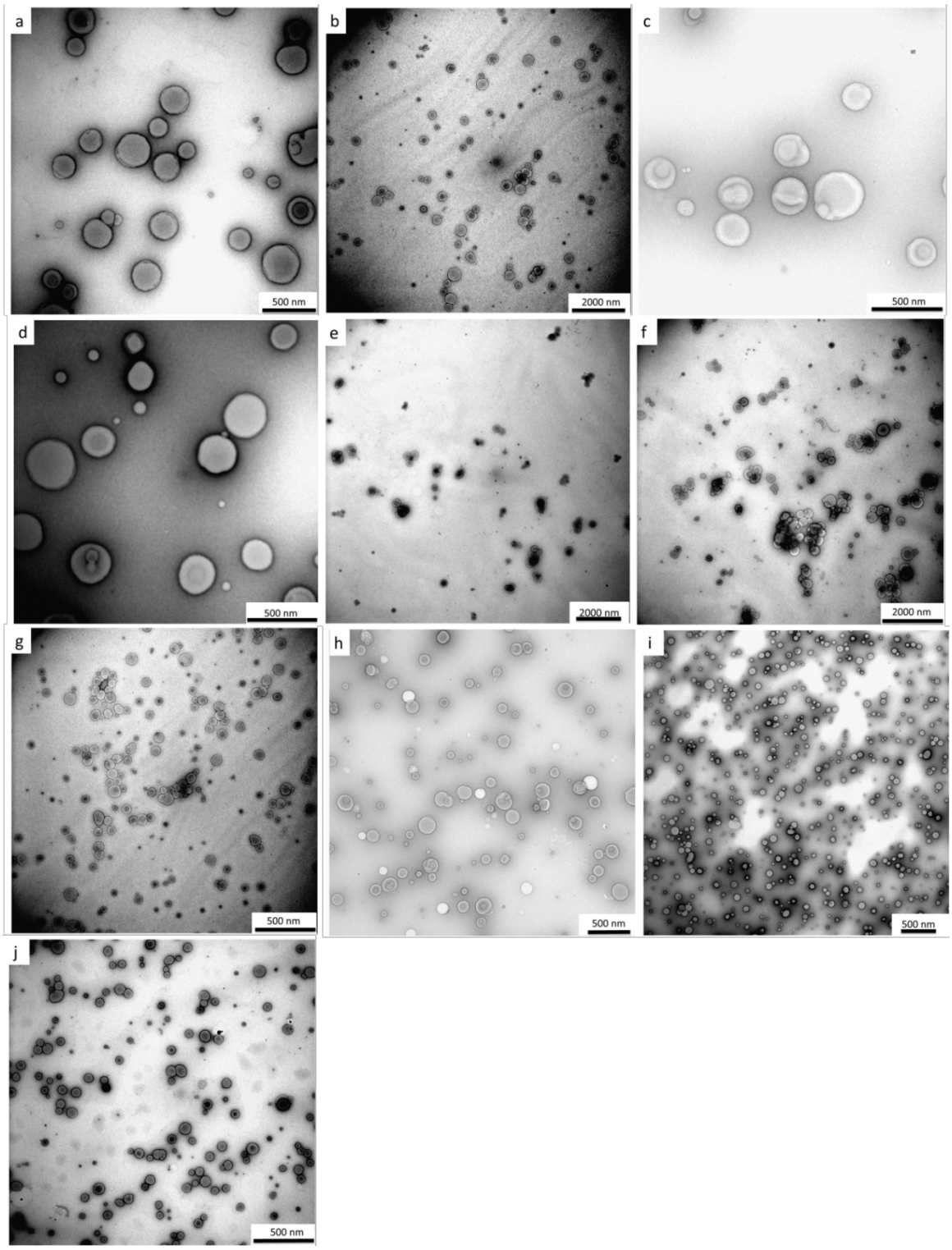

Figure 22. TEM images of morphologies formed by $PDMS_{65}$-*b*-$PMOXA_{14}$ with different initial concentration. a. 0.1 mg/mL; b. 0.3 mg/mL; c. 0.5 mg/mL; d. 0.7 mg/mL; e. 0.9 mg/mL; f. 1 mg/mL; g. 3 mg/mL; h. 5 mg/mL; i. 7 mg/mL; j. 9 mg/mL.

2.2.2.4. Effect of content of solution on the architectures of supramolecular assemblies of $PDMS_x$-*b*-$PMOXA_y$.

The self-assembly behavior of ABPs can also be influenced by the buffer composition, such as the presence of salts, pH, or traces of organic solvent.[52, 59] To investigate the effect of pH on the architectures of the supramolecular assemblies of $PDMS_{65}$-*b*-$PMOXA_{14}$ formed by the film rehydration method we used various buffers: tris/HCl (pH = 8.0), PBS (pH = 7.2) and acetate (pH = 5.0). As seen by a combination of TEM micrographs and DLS data, pH and salt type did not affect the self-assembled supramolecular structures leading to polymersomes with around 200 nm diameter in all buffer solutions. In addition, polymersomes exhibited storage stability of more than one month at room temperature in each buffer solution (Figure 23, 24, 25). We attributed this stability to the neutral hydrophilic block PMOXA, which acted as a protecting shell. [17, 142]

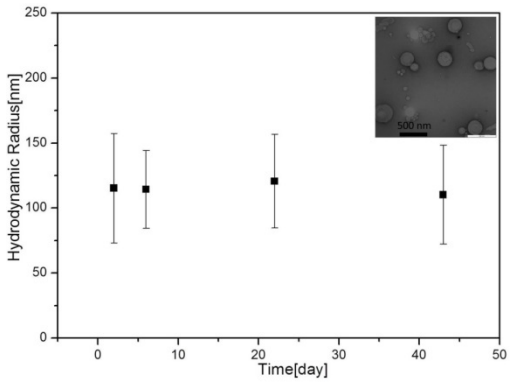

Figure 23. Hydrodynamic radius and stability of $PDMS_{65}$-*b*-$PMOXA_{14}$ polymersomes in Tris/HCl buffer (pH 8.0). Inset: representative TEM image of polymersomes.

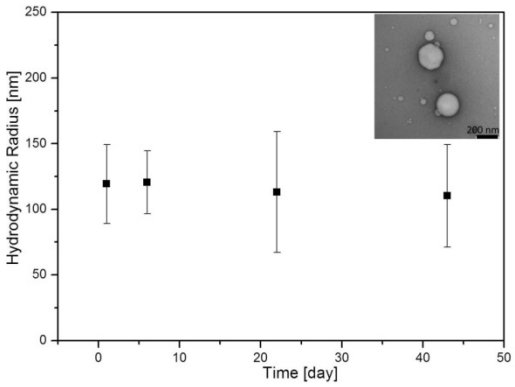

Figure 24. Hydrodynamic radius and stability of $PDMS_{65}$-*b*-$PMOXA_{14}$ polymersomes in PBS buffer (pH 7.2). Inset: representative TEM image of polymersomes.

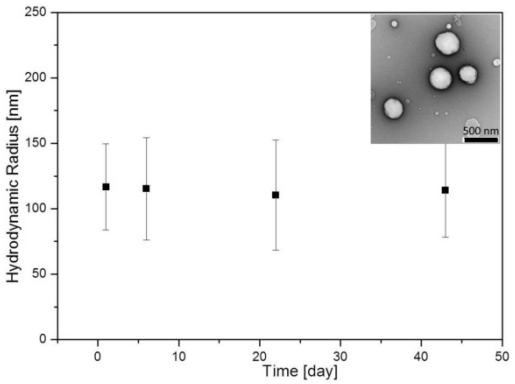

Figure 25. Hydrodynamic radius and stability of $PDMS_{65}$-*b*-$PMOXA_{14}$ polymersomes in acetate buffer (pH 5.0). Inset: representative TEM image of polymersomes.

2.2.3. Discussion and analysis of effect of f_{PMOXA} on the 3D assemblies of $PDMS_x$-*b*-$PMOXA_y$.

Three types of phase diagrams were obtained based on the M_n of PDMS and f_{PMOXA} values (Figure 26). For the ABP series with 5.0 kDa PDMS ($PDMS_{65}$), ABPs formed large polymer aggregates when the DP of PMOXA was less than 10 ($f_{PMOXA} \leq 16\%$). The presence of aggregates was due to the shorter length of hydrophilic PMOXA block not supporting the self-assembly structures.[131] However, upon filtration, spherical objects were present in the turbid solution of $PDMS_{65}$-*b*-$PMOXA_{10}$ (Figure 26A). The ratio ρ = 0.99 between the radii of gyration, R_g, obtained by SLS, and the hydrodynamic radius, R_H obtained by DLS indicates that these spherical objects are polymersomes (Table 3). An f_{PMOXA} value of 16% represented the lowest limitation for polymersomes formation.

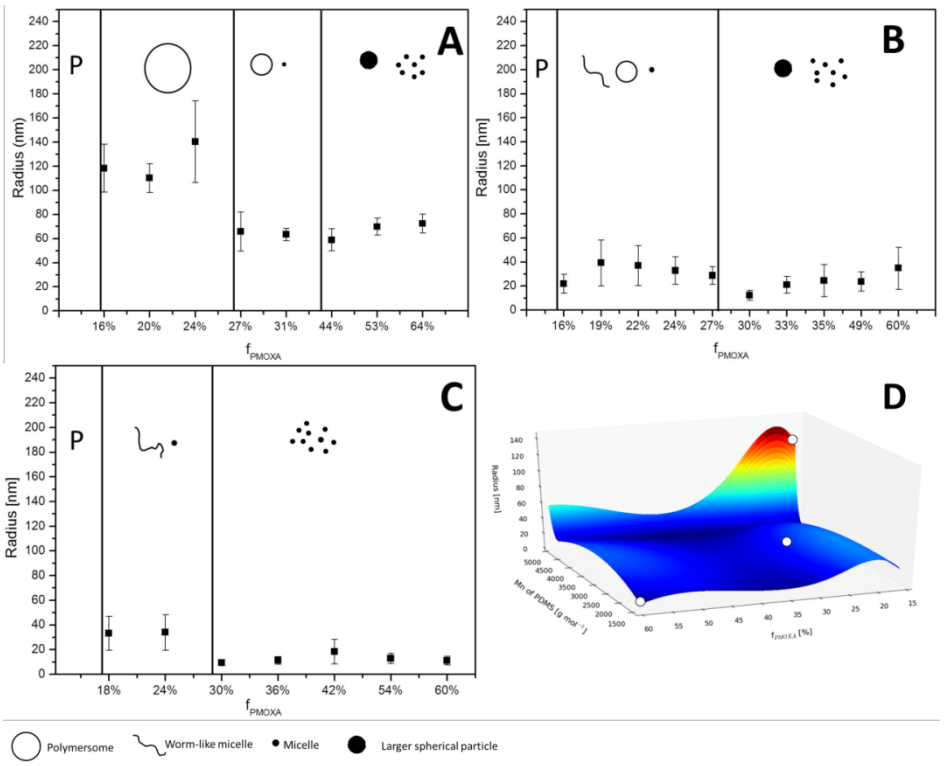

Figure 26. Phase diagrams for $PDMS_x$-*b*-$PMOXA_y$ based on the self-assembled structures and polymer chemical structure. A: $PDMS_{65}$-*b*-$PMOXA_{10\text{-}38}$, B: $PDMS_{39}$-*b*-$PMOXA_{6\text{-}22}$, C: $PDMS_{16}$-*b*-$PMOXA_{3\text{-}10}$, D: 3D phase diagram of $PDMS_{65}$-*b*-$PMOXA_{10\text{-}38}$, $PDMS_{39}$-*b*-$PMOXA_{6\text{-}22}$ and $PDMS_{16}$-*b*-$PMOXA_{3\text{-}10}$, the three points represent $PDMS_{65}$-*b*-$PMOXA_{10}$, $PDMS_{39}$-*b*-$PMOXA_{10}$ and $PDMS_{16}$-*b*-$PMOXA_{10}$.

By increasing f_{PMOXA} to 25%, polymersomes with radii ≥ 100 nm, and a very minor fraction of micelles were formed (Figure 26A and Figure 27b, c, d). The ρ values, namely the ratio of the radius of gyration divided by the hydrodynamic radius, of $PDMS_{65}$-*b*-$PMOXA_{12}$ and $PDMS_{65}$-*b*-$PMOXA_{14}$ with f_{PMOXA} of 16% and 19%, were 1.07 and 0.91 respectively, indicating the formation of hollow-sphere structures (Table 3).[143] A further increase in f_{PMOXA} from 25% to 44% induced a decrease of the polymersomes hydrodynamic radii to < 100 nm, but also resulted in increasing amount of micelles (Figure 26A and Figure 27e, f). The ρ value for $PDMS_{65}$-*b*-$PMOXA_{19}$ was determined as 0.94 (Table 3), thus proving the formation of polymersomes. Further increasing the f_{PMOXA} to 65% induced a change in the architecture of the supramolecular assemblies, and a mixture of small micelles and larger spherical particles with diameter around 70 nm was observed (Figure 27g, h, i). The aspect of cryo-TEM micrograph (Figure 30A, B) is similar to recently reported multicompartment micelles.[144,145] However, the resolution of cryo-TEM prevented a more detailed structural analysis. SAXS

was also applied to further characterize the spherical particles formed by $PDMS_{65}$-*b*-$PMOXA_{32}$ (Figure 31). SAXS data of the weakly scattering polymer solution were fitted by a form factor of spherical particles with almost homogenous density. Owing to the weak scattering, a more detailed analysis of the inner structure of the spherical object was not possible. Therefore, the combined cryo-TEM and SAXS was unable to provide more insight into the internal structure of spherical particles (Ø ~ 70 nm). In addition, a smaller ρ value for $PDMS_{65}$-*b*-$PMOXA_{32}$ of 0.82 (Table 3) supported the presence of soft spheres, but did not give information on the internal structure.[146]

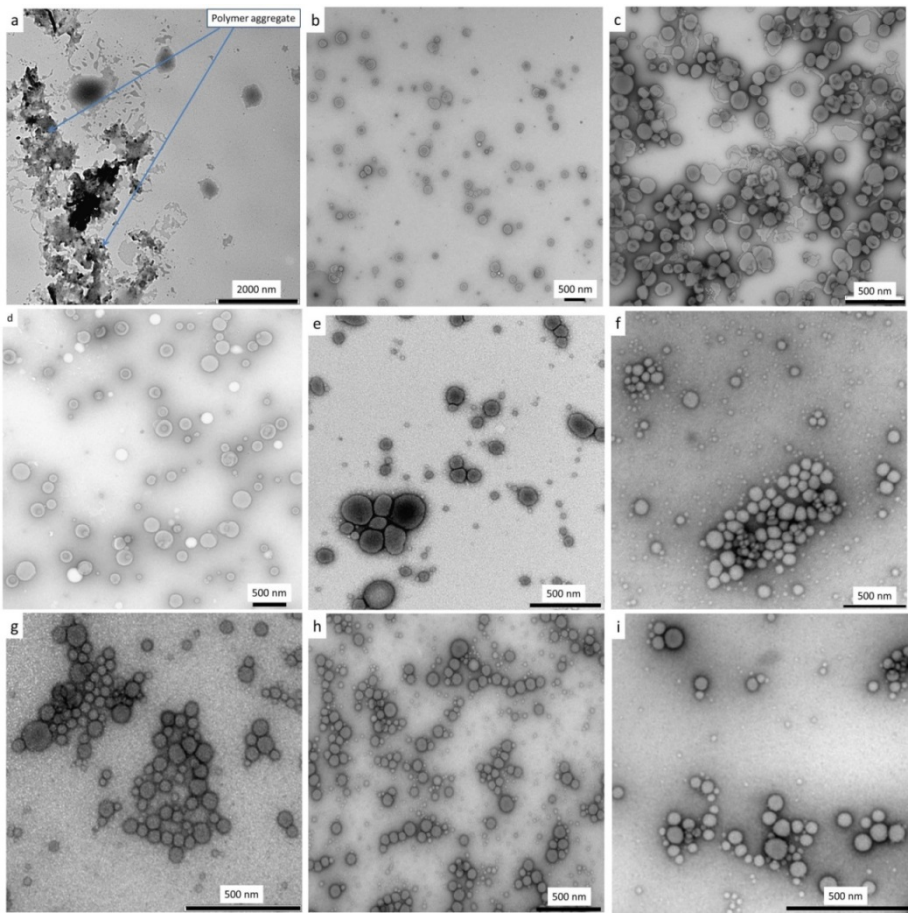

Figure 27. TEM images of self-assemblies formed by $PDMS_{65}$-*b*-$PMOXA_y$. a: $PDMS_{65}$-*b*-$PMOXA_{10}$ ($f_{PMOXA} = 16\%$); b: $PDMS_{65}$-*b*-$PMOXA_{10}$ ($f_{PMOXA} = 16\%$) after extrusion; c: $PDMS_{65}$-*b*-$PMOXA_{12}$ ($f_{PMOXA} = 20\%$); d: $PDMS_{65}$-*b*-$PMOXA_{14}$ ($f_{PMOXA} = 24\%$); e: $PDMS_{65}$-*b*-$PMOXA_{16}$ ($f_{PMOXA} = 27\%$); f: $PDMS_{65}$-*b*-$PMOXA_{19}$ ($f_{PMOXA} = 31\%$); g: $PDMS_{65}$-*b*-$PMOXA_{26}$ ($f_{PMOXA} = 44\%$); h: $PDMS_{65}$-*b*-$PMOXA_{32}$ ($f_{PMOXA} = 53\%$); i: $PDMS_{65}$-*b*-$PMOXA_{38}$ ($f_{PMOXA} = 64\%$).

The transition from polymersomes to micelles was observed for ABPs of poly(ethylene oxide)-*block*-poly(*N,N*-diethylaminoethyl-methacrylate) (PEO-*b*-PDEAMA), polystyrene-*b*-poly(4-vinylpyridine) (PS-*b*-P4VP), and polystyrene-dendrimer with increasing length of hydrophilic blocks.[131, 147, 148] In the PS-*b*-P4VP system, the polymersomes formed in the range of f_{P4VP} 13 - 24%, which was similar with the range of f_{PMOXA} for our PDMS-*b*-PMOXA polymer system. The f_{PMOXA} value mainly determined the shape of the polymeric chains, and therefore influenced the size and morphologies of the self-assembled structures.[149, 55] The formation of larger spherical particles is presumably caused by increasing the length of the hydrophilic PMOXA, which combines spherical micelles into larger spherical particles.

The phase diagram of PDMS-*b*-PMOXA with a 3.1 kDa PDMS ($PDMS_{39}$) shows a self-assembly behavior similar to that of the higher M_n PDMS (for f_{PMOXA} values > 25%). In contrast, this series of copolymers did not generate polymersomes with diameter > 100 nm for the whole domain of f_{PMOXA} values (Figure 26B). Polymer aggregates were present during the self-assembly of block copolymers with f_{PMOXA} < 19%, whereas increasing the f_{PMOXA} value to 27% induced the formation of mixtures of polymersomes with diameter < 100 nm, spherical micelles, and worm-like micelles. (Figure 26B and Figure 28a-e). A further increase in f_{PMOXA} to 60% resulted in the formation of a mixture of small micelles and larger spherical micelles. (Figure 26B, Figure 28f-g and Figure 30C).

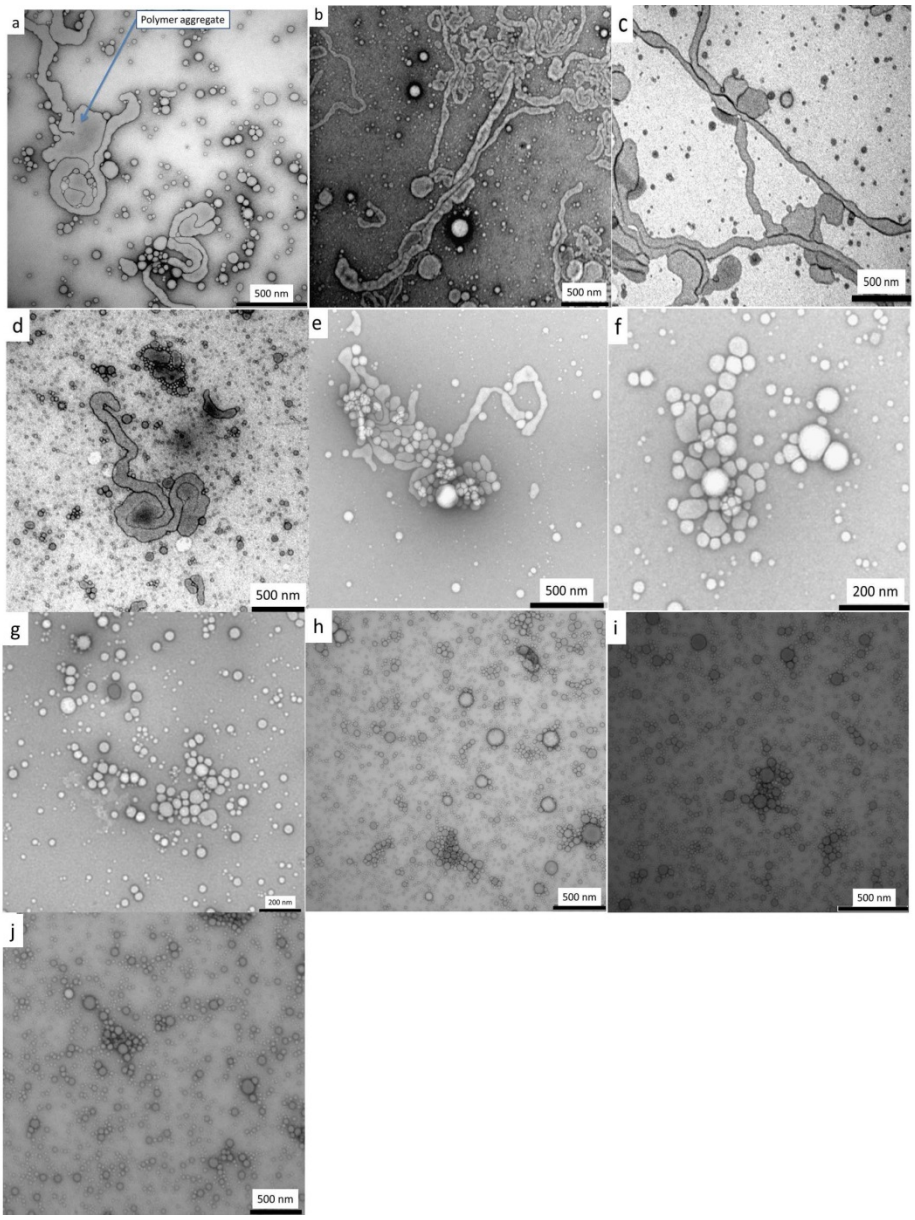

Figure 28. TEM images of self-assemblies formed by $PDMS_{39}$-*b*-$PMOXA_y$ a: $PDMS_{39}$-*b*-$PMOXA_6$ ($f_{PMOXA} = 16\%$); b: $PDMS_{39}$-*b*-$PMOXA_7$ ($f_{PMOXA} = 19\%$); c: $PDMS_{39}$-*b*-$PMOXA_8$ ($f_{PMOXA} = 22\%$); d: $PDMS_{39}$-*b*-$PMOXA_9$ ($f_{PMOXA} = 24\%$); e: $PDMS_{39}$-*b*-$PMOXA_{10}$ ($f_{PMOXA} = 27\%$); f: $PDMS_{39}$-*b*-$PMOXA_{11}$ ($f_{PMOXA} = 30\%$); g: $PDMS_{39}$-*b*-$PMOXA_{12}$ ($f_{PMOXA} = 33\%$); h: $PDMS_{39}$-*b*-$PMOXA_{13}$ ($f_{PMOXA} = 35\%$); i: $PDMS_{39}$-*b*-$PMOXA_{18}$ ($f_{PMOXA} = 49\%$); j: $PDMS_{39}$-*b*-$PMOXA_{22}$ ($f_{PMOXA} = 60\%$).

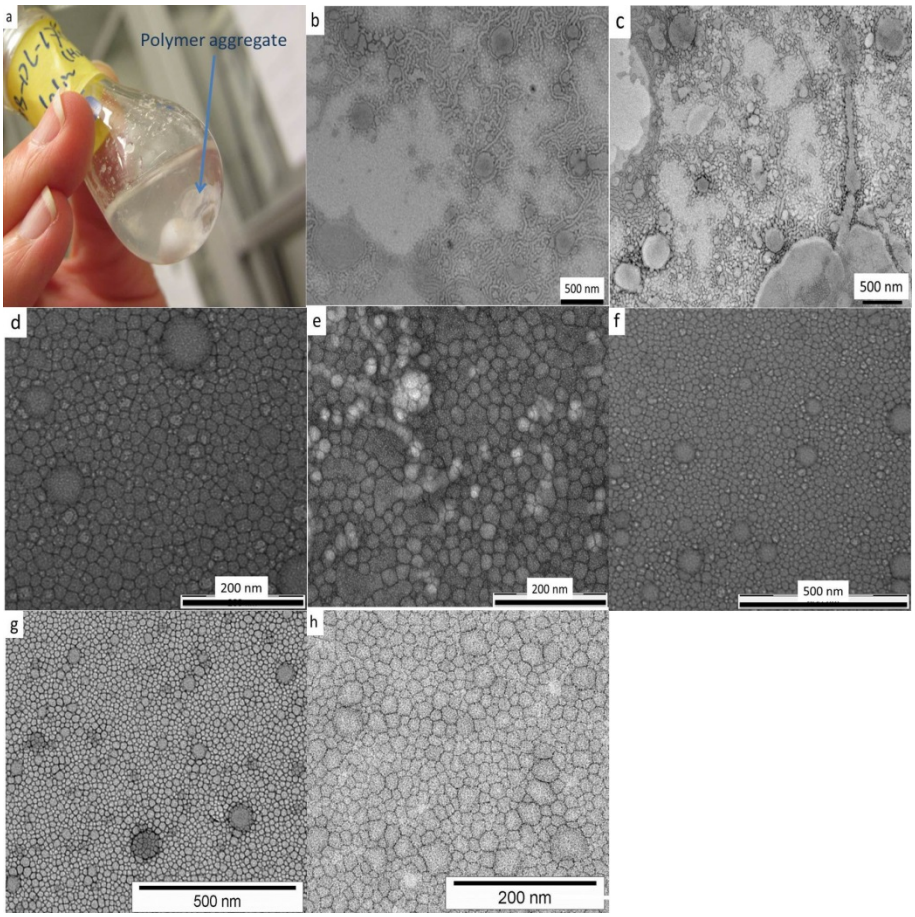

Figure 29. TEM images of self-assemblies formed by $PDMS_{16}$-*b*-$PMOXA_y$ a: $PDMS_{16}$-*b*-$PMOXA_2$ ($f_{PMOXA} = 12\%$); b: $PDMS_{16}$-*b*-$PMOXA_3$ ($f_{PMOXA} = 18\%$); c: $PDMS_{16}$-*b*-$PMOXA_4$ ($f_{PMOXA} = 24\%$); d: $PDMS_{16}$-*b*-$PMOXA_5$ ($f_{PMOXA} = 30\%$); e: $PDMS_{16}$-*b*-$PMOXA_6$ ($f_{PMOXA} = 36\%$); f: $PDMS_{16}$-*b*-$PMOXA_7$ ($f_{PMOXA} = 42\%$); g: $PDMS_{16}$-*b*-$PMOXA_9$ ($f_{PMOXA} = 54\%$); h: $PDMS_{16}$-*b*-$PMOXA_{10}$ ($f_{PMOXA} = 60\%$).

The phase diagram of PDMS-*b*-PMOXA with 1.4 kDa PDMS showed a completely different self-assembly behavior (Figure 26C). For f_{PMOXA} values < 18%, the copolymer was in an aggregate phase, while for f_{PMOXA} values in the range 24 - 30%, mixtures of worm-like and spherical micelles were obtained (SI, Figure 29b, c). For f_{PMOXA} values of 36 - 60%, only spherical micelles with radii around 20 nm were observed (Figure 26C and Figure 29d-h, Figure 30D), but with no clustering to generate larger spherical particles.

Analogous to increasing f_{PMOXA}, increases in f* values for different ABP series resulted in changes in the morphologies of the self-assembled structures from larger to smaller polymersomes, and finally to a mixture of small micelles and larger spherical particles for the first block copolymers series (f* 14 - 39%); from a mixture of polymersomes and wormlike

micelles and spherical micelles to the mixture of small micelles and larger spherical particles for the second block copolymers series (f* 14 - 37%); from wormlike micelles and spherical micelles to spherical micelles for the third block copolymers series (f* 11 - 38%).

In order to understand the role of the hydrophobic block in determining the architecture of the supramolecular assembles, we analyzed the behavior of $PDMS_{65}$-*b*-$PMOXA_{10}$, $PDMS_{39}$-*b*-$PMOXA_{10}$, and $PDMS_{16}$-*b*-$PMOXA_{10}$ copolymers (Figure 26D). With increasing hydrophobic block lengths, the copolymers self-assembled into morphologies starting with spherical micelles (for short PDMS length), progressing to a mixture of spherical micelles, wormlike micelles, and small polymersomes (for medium PDMS length), and finally to polymersomes (for long PDMS length). This self-assembly trend as a function of the hydrophobic domain was in agreement with previous reports for poly(ethyleneoxide)-*block*-poly(*γ*-methyl-*ε*-caprolactone) (PEO-*b*-PMCL), poly(ethyleneoxide)-*block*-poly(N,N-diethylaminoethylmethacrylate) (PEO-*b*-PDMAEMA), and poly(styrene-*block*-4-vinylpyridine) (PS-*b*-P4VP) ABPs.[131, 143, 147] In order to identify the combined effect of two molecular factors (f_{PMOXA} and the M_n of the hydrophobic domains), the self-assembly process was expressed as a 3D phase diagram (Figure 26D) for the mean hydrodynamic radii calculated for spherical objects formed by self-assembly in solution as function of M_n of the PDMS and f_{PMOXA}. There was a specific domain of molecular properties, which supported the formation of polymersomes with radii larger than 100 nm: a long hydrophobic block ($PDMS_{65}$) combined with small hydrophilic domains (f_{PMOXA} values < 25%). Polymersome formation was favored by adjusting the sizes of the hydrophobic and hydrophilic domains to produce f_{PMOXA} values of < 25%. Both molecular properties played a role in the self-assembly process of hollow sphere architecture. Once the M_n of hydrophobic block decreased, the hydrodynamic radius of spherical objects decreased dramatically, and micelles were the predominant architecture. Interestingly, the formation of micelles was independent on the hydrophilic domain (for the whole range of f_{PMOXA} we tested) once the hydrophobic block was small enough to prevent the formation of polymersomes. For both small hydrophilic and hydrophobic domains mixtures of micelles with small radii and worm-like structures were generated. This was due to the balance between the hydrophilic and hydrophobic domains not supporting the formation of membranes with curvature.[50]

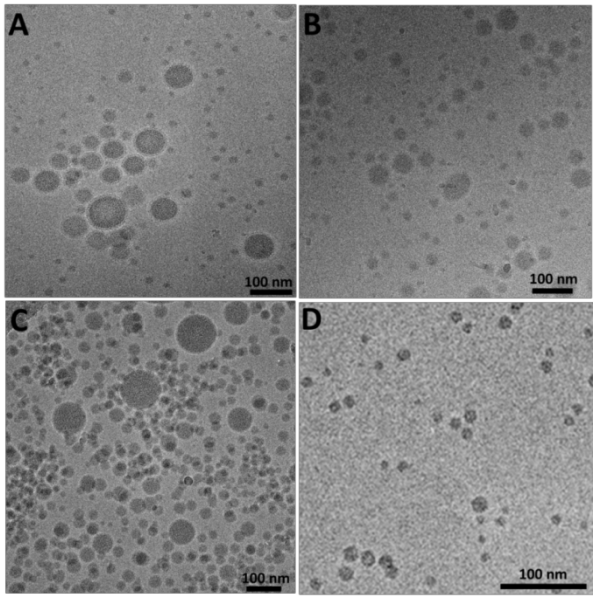

Figure 30. Cryo-TEM images of self-assemblies formed by $PDMS_x$-*b*-$PMOXA_y$. (A) $PDMS_{65}$-*b*-$PMOXA_{26}$ ($f_{PMOXA} = 44\%$), (B) $PDMS_{65}$-*b*-$PMOXA_{38}$ ($f_{PMOXA} = 64\%$), (C) $PDMS_{39}$-*b*-$PMOXA_{10\text{-}22}$ ($f_{PMOXA} = 30 - 60\%$) and (D) $PDMS_{16}$-*b*-$PMOXA_{5\text{-}10}$ ($f_{PMOXA} = 30 - 60\%$).

The self-assembly behavior is governed by two factors: the curvature of the membrane, which is formed during the self-assembly process, and the intrinsic water solubility of the copolymers. First, copolymers with lower f_{PMOXA} induce supramolecular assemblies with lower curvature values,[134] and are therefore expected to self-assemble into polymersomes. Due to the chain segregation occurring from hydrophobic-hydrophilic mismatch, the short hydrophilic block is in a stretched conformation, thereby reducing its contribution to an additional curvature effect.[50, 150] In contrast, copolymers with higher f_{PMOXA} values induce supramolecular assemblies with higher curvature. This prevents the formation of polymersomes and increases the probability of forming micellar structures, due to higher steric repulsion of hydrophilic chains tethered at the interface.[151]

Table 3. Gyration, hydrodynamic radii and resulting ρ-value ($\rho = \frac{Rg}{Rh}$) of self-assemblies of selected PDMS-*b*-PMOXA ABPs.

Sample	R_g (nm)	R_h (nm)	ρ ($\rho = \frac{Rg}{Rh}$)
$PDMS_{65}$-*b*-$PMOXA_{10}$	131	132	0.99
$PDMS_{65}$-*b*-$PMOXA_{12}$	132	123	1.07
$PDMS_{65}$-*b*-$PMOXA_{14}$	104	115	0.91
$PDMS_{65}$-*b*-$PMOXA_{19}$	71	75	0.94
$PDMS_{65}$-*b*-$PMOXA_{32}$	80	98	0.82

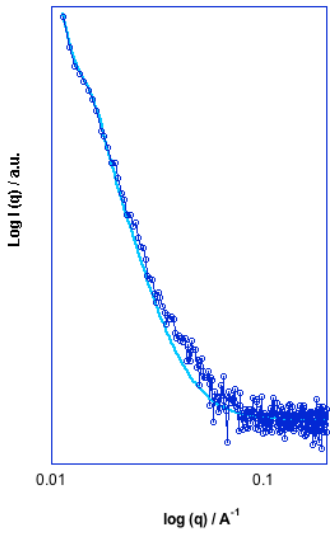

Figure 31. SAXS patterns (dark blue) and data fits (lighter blue) obtained for the respective $PDMS_{65}$-*b*-$PMOXA_{32}$ self-assemblies PBS buffer solution (5 mg/mL). The figure shows the scattering curve (dark blue) of "CH4-micelles" (intensity *I* vs momentum transfer *q*). The lighter blue line is a fit taking into account a spherical particle with a radius of *r* = (315 ± 68) Å. An additional scattering feature from 0.03 - 0.06 Å can be seen. However, it is difficult to interpret it in more detail.

In addition, Cryo-TEM micrographs indicated that the membrane thickness increased with increasing M_n of the hydrophobic block: $PDMS_{39}$-*b*-$PMOXA_8$ polymersomes had a thickness of 16.0 ± 1.1 nm, whilst $PDMS_{65}$-*b*-$PMOXA_{14}$ polymersomes had a thickness of 21.3 ± 1.2 nm (Figure 32A and 32B). The hydrophilic blocks did not contribute to the membrane thickness since they were in a fully hydrated state.

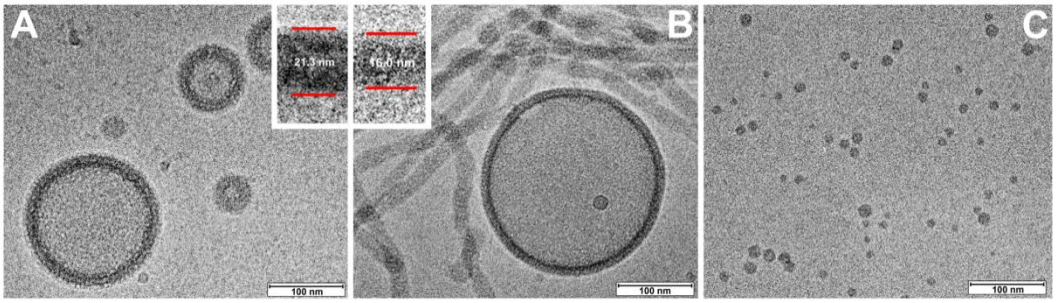

Figure 32. Cryo-TEM micrographs of different PDMS-*b*-PMOXA ABPs supramolecular assemblies formed by self-assembly of A: $PDMS_{65}$-*b*-$PMOXA_{14}$, B: $PDMS_{39}$-*b*-$PMOXA_{8}$, C: $PDMS_{16}$-*b*-$PMOXA_{7}$. Inset: enlarged view of the membrane thicknesses of $PDMS_{65}$-*b*-$PMOXA_{14}$ (A) and $PDMS_{39}$-*b*-$PMOXA_{8}$ (B).

2.2.4. Membrane properties of self-assemblies investigated by EPR

While there are various studies indicating that the thickness of polymersome membranes depends on the hydrophobic block, as shown by cryo-TEM micrographs,[152] until now, there have been no reports on the local flexibility and polarity of polymer membranes. However, these are essential factors to take into account when planning to insert membrane proteins into polymersome membranes for nanoreactor development. In order to get insight into membrane properties, we investigated the local microviscosity and micropolarity by spin probe EPR. While the local microviscosity is determined from the rotation correlation time of the spin probes, the micropolarity is determined from the hyperfine coupling, and the line-width of the spin probes inserted in the polymer membranes (in various depths). Micropolarity was estimated by measuring the ^{14}N hyperfine coupling constants of nitroxide spin probes, and the spectral linewidths (especially the high-field line), known to be strongly affected by the local polarity around the nitroxide moiety.[153] Although nitroxide spin probes are commonly employed to characterize self-assembly behavior in solution and the critical micellar concentration for various polymers, a careful selection of spin probes in terms of their compatibility with the size and structure of the polymer assembly is necessary. The selection aims to avoid the localization of the spin probe inside water pockets that will give no information about the self-assembling characteristics.[154-156] The hydrophobic spin probes 5 DSA and 16 DSA were chosen because they are large enough to avoid being trapped in small water pockets. In addition, they are expected to be compatible with the hydrophobic PDMS block and avoid electrostatic repulsions. First, the EPR spectra of both spin-probes

were analysed at temperatures ranging from 150 to 320 K in 0.1 M NaOH and 20% glycol to voids line-broadening caused by formation of water crystalline structure. They consist of an isotropic triplet, which indicates rapid tumbling, and hence no aggregation (Figure 33). The ^{14}N coupling constants a_N have values in the range 15.8 - 16.0 G, which are similar to those reported in the literature (15.8 G for 5 DSA in 0.1 M NaOH,[157] and 15.9 for 16 DSA in 0.1 M NaOH respectively).[158] At 100 K the EPR spectrum of 5 DSA in pure water is a broad singlet, due to phase separation and spin-spin interactions. Therefore the hyperfine coupling constant $2A_{zz}$ cannot be determined. However, addition of glycol (20%), resulted in an anisotropic EPR spectra typical of rigid molecules in a random orientation, and revealed $2A_{zz}$ values of 71.3 G for 5 DSA and 72.1 G for 16 DSA (Figure 33).

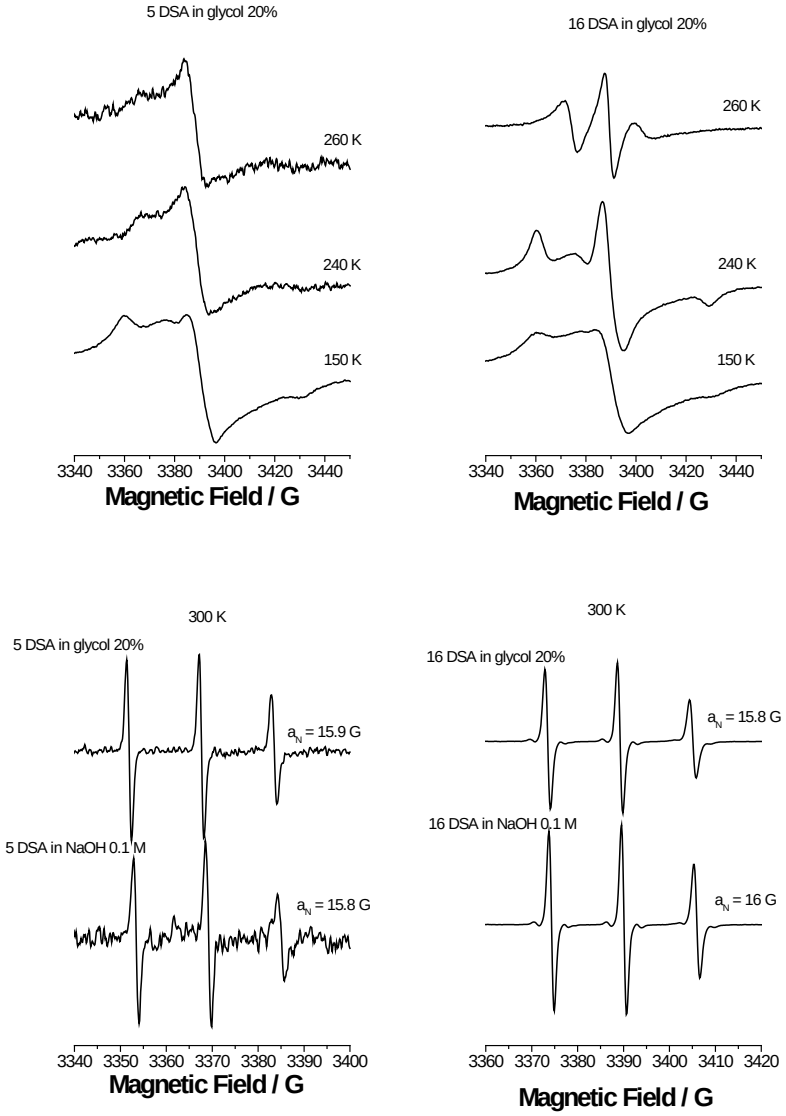

Figure 33. Rigid limit and fast motional spectra of 5 DSA and 16 DSA in 0.1 M NaOH (300 K) and 20% glycol at temperatures ranging from 150 K to 260 K and 300 K, respectively.

Second, the mobility of both nitroxide spin probes in $PDMS_{65}$-*b*-$PMOXA_y$ membranes was studied in two situations: i. when entrapped during the self-assembly process of polymersome formation, and ii. when added pre-assembled polymersomes.

i. The spectra of 5 DSA entrapped during the self-assembly process of $PDMS_{65}$-*b*-$PMOXA_{12}$, $PDMS_{65}$-*b*-$PMOXA_{14}$, $PDMS_{65}$-*b*-$PMOXA_{19}$ and $PDMS_{65}$-*b*-$PMOXA_{32}$ are significantly different from that of free 5 DSA (Figure 34A, 35). For $PDMS_{65}$-*b*-$PMOXA_{12}$, $PDMS_{65}$-*b*-$PMOXA_{14}$ and $PDMS_{65}$-*b*-$PMOXA_{32}$ at temperatures varying from 150 K to 290 K, a broad EPR signal, typical of slow-motion regime of aggregated spin-probes, was obtained. At higher temperatures, up to 320 K, both an isotropic triplet (characteristic for free rotation of the spin probe), and a broad signal (due to hindered rotation) are detected. The isotropic triplet has a_N values for $PDMS_{65}$-*b*-$PMOXA_{12}$ and $PDMS_{65}$-*b*-$PMOXA_{14}$ polymersomes of 15.3 G and 15.6 G, respectively, which differs slightly from that of free 5 DSA. a_N values for $PDMS_{65}$-*b*-$PMOXA_{32}$ assemblies are similar to that of the free 5 DSA (15.9 G). a_N values indicate that the spin-probes face two different environments which depend on the copolymer molecular properties. The smaller a_N values for $PDMS_{65}$-$PMOXA_{12}$ and $PDMS_{65}$-*b*-$PMOXA_{14}$ polymersomes are consistent with a more hydrophobic environment and indicate the insertion of the spin probe in the siloxane layer.[155] The similar a_N value $PDMS_{65}$-*b*-$PMOXA_{32}$ as that obtained in pure water indicates that the spin probe is located at the hydrophilic interface of the PMOXA layer. The broad EPR signal superposed on an isotropic triplet spectrum at the higher temperatures indicates either an aggregation of the spin probe due to its insertion into the spherical particles, or a limited rotation, due to a high density of the hydrophobic domain.

With $PDMS_{65}$-*b*-$PMOXA_{19}$ the behavior of the spin probe was completely different from that described above (Figure 35). In the temperature range 150 - 290 K, typical rigid limit spectra were obtained, with $2A_{zz}$ values of 70.2 G. Well resolved spectra, and smaller value for $2A_{zz}$ compared to that detected for 5 DSA in glycol (71.3 G) indicate that there is no aggregation, normally accompany of spin probe insertion in hydrophobic region of membranes. This indicates that the spin probe was located in the PDMS domain, which had a higher flexibility than that observed inside the copolymer micelles for the other three types of polymer. At 290 K a two component EPR spectrum was obtained: an anisotropic component with a value of 51 G for $2A_{zz}$, and a broad signal similar to that described in the literature for a spin probe in a lipid bilayer in the presence of sodium dodecyl sulfate.[159] The significantly smaller value

for $2A_{ZZ}$ is obtained because of motion that is not sufficient to produce an isotropic spectrum. The broad spectrum indicates slow tumbling of the spin probe because of the high viscosity of the microenviroment in the copolymer micelles. In addition, the presence of a two component signal suggests that the spin probe was incorporated into two different types of architectures (micelles and polymersomes membranes, or micelles and spherical particles). When the temperature was increased to 320 K, an isotropic triplet was observed superposed on a broad signal, similar to the spectra of the other copolymer polymersomes. For $PDMS_{65}$-*b*-$PMOXA_{19}$ polymersomes, the isotropic component was less well defined than for the other three copolymers. A rough estimation of a_N value of 15.7 G was estimated, which is higher than for $PDMS_{65}$-*b*-$PMOXA_{14}$ and smaller than that for $PDMS_{65}$-*b*-$PMOXA_{32}$. With increasing PMOXA length, the spin probe is located much closer to the PMOXA than the PDMS hydrophobic domain. This suggests that $PDMS_{65}$-*b*-$PMOXA_{32}$ diblock polymers arrange in hydrophilic-hydrophobic-hydrophilic membrane architecture. The use of 16 DSA as a spin-probe, which is known to penetrate much deeper into hydrophobic layers, indicated a similar behaviour involving insertion in the hydrophobic domain of polymer membrane of $PDMS_{65}$-*b*-$PMOXA_{12}$, but for $PDMS_{65}$-*b*-$PMOXA_{14}$ and $PDMS_{65}$-*b*-$PMOXA_{32}$ the spin-probe was only present at the interface between PDMS and PMOXA domains (Figure 35).

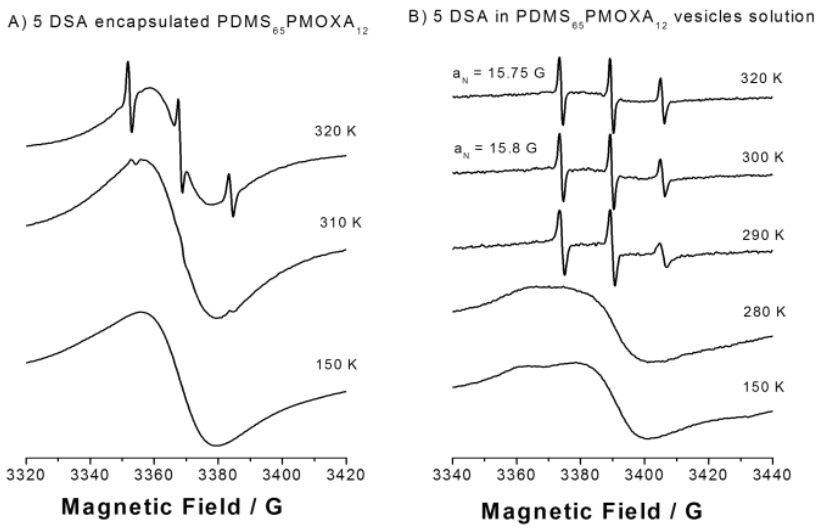

Figure 34. Temperature dependence of the EPR spectra of A) 5 DSA entrapped inside polymeric membrane during polymersome preparation by the film rehydration method and B) 5 DSA mixed with preformed polymersome solutions.

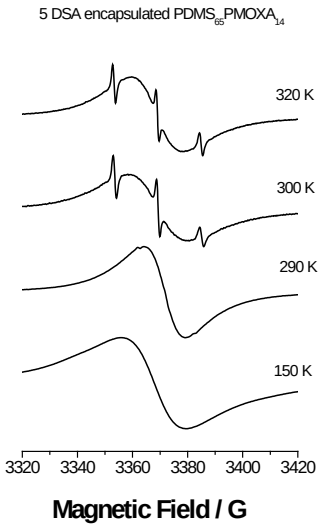
5 DSA encapsulated PDMS65PMOXA14
320 K
300 K
290 K
150 K
3320 3340 3360 3380 3400 3420
Magnetic Field / G

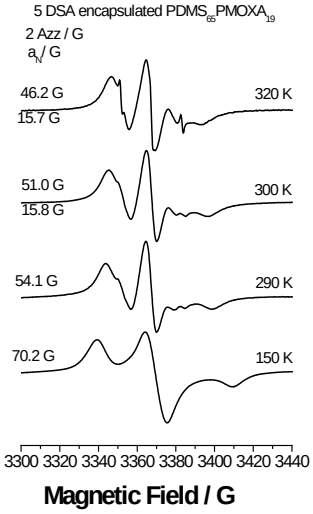
5 DSA encapsulated PDMS65PMOXA19
2 Azz / G
aN / G
46.2 G
15.7 G
320 K
51.0 G
15.8 G
300 K
54.1 G
290 K
70.2 G
150 K
3300 3320 3340 3360 3380 3400 3420 3440
Magnetic Field / G

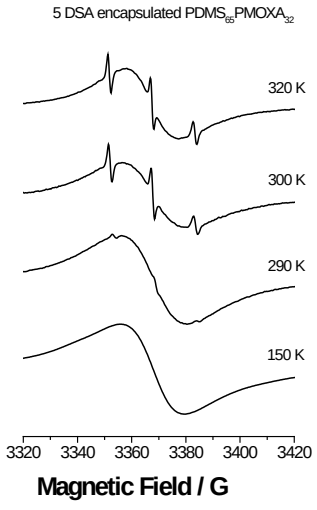
5 DSA encapsulated PDMS65PMOXA32
320 K
300 K
290 K
150 K
3320 3340 3360 3380 3400 3420
Magnetic Field / G

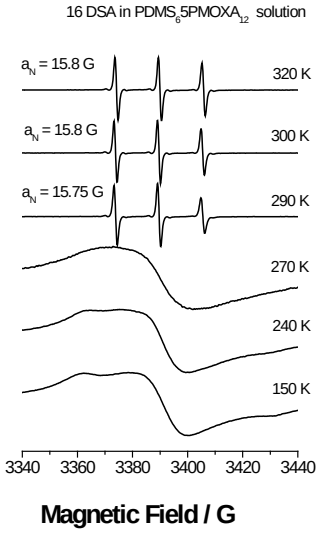
16 DSA in PDMS65PMOXA12 solution
aN = 15.8 G
320 K
aN = 15.8 G
300 K
aN = 15.75 G
290 K
270 K
240 K
150 K
3340 3360 3380 3400 3420 3440
Magnetic Field / G

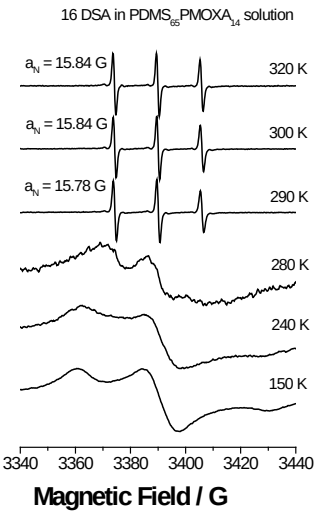
16 DSA in PDMS65PMOXA14 solution
aN = 15.84 G
320 K
aN = 15.84 G
300 K
aN = 15.78 G
290 K
280 K
240 K
150 K
3340 3360 3380 3400 3420 3440
Magnetic Field / G

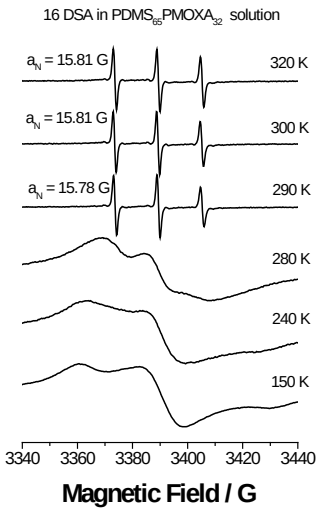
16 DSA in PDMS65PMOXA32 solution
aN = 15.81 G
320 K
aN = 15.81 G
300 K
aN = 15.78 G
290 K
280 K
240 K
150 K
3340 3360 3380 3400 3420 3440
Magnetic Field / G

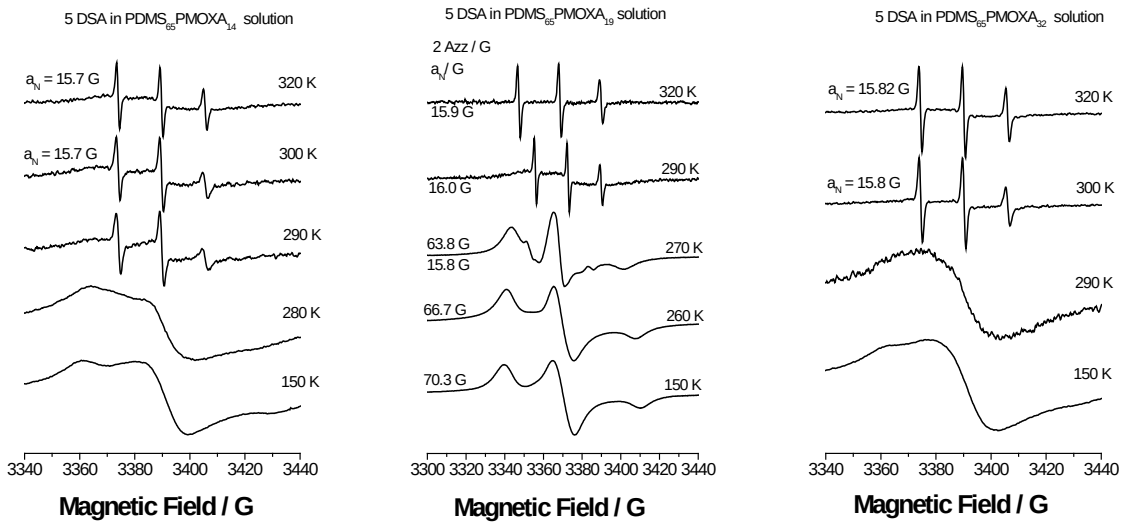

Figure 35. Rigid limit and fast motional spectra of 5 DSA encapsulated in $PDMS_{65}$-*b*-$PMOXA_{14}$, $PDMS_{65}$-*b*-$PMOXA_{19}$, $PDMS_{65}$-*b*-$PMOXA_{32}$ and 5 DSA and 16 DSA inserted in preformed structures.

ii. When the 5 DSA spin probe was mixed with preformed polymersome solutions, its behaviour was completely different from that observed for incorporation during the self-assembly process. At temperatures < 280 K anisotropic EPR spectra typical of slow motion were observed with solutions of $PDMS_{65}$-*b*-$PMOXA_{12}$, $PDMS_{65}$-*b*-$PMOXA_{14}$ and $PDMS_{65}$-*b*-$PMOXA_{32}$ (Figure 34B, 35). $2A_{zz}$ values calculated from spectra recorded at 150 K (69.2 G for both $PDMS_{65}$-*b*-$PMOXA_{12}$ and $PDMS_{65}$-*b*-$PMOXA_{14}$ polymersomes) are slightly smaller than those recorded in glycerol (71.2 G), indicating that the spin probe penetrated the hydrophobic domain. No resolved anisotropic components were observed for $PDMS_{65}$-*b*-$PMOXA_{32}$ spherical particles, probably due to the aggregation of the spin probe. For $PDMS_{65}$-*b*-$PMOXA_{19}$ polymersomes, the value of 70.3 G for $2A_{zz}$ at 150 K is much closer to the value for 5 DSA in glycerol, and suggests that the spin probe is present at the interface between the hydrophobic and hydrophilic domain, with the nitroxide group oriented toward the PMOXA domain. At 270 K the EPR spectrum contained three components; a rigid-limit spectrum, an isotropic spectrum, and a broad anisotropic spectrum. This complex EPR spectrum is probably the consequence of insertion of the spin probe into two different structures micelles and polymersomes/soft particles.

At temperature ≥ 290 K three-peak EPR spectra, characteristic of fast motional averaging were observed with all copolymer 3D assemblies. The a_N values of 15.7-15.9 G at 300 K

indicate localization of the nitroxide group of the spin probe in a hydrophilic, polar environment, similar to that in glycol. To get more insight into the dynamics of the spin probe inside the hydrophilic domain of particles, we calculated the rotation correlation time of 5 DSA spin probe.[160] The rotation correlation time of 0.77 ns for 5 DSA in NaOH (0.72 ns)[158] increased to 2.7 ns in $PDMS_{65}$-*b*-$PMOXA_{12}$ polymersomes, 1.18 ns in $PDMS_{65}$-*b*-$PMOXA_{14}$ polymersomes, 0.98 ns in $PDMS_{65}$-*b*-$PMOXA_{19}$ polymersomes, and 0.86 ns in $PDMS_{65}$-*b*-$PMOXA_{32}$ preformed structures. The increase of the rotation time and the broading of the high-field peak of EPR spectra, caused by an increase of the rotation correlation time, indicate the localization of the spin probe in a more viscous environment, such as the PMOXA hydrophilic layer ($PDMS_{65}$-*b*-$PMOXA_{12}$ to $PDMS_{65}$-*b*-$PMOXA_{19}$ polymersomes). These values are comparable to that determined for 5 DSA in 20% glycerol solution (1.2 ns), characterized by an increased viscosity. With $PDMS_{65}$-*b*-$PMOXA_{32}$, the rotation correlation time is closer to that in water (0.77 ns) and indicates that the spin probe is inserted into the PDMS domain with the nitroxide group oriented toward aqueous medium.

The rotation correlation time values decreasing to that for 5 DSA in water correlated with higher $2A_{zz}$ and a_N values, and shows that the PMOXA layer serves as a protecting layer for the hydrophobic domain. The effect is more pronounced with the increase of the hydrophilic block thickness.

EPR results provide a deep insight into the flexibility of polymer membranes with a hydrophobic dense domain of PDMS, which hinders the free rotation of the spin probe and induces broadening even at high temperatures, and the more elastic hydrophilic PMOXA layers. The different flexibility and the nature of each block induces a change in a_N values (related to the polarity), and of the slow motion broad signal of 5 DSA entrapped in membranes. The values of EPR parameters indicate clearly the spin probe insertion in the rigid PDMS layer. Moreover, the combination of a change in correlation time with no change in a_N value for 5 DSA in the presence of preformed $PDMS_{65}$-*b*-$PMOXA_{12}$, $PDMS_{65}$-*b*-$PMOXA_{14}$ and $PDMS_{65}$-*b*-$PMOXA_{32}$ 3D assemblies, clearly suggests insertion of the spin probe only inside the PMOXA hydrophilic layer. With an increase in the PMOXA block length from $PDMS_{65}$-*b*-$PMOXA_{12}$ to $PDMS_{65}$-*b*-$PMOXA_{19}$, and $PDMS_{65}$-*b*-$PMOXA_{32}$ the flexibility of the PMOXA hydrophilic domain was reduced, and induced localization of the spin probe in the PMOXA domain when added to the preformed 3D assemblies. Thus the hydrophilic region

exposed at the surface of preformed 3D assemblies acts as a protective layer for the hydrophobic (PDMS) domain, and accessibility to the PDMS domain decreases with increasing PMOXA domain length. The shielding property of PMOXA domain is important for developing medical applications, where interactions with biological molecules should be avoided (to increase the circulation times). This represents the first evidence of a significant change in the behavior of the membrane as a function of the hydrophilic block length. The difference between the hyperfine coupling of the spin probe entrapped during the formation of supramolecular assemblies from $PDMS_{65}$-*b*-$PMOXA_{12}$, $PDMS_{65}$-*b*-$PMOXA_{14}$, $PDMS_{65}$-*b*-$PMOXA_{19}$ to $PDMS_{65}$-*b*-$PMOXA_{32}$ can be explained by the transition from polymersomes, to mixtures of micelles and smaller polymersomes, and finally a mixture of micelles and spherical particles, in agreement with the LS and Cryo-TEM data.

Detergents are needed for extracting membrane proteins from biological membranes and mediating their solubility in aqueous solutions, and are important for their purification and stabilization.[161] Since channel proteins are usually inserted into polymersome membranes to render them permeable, the nanoreactor solutions might contain detergent molecules.[81] In order to check the influence of detergent on the permeability and fluidity of polymersomes membranes, the effect of adding 1% detergent (Triton X-100), a concentration reported to destroy lipid vesicles,[162] on the depth of penetration of the 5 DSA spin probe inside polymer membranes was investigated. The EPR parameters of 5 DSA obtained in polymersome solution after addition of detergent with those for 5 DSA in the presence of the detergent in distilled water were analysed. At 150 K the EPR spectra were anisotropic, with $2A_{zz}$ values of 66.2 G for free 5 DSA and 69.1-69.3 G for 5 DSA in preformed polymersome solutions of $PDMS_{65}$-*b*-$PMOXA_{12}$, $PDMS_{65}$-*b*-$PMOXA_{14}$ polymers, respectively (Figure. 36). At temperatures ranging from 290 K (Figure. 36) to 320 K, the EPR spectra of free 5 DSA in detergent showed broad three lines isotropic spectra with a_N of 14.8 G, which indicate a slow tumbling of the spin probe due to the higher viscosity inside detergent micelles.[159] When polymersomes were mixed with detergent, the spectra were similar to that described for a spin probe location in a lipid bilayer in the presence of sodium dodecyl sulfate (with an anisotropic broad component and an isotropic one).[163] Therefore in this situation, the nitroxide spin probe is immobilized and cannot freely rotate.

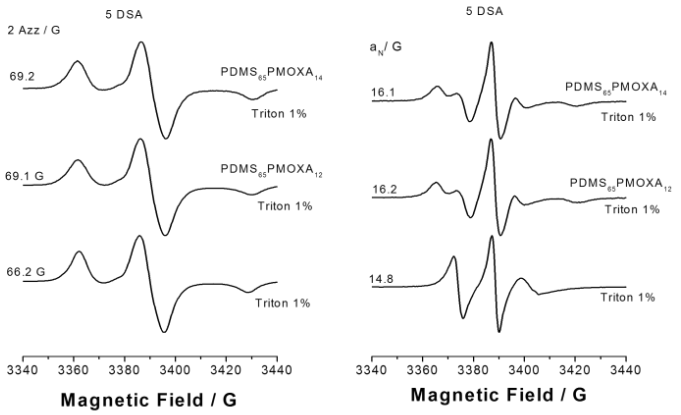

Figure 36. Rigid limit and fast motional EPR-spectra of 5 DSA inserted in preformed polymersomes treated with 1% Triton X-100, at 100 K, respectively 300 K.

At temperatures above 290 K, a_N values were 14.6 G for 5 DSA in detergent solution and 16.1-16.2 G in preformed polymersome solutions while in the presence of detergent. This indicates that the spin probe was inside the PDMS layer, which is denser and less flexible than the detergent. In addition, it suggests that the nitroxide group is oriented toward the PMOXA domain. The higher values of a_N exclude the possibility of nitroxide location in micelles, as observed for the $PDMS_{65}$-*b*-$PMOXA_{19}$ polymer. In order to check if the detergent treatment did not influence the integrity of the $PDMS_{65}$-*b*-$PMOXA_{12}$ and $PDMS_{65}$-*b*-$PMOXA_{14}$ membranes, TEM micrographs, and DLS analysis were performed as well. After Triton treatment, spherically shaped structures were preserved, as shown by TEM micrographs (Figure 37). In addition, R_h value of 120 nm for $PDMS_{65}$-*b*-$PMOXA_{12}$ and 112 nm for $PDMS_{65}$-*b*-$PMOXA_{14}$ polymersomes were determined by DLS.

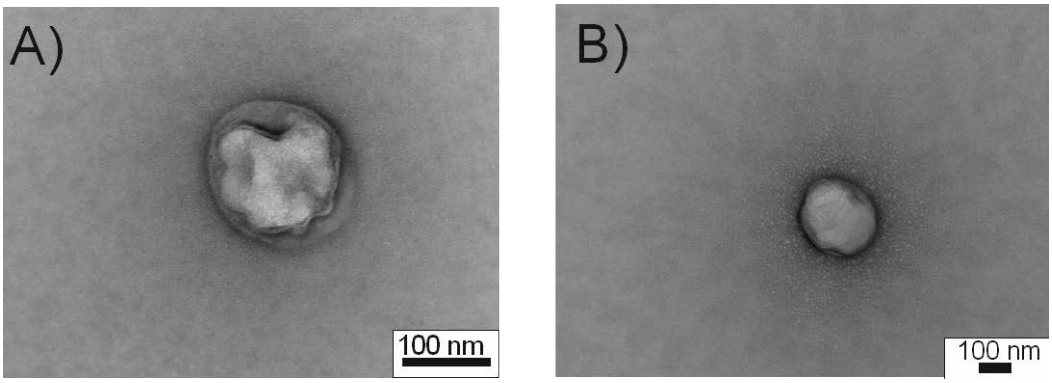

Figure 37. TEM micrographs of (A) $PDMS_{65}$-*b*-$PMOXA_{12}$ and (B) $PDMS_{65}$-*b*-$PMOXA_{14}$ polymersomes formed by self-assembly of block copolymers in PBS in presence of 5 DSA with 1% Triton X-100.

2.3. Conclusions

In order to study the influence of molecular parameters and preparation methods on the architecture of supramolecular assemblies generated by self-assembly, we have synthesized a library of three PDMS-*b*-PMOXA ABPs: $PDMS_{65}$-*b*-$PMOXA_{10-38}$, $PDMS_{39}$-*b*-$PMOXA_{6-22}$, and $PDMS_{16}$-*b*-$PMOXA_{3-10}$. 3D phase diagrams indicate that both PDMS and PMOXA domains play a key role in the self-assembly process in aqueous solutions. For a PDMS block length of 5.0 kDa, increasing the length of hydrophilic PMOXA blocks lead to changes in the self-assembly architectures from polymer aggregates, polymersomes with radii > 100 nm, to a mixture of micelles and polymersomes with radii around 50 nm, and finally to a mixture of micelles and spherical particles. In contrast, decreasing the M_n of hydrophobic domain prevented the formation of polymersomes but lead to micelles. For copolymers with the same hydrophilic/hydrophobic ratio, the M_n of the hydrophobic block representd the key factor that governed the self-assembly process. The polymersome membrane presents an internal structure with a dense hydrophobic middle layer, and two more elastic hydrophilic PMOXA inner and outer domains. The outer PMOXA layer has a protective role and prevented the penetration of spin probes into the polymersome membrane before detergent treatment even if they were highly hydrophobic. This protection effect was enhanced by increasing the PMOXA block, and indicated low membrane fluidity, which is known to correlate with a high mechanical stability. Destabilization of the membrane by 1% Triton X-100 resulted in easier penetration of the spin probes into the siloxane membrane. However, the structure of polymersomes was preserved upon treatment with detergent, and only the permeability of the membrane for hydrophobic cargo was increased. To the best of our knowledge, this represents the first characterization of the intrinsic aspects of a membrane generated by self-assembling amphiphilic block copolymers, and provides insight into the finer details regarding the flexibility and permeability of polymersomes. Thus, appropriate selection of molecular parameters and preparation method are essential for generating polymersomes with desired membrane properties, for example the insertion of membrane proteins or engineering artificial organelles.

3. Reduction responsive amphiphilic PMOXA-graft(ss)-PCL copolymers synthesis and their potential application as smart nanocarriers

Dalin Wu, Martin Nussbaumer, Adrian Najer, Cornelia Palivan, Wolfgang Meier*

The manuscript about this work is being writing and will be submitted.

3.1 Introduction

Nanocarriers are nanosized materials with a large surface area and inner volume, which can carry multiple small functional molecules encapsulated inside their cavity or on their surface.[164] Due to their ability of loading diverse molecules, nanocarriers are applied as potential platforms for disease therapy,[165, 166] imaging,[167] biomolecules detection,[168] sensoring,[169] and antimicrobial,[89, 170] application. Benefitting from the development of nanotechnology, nanocarriers are prepared by metal-organic frameworks,[167] functionalized inorganic nanoparticles,[109, 171] cavity proteins,[169] metal nanoparticles,[168, 172, 173]dendrimers,[174] and self-assemblies of ABPs.[95, 132, 175, 176] During the self-assembly process of ABPs in aqueous solution, hydrophobic molecules such as anticancer drugs[177] or quantum dots[80] can be encapsulated into the hydrophobic domains of the self-assembled structures. All of these factors have led self-assembled ABPs to be a leading field of nanocarriers research.[178, 179]

The functional properties of ABPs and their self-assembled nanostructures are determined by the nature and chemical properties of their constituting polymer blocks, and their functional groups.[70, 72, 180] By using polyesters such as PCL, PLA, or polypeptides as hydrophobic polymer building blocks, the formed nanostructures can be endowed with biodegradability and biocompatibility, which is favored if intended for bio-applications.[181-184] PEG and PMOXA two often used as hydrophilic polymer building blocks due to their biocompatibility as well as ability to limit interaction with blood components, toxicity, and first pass clearance.[17] Recently, results demonstrated that PMOXA show a higher chemical stability compared to PEG upon exposure to physiological conditions,[185] and PMOXA decorated liposomes also showed higher circulation time in blood.[186] The reason why PMOXA is less prone to degradation than PEG is that *N*-vicinal C−H bonds are less polarized than *O*-vicinal C−H bonds and are known to be stable against biological degradation.[187,188,189]

Self-assemblies of ABPs with stimuli-responsiveness: pH,[68] temperature,[190] irradiated light,[191] enzyme[127, 180] or a combination thereof,[192] are some of the most promising candidates in drug delivery research and application. Due to their stimuli-responsiveness, these self-assemblies can disassemble rapidly and release their encapsulated cargoes upon a desired stimuli in short time, which can maximize therapeutic efficiency.[71, 72] Responsive functional groups can be introduced on one of the ABP building blocks the side chains, or as the linker between hydrophobic and hydrophilic blocks.[193-195] Among all stimuli-responsive functional groups, redox-responsive disulfide bonds (-SS-) which can be cleaved by reducing agents,[196] are one of the most interesting responsive groups. This is due to the existence of a large difference in reducing potential between extracellular fluids and the intracellular environment (2-20 μM and 0.5-10 mM of glutathione (GSH) respectively).[197] Two examples of nanoparticles self-assembled by ABPs containing disulfide bonds are dextran-SS-poly(ε-caprolactone) and poly(ethylene glycol)-SS-poly(methacrylate). Both nanoparticles released their encapsulated cargoes upon addition of the reducing agents dithiothreitol (DTT) or GSH faster than dextran-*block*-poly(ε-caprolactone) and poly(ethylene glycol)-*block*-poly(methacrylate) without redox responsive disulfide groups.[77,140]

Here, we report the synthesis of a new reduction responsive ABP, poly(2-methyl-2oxazoline)-graft(ss)-poly(ε-caprolactone) (PMOXA-graft(ss)-PCL), composed of hydrophilic PMOXA and hydrophobic biodegradable PCL with grafted molecular structure, in which the reduction responsive disulfide group acts as the linker between PMOXA and PCL. The reason and motivation of synthesizing PMOXA-graft(ss)-PCL with graft molecular structure are i) the graft hydrophilic PMOXA can provide more steric hindrance on the surface of the self-assemblies which is possible to keep stable self-assembled nanostructure; ii) the polymers with graft structure are easier to obtained comparing with linear ones through two blocks coupling synthesis procedure. Technologies of ^{1}H NMR, FTIR, and GPC were applied to analyze the chemical structures and parameters of PMOXA-graft(ss)-PCL. DLS and TEM were used to characterized the self-assembly nanostructures of PMOXA-graft(ss)-PCL in aqueous solution. In addition, the reduction responsive behavior of self-assembled nanostructures is characterized by DLS, FCS, and TEM. Finally, cell culture experiments to determine the toxicity of PMOXA-graft(ss)-PCL and DOX loaded self-assembly nanostructures were carried out in Hela cells.

3.2. Results and discussion

3.2.1. Synthesis and characterization of PMOXA-SAc, PMOXA-SH, PCL-*co*-PBCL, PCL-*co*-PCCL and PMOXA-graft(ss)-PCL copolymer

3.2.1.1. The synthesis scheme of PMOXA-SAc, PMOXA-SH, PCL-*co*-PBCL, PCL-*co*-PCCL and PMOXA-graft(ss)-PCL copolymer

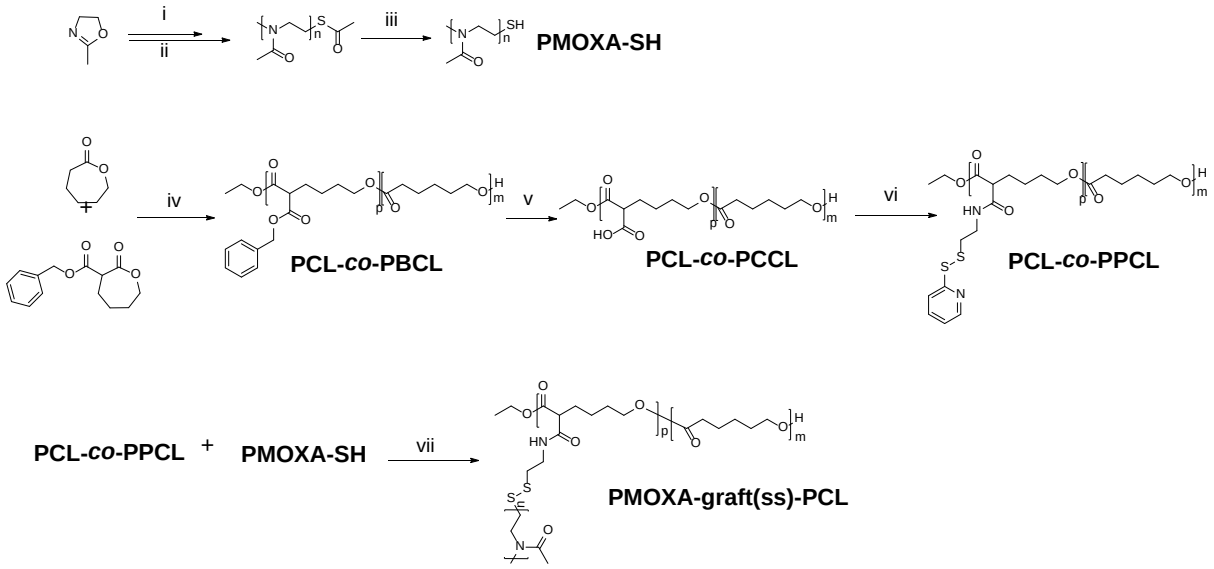

Scheme 9. The synthetic route for PMOXA-SH, PCL-*co*-PPCL and PMOXA-graft(ss)-PCL.[a]

[a] Reagents and conditions: (i) methyl trifluoromethanesulfonate, acetonitrile, 80 °C for 24 h under argon; (ii) potassium thioacetate, RT for 24 h under argon; (iii) triphenylphosphine, anhydrous MeOH, RT for 48 h under argon; (iv) anhydrous EtOH, Tin(II) 2-ethylhexanoate, toluene, 110 °C for 24 h under argon; (v) Pd/C (10 wt. %), ethyl acetate, RT for 42 h under hydrogen; (vi) 2-pyridylthiol cysteamine hydrochloride, N,N'-dicyclohexylcarbodiimide, 4-dimethylaminopyridine, triethylamine, DCM, RT for 60 h under argon; (vii) acetic acid, DMF, RT for 60 h under argon.

3.2.1.2. Characterization of PMOXA-SAc, PMOXA-SH, PCL-*co*-PBCL, PCL-*co*-PCCL and PMOXA-graft(ss)-PCL copolymer

Synthesis of thiolated PMOXA (PMOXA-SH). Living ROP of 2-methyl-2-oxazoline was initiated by methyl trifluoromethanesulfonate in acetonitrile.[17] After the polymerization, potassium thioacetate was used in excess to quench the polymerization and introduce the

thiolacetate group to synthesize PMOXA-SAc. The appearance of peaks at δ 2.34 ppm and 2.94 ppm were characteristic of the protons of methyl group of thiolacetate and methylene group next to the thiol group (Figure 38A).[198] The PMOXA-SAc was further reduced by PPh_3 in anhydrous MeOH to synthesize PMOXA-SH. The disappearance of the peaks at δ 2.34 ppm and appearance of a peak at δ 2.94 ppm demonstrated the successful reduction and synthesis of PMOXA-SH (Figure 38B). Fast operation was necessary to avoid disulfide formation between two thiol ended PMOXA polymers (PMOXA-SH) during the purification.

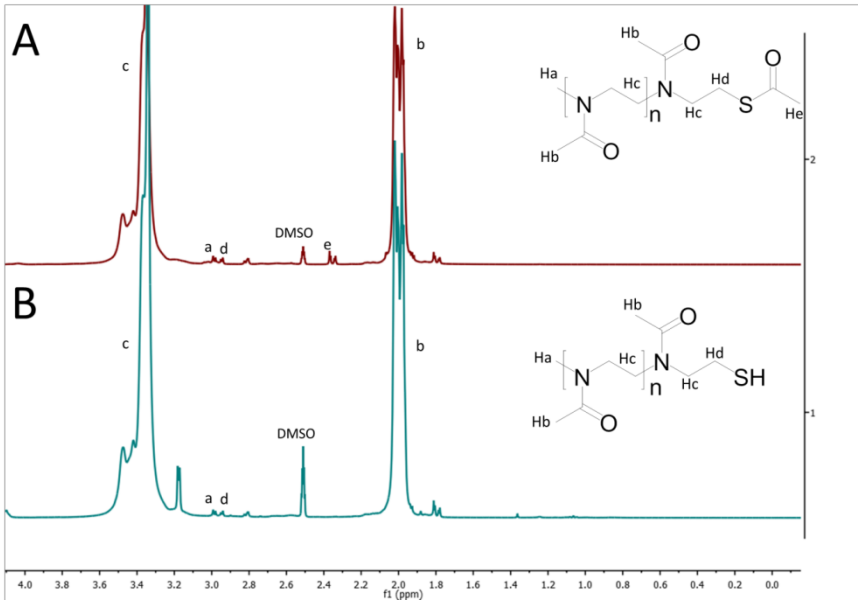

Figure 38. ^{1}H NMR spectrums of PMOXA-SAc (A) and PMOXA-SH (B) in d6-DMSO.

Synthesis of poly(ε-caprolactone)-*co*-poly(α-pyridyldisulfide-ε-caprolactone) (PCL-*co*-PPCL). The monomer α-benzyl carboxylate-ε-caprolactone was synthesized according to a previous published method.[199] Ethanol was used to initiate the copolymerization of monomer ε-caprolactone and α-benzyl carboxylate-ε-caprolactone with varying molar ratios in toluene at 110 °C to synthesize PCL-*co*-PBCL with a ≥ 80% yield. The appearance of the characteristic peaks of benzyl carboxylate group protons (δ 5.23 ppm and 7.26 ppm) demonstrated successful copolymerization of ε-caprolactone and α-benzyl carboxylate-ε-caprolactone (Figure 39A). The block ratio of PCL-*co*-PBCL could be calculated by integration of the signals at δ 5.23 ppm (methylene protons on benzyl in α-benzyl carboxylate-ε-caprolactone units), δ 3.33 ppm (methylene protons on ε-caprolactone units) and δ 1.19 ppm (the end methyl group). The corresponding M_ns determined from ^{1}H NMR of two PCL-*co*-PBCLs were 33.4 KDa and 15.2 KDa respectively, while the values determined by GPC were 40 KDa and 13 KDa

respectively (Table 4). The PDIs of the two synthesized PCL-*co*-PBCL samples were 1.5 and 2.0 (Table 4). Subsequently, PCL-*co*-PBCL was reduced by Pd/C at RT under hydrogen to synthesize the PCL-*co*-PCCL. The disappearance of the characteristic peaks for methylene protons near the phenyl ring at 5.23 ppm and for phenyl ring protons 7.26 ppm demonstrated that the benzyl alcohol was successfully eliminated (Figure 39B). Finally, the PCL-*co*-PCCL reacted with 2-pyridylthio cysteamine hydrochloride in the presence of DCC to yield PCL-*co*-PPCL. The appearance of new peaks corresponding to methylene protons next to the disulfide group (δ 2.93 ppm) and pyridyl group protons (δ 7.0-8.6 ppm) proved the successful esterification and synthesis of PCL-*co*-PPCL (Figure 39C).

Table 4. Chemical parameters of PCL-*co*-PBCLs and PMOXA-graft(ss)-PCLs .

Samples	^{1}H NMR			GPC		
	Block ratio	M_n (KDa)	$f_{(PMOXA)}$ [a]	M_w (KDa)	M_n (KDa)	PDI
PCL-*b*-PBCL 1	264:13	33.4		40000	19.4	2.0
PCL-*b*-PBCL 2	126:3	15.2		13000	19.7	1.50
PMOXA-graft(ss)-PCL2	88:238	34.8	22%	22300	13.0	1.72
PMOXA-graft(ss)-PCL1	127:165	30.0	36%	18400	13.3	1.38
PMOXA-graft(ss)-PCL3	135:135	27.0	43%	~	~	~

[a] The values of $f_{(PMOXA)}$ were calculated by the equation $\frac{Mn\ of\ PMOXA}{Mn\ of\ whole\ copolymer}$.

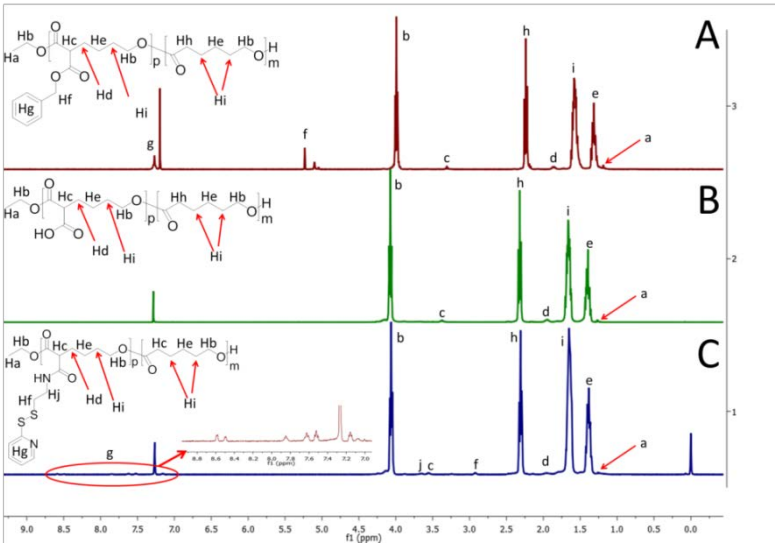

Figure 39. ^{1}H NMR spectra of PCL-*co*-PBCL (A), PCL-*co*-PCCL (B) and PCL-*co*-PPCL (C) in $CDCl_3$.

Synthesis of poly(2-methyl-2-oxazoline)-graft(ss)-poly(ε-caprolactone) (PMOXA-graft(ss)-PCL).

PMOXA-graft(ss)-PCL was synthesized through the thiol-disulfide exchange reaction between PMOXA-SH and PCL-PPCL in the presence of a catalytic amount of acetic acid.[8] The final product was purified by precipitation in cold MeOH in order to remove the unreacted PMOXA-SH. The appearance of the proton signals at f, g corresponding to PMOXA and c, d, e, f corresponding to PCL in Figure 40 proving the successful synthesis of PMOXA-graft(ss)-PCL. The h peak (δ 2.84 ppm) corresponds to the protons on the carbon next to the disulfide, which also proves the successful formation of the disulfide group. FT-IR was also used to characterize the chemical structure (Figure 41). The absorbance bands at 1720 cm^{-1} and 1160 cm^{-1} in the FT-IR spectrum of PMOXA-graft(ss)-PCL, assigned to stretching vibration of C=O and C-O on PCL, and 1724 cm^{-1} due to the stretching vibration of C=O on PMOXA, indicate the synthesis of PMOXA-graft(ss)-PCL copolymers. Three PMOXA-graft(ss)-PCL copolymers with different molecular structures and M_n varying from 27 KDa to 34.8 KDa and PMOXA fraction ($f_{(PMOXA)}$) from 22% to 43% were synthesized. The PDIs of the first two PMOXA-graft(ss)-PCLs were 1.72 and 1.38. However, due to insolubility of PMOXA-graft(ss)-PCL 3 in THF, the GPC could not be recorded (Table 4). The M_n of PMOXA-graft(ss)-PCL 1 and PMOXA-graft(ss)-PCL 2 determined from ^{1}H NMR were higher than from GPC, which might be caused by the grafted structure of the copolymer.[8]

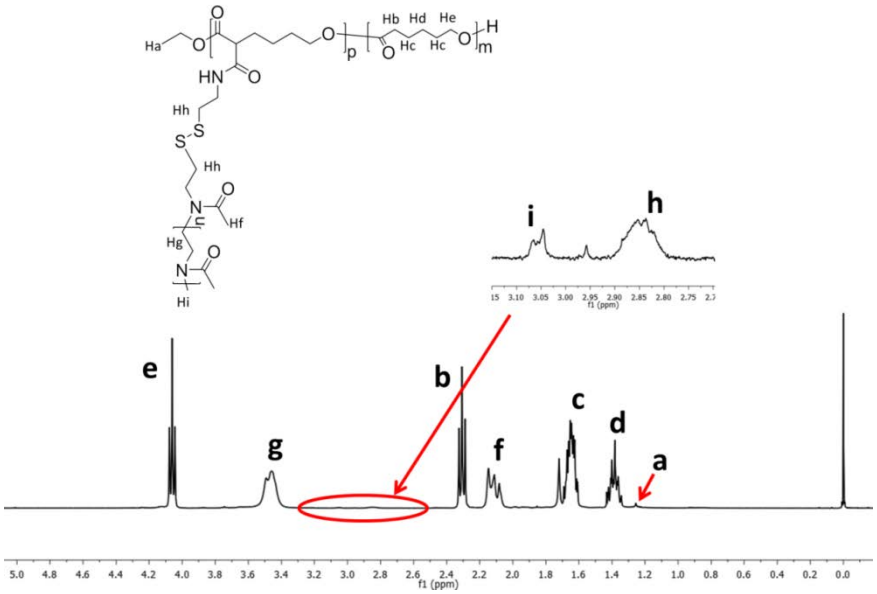

Figure 40. The ^{1}H NMR spectrum of PMOXA-graft(ss)-PCL copolymer in $CDCl_3$.

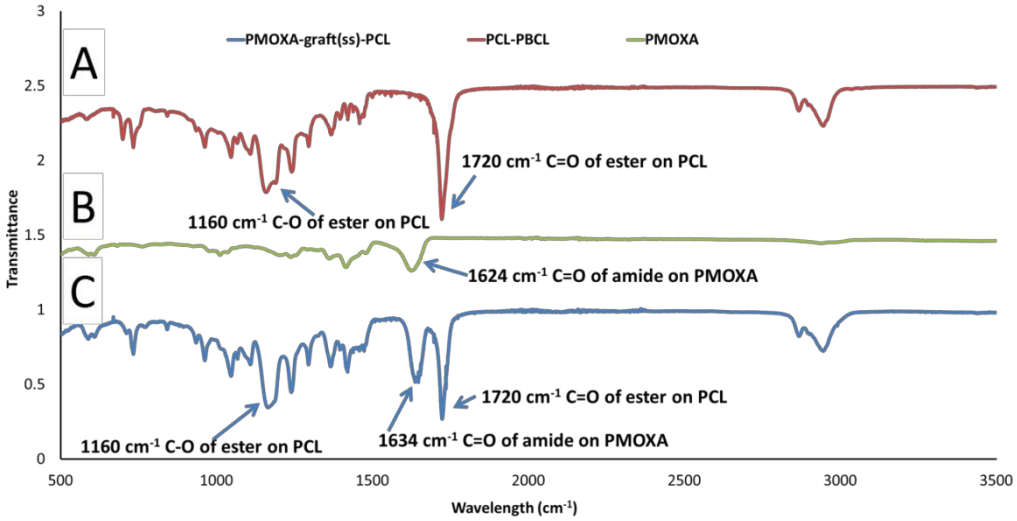

Figure 41. The FT-IR spectrums of PCL-*co*-PBCL (A), PMOXA-SH (B) and PMOXA-graft(ss)-PCL (C).

Synthesis of poly(2-methyl-2-oxazoline)-*block*-poly(ε-caprolactone) (PMOXA-*b*-PCL)

PMOXA-OH with M_n 7650 (70 mg) was first dissolved into freshly distilled ε-caprolactone (2 mL). After Tin(II) 2-ethylhexanoate (3 µL) was added, the reaction was carried out at 110 °C for 30 min. After cooling down the reaction mixture to RT, PMOXA-*b*-PCL was dissolved in DCM and precipitated twice into diethyl ether in order to purify the final product. PMOXA-*b*-PCL is being used as a control ABP. The peaks of H_a and H_b corresponding to PMOXA and H_c, H_d, H_e and H_f corresponding to PCL ^{1}H NMR spectrum in Figure 42 demonstrated the right structures of PMOXA-*b*-PCL.

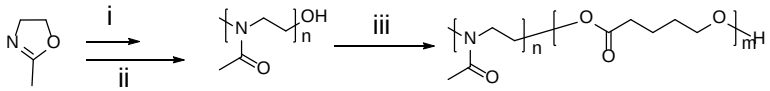

Scheme 9. The synthetic route for PMOXA-*b*-PCL.[a]

[a] Reagents and conditions: 1. methyl trifluoromethanesulfonate, acetonitrile, 80 °C for 24 h under argon; 2. KOH/MeOH solution (0.5 M), RT for 24 h; 3. ε-caprolactone, Tin(II) 2-ethylhexanoate, 110 °C for 0.5 h under argon.

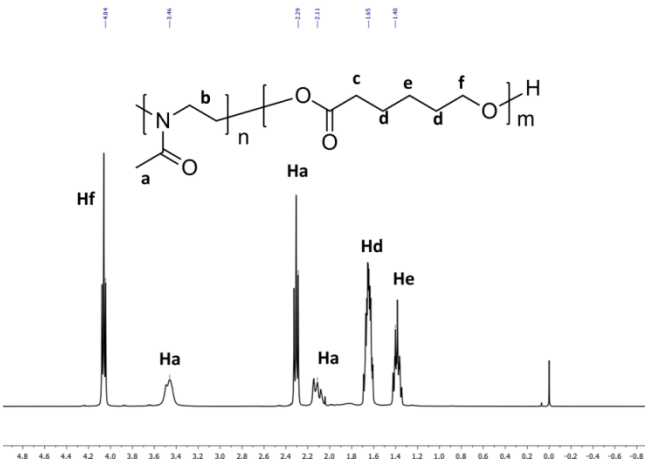

Figure 42. The ^{1}H NMR spectrum of PMOXA-*b*-PCL in $CDCl_3$.

3.2.2. Preparation and characterization of PMOXA-graft(ss)-PCL self-assemblies.

PMOXA-graft(ss)-PCL self-assemblies of were prepared by the solvent exchange method.[144] The diameters of the self-assemblies ranged from 27 nm to 51 nm with a narrow PDI of 0.09-0.18 according to DLS measurements (Figure 43D). Interestingly, the average diameter of self-assemblies decreased with the increase of hydrophilic PMOXA content from 22% to 43% (Figure 43D). The decrease can be attributed to a higher interfacial curvature value corresponding to the larger hydrophilic block size. The smaller diameter of self-assembled nanostructures is correlated with a higher interfacial curvature values.[50, 65] From the TEM images and DLS results, we can conclude that the self-assemblies are nanoparticles. The CMC was measured using pyrene as a fluorescence probe in PBS buffer.[200-202] CMC values of these three PMOXA-graft(ss)-PCL samples were between $0.05*10^{-3}$ - $0.29*10^{-3}$ mg/mL (Figure 44). In addition, the CMC values increased with the increasing content of hydrophilic PMOXA ($f_{(PMOXA)}$), which was caused by the enhancement of its hydrophilic properties.[61]

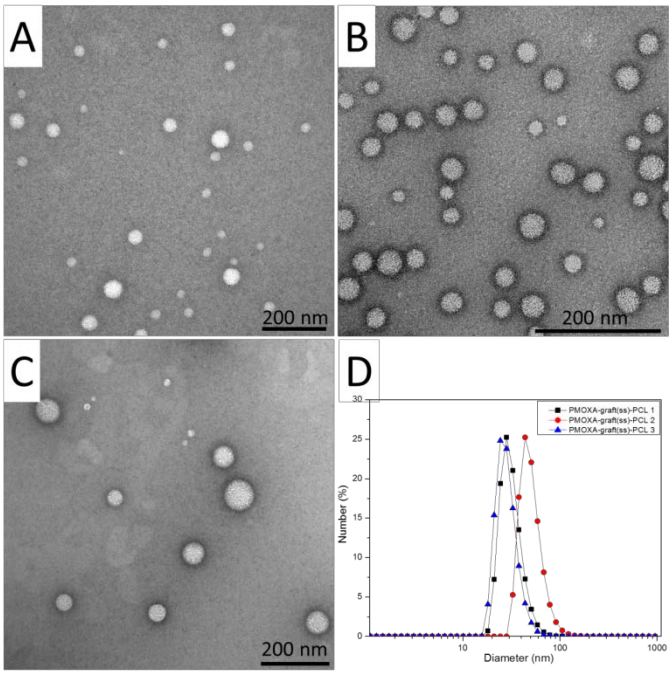

Figure 43. Morphologies of nanoparticles formed by PMOXA-graft(ss)-PCLs imaged by TEM and diameters measured by DLS. (A) Nanoparticles formed by PMOXA-graft(SS)-PCL 1; (B) nanoparticles formed by PMOXA-graft(SS)-PCL 2; (C) nanoparticles formed by PMOXA-graft(SS)-PCL 3; (D) diameters and distribution of nanoparticles measured by DLS.

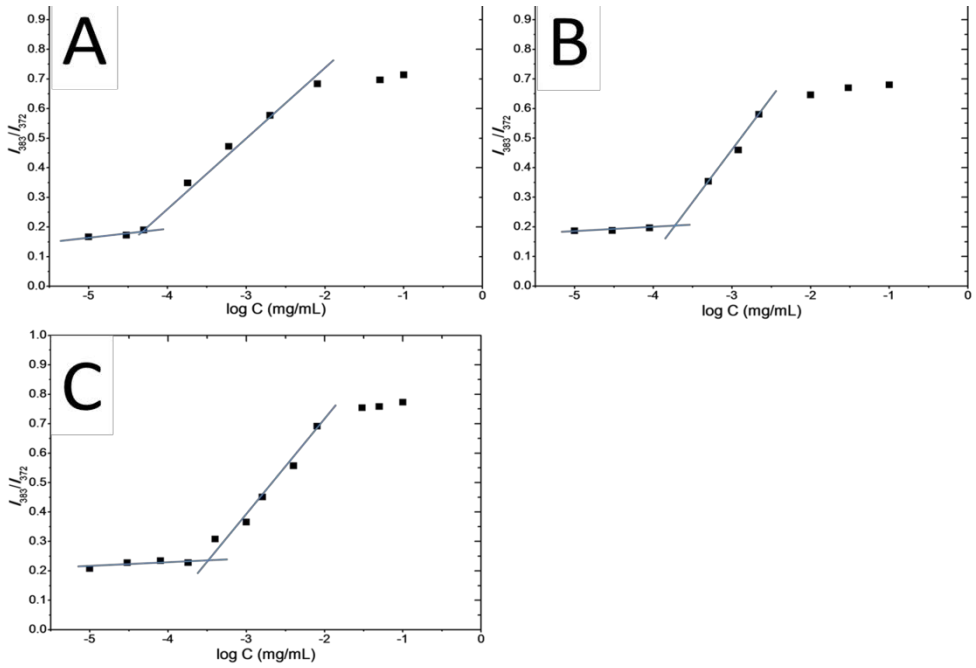

Figure 44. The fluorescence intensity ratio I_{383}/I_{372} of pyrene as a function of PMOXA-graft()ss)-PCL copolymers concentration. The intersection is the value of CMC. (A) PMOXA-graft(ss)-PCL 2; (B) PMOXA-graft(ss)-PCL 1 and (C) PMOXA-graft(ss)-PCL 3.

3.2.3. Reduction responsive properties of PMOXA-graft(ss)-PCLs and their self-assemblies.

DLS was used to investigate the reductive properties of PMOXA-graft(ss)-PCL 1 self-assembled nanoparticles addition of the reducing agent DTT (10 mM) in PBS. DLS demonstrated by that 13 minutes after adding DTT, the diameter of the nanoparticles changed from 32 nm to 85 nm. After 47 minutes, the diameter of nanoparticle increased to 2274 nm yielding a very turbid solution (figure 45 and Figure 46B). After 4 h, only white, macroscopic aggregates were observed (Figure 46C).

After filtering and washing the precipitate with MeOH, ^{1}H NMR spectrum was recorded showing only the proton signals characteristic of PCL – no peaks from the hydrophilic PMOXA were found – proving that the white precipitate was only hydrophobic PCL (Figure 47). These results clearly indicated that disulfide between PMOXA and PCL was reduced by DTT and it led to the disintegration of the nanoparticles. Without DTT, the nanoparticles were stable for 24 h without changing their diameter and PDI (Figure 45). Additionally, TEM results proved the nanoparticle structure is stable at 37 °C for 48 h. However, in presence of DTT, no nanoparticles can be identified in TEM images (Figure 48B).

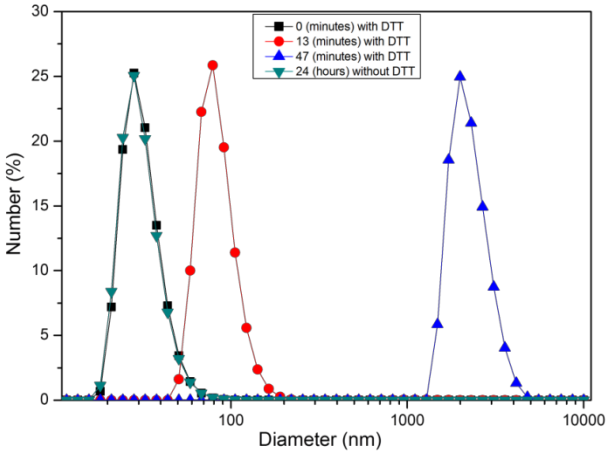

Figure 45. Changes in the diameter of nanoparticles formed by PMOXA-graft(SS)-PCL 1 in response to 10 mM DTT over time measured by DLS.

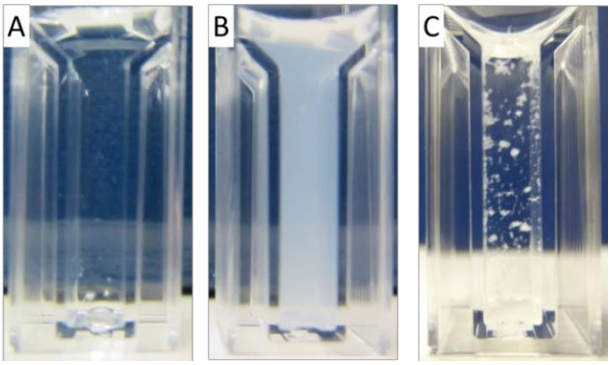

Figure 46. Digital imagines of nanoparticle solutions formed by PMOXA-graft(ss)-PCL 1 (1mg/mL) after DTT (final concentration 10 mM) treatment. (A) 13 minutes after DTT was added; (B) 47 minutes after DTT was added and (C) 4 h after DTT was added.

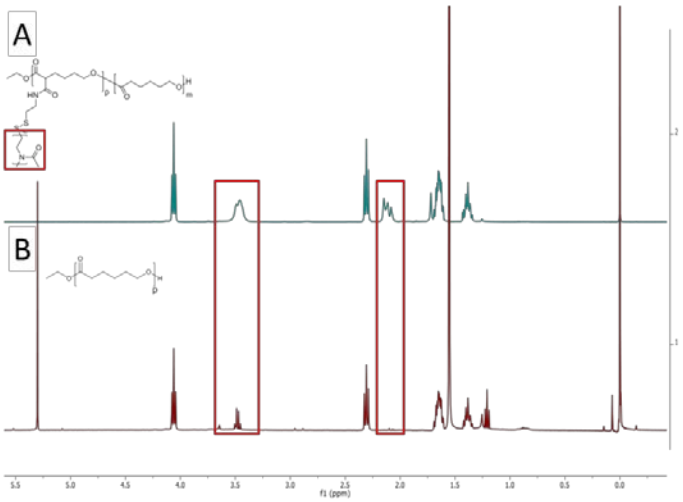

Figure 47. The ^{1}H NMR spectrums: (A) PMOXA-graft(ss)-PCL 1; (B) the white precipitation in the nanoparticles solution after being treated with DTT (10 mM).

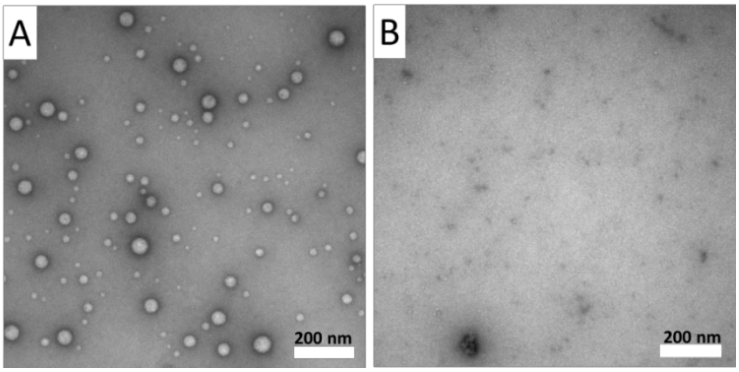

Figure 48. (A) TEM image of PMOXA-graft(ss)-PCL 1 nanoparticles in PBS at 37 °C for 48 h. (B) TEM image of PMOXA-graft(ss)-PCL 1 nanoparticles in PBS containing DTT (10 mM) at 37 °C for 48 h.

3.2.4. Triggered release of hydrophobic molecules from reduction responsive nanoparticles

Fluorescence correlation spectroscopy (FCS) was used to follow the disintegration of reduction responsive nanoparticles and the release of a model hydrophobic dye. By following the diffusion times of fluorescent molecules it is possible to determine whether the dye is encapsulated or freely diffusing. Therefore, a stable hydrophobic fluorophore (BODIPY 630) was encapsulated into nanoparticles formed by PMOXA-graft(ss)-PCL and PMOXA-*b*-PCL and time series of FCS curves were recorded in the presence or absence of the reducing agent DTT (Figure 49A). In case of reduction responsive nanoparticles (PMOXA-graft(ss)-PCL) in the presence of DTT, the free dye population increased over time, reaching more than 90% free dye after 1.5 h. Without DTT or nanoparticles without reduction responsibility (PMOXA-*b*-PCL), the additional DTT did not result in any free dye population in the FCS curves after 24 h. By determining hydrodynamic diameters of nanoparticles from nanoparticle diffusion time in Figure 49B, the changing bigger trend of diameter was the same with DLS measurements in Figure 45. Rapidly after addition of DTT, the diameter of nanoparticle and the percentage of free dye population increased. This can be explained by a loss of PMOXA – due to reduction-triggered cleavage of PMOXA from the copolymer and subsequent PCL aggregation.

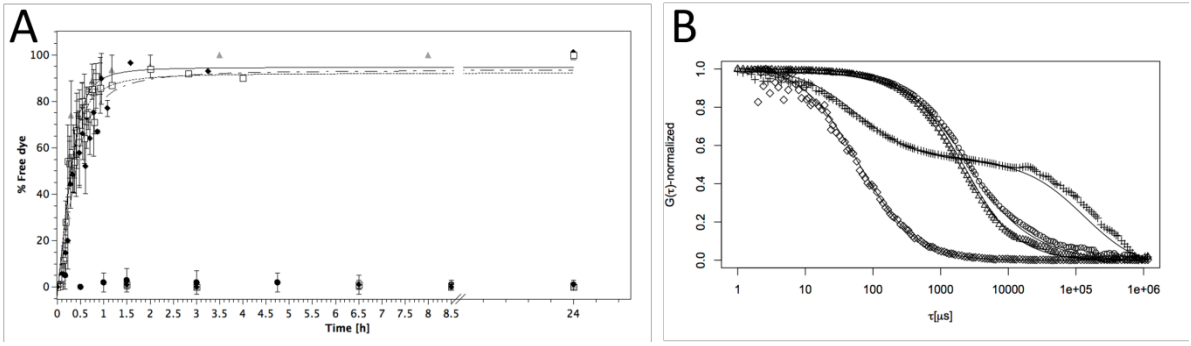

Figure 49. Reduction-triggered disassembly and dye release from PMOXA-graft(ss)-PCL nanoparticles studied by FCS. (A): Percentage of free dye measured by FCS curves: PMOXA-graft(ss)-PCL 1 (grey triangles), PMOXA-graft(ss)-PCL 2 (white rectangles), PMOXA-graft(ss)-PCL 3 (black diamonds), and PMOXA-*b*-PCL (black circles). Free dye only appeared for the PMOXA-graft(ss)-PCLs in presence of 10 mM DTT (upper curves), whereas incubation in PBS or PMOXA-*b*-PCL nanoparticles in 10 mM DTT did not show free dye up to 24 h (lower curves). (B): Normalized autocorrelation curves for PMOXA-graft(ss)-PCL 1 nanoparticles in

10 mM DTT: t = 0 min (circles), t = 24 min (crosses, 46% free dye), t = 24 h (diamonds, 100% free dye), t = 24 h no DTT (triangles).

3.2.5. Loading properties of hydrophobic DOX inside nanoparticles formed by PMOXA-graft(ss)-PCLs

DOX was used as hydrophobic model drug to be encapsulated into nanoparticles formed by PMOXA-graft(ss)-PCLs. All three PMOXA-graft(ss)-PCL nanoparticles were loaded with increasing amounts of DOX ranging from 50 to 250 µg with theoretical drug loading contents (DLC) of 4.8 wt%, 13 wt% and 20 wt%. The drug loading efficiencies (DLE) were around 40% for all the samples, which indicated that the theoretical drug loading contents and the difference of polymer chemical structures had very little influence on DLE (Table 5). The calculated 40% DLE was slightly lower than the DLE values (50%) reported recently for nanoparticles based on cross-linked polyurethane micelles (CCL-PUMs) and PCL-g-SS-PEG copolymers (M_n (^{1}H NMR): 35.6 KDa - 66 KDa),[8, 203] this could be explained by the non-crosslinked molecule structure and lower M_n of our PMOXA-graft(ss)-PCLs. Our results demonstrated that the nanoparticles were loaded with more drugs when higher amounts of drug were added in the self-assembly solution. The final diameter and PDI of DOX loaded nanoparticles increased with increasing theoretical drug loading contents for all three PMOXA-graft(ss)-PCLs (Table 5 and Figure 50), which was caused by more encapsulated DOX occupied more 3D space in the nanoparticles. The diameter and PDI of DOX loaded nanoparticles changed from small to large with increasing theoretical DLC. This is similar to the results reported recently using PCL-g-SS-PEG ABPs.[8]

Table 5. DOX loading content (DLC), DOX loading efficiency (DLE), size and PDI of DOX loaded PMOXA-graft(SS)-PCL Nanoparticles.

Polymer	DLC (wt %)[a]		DLE (%)[b]	DLS	
	in feed	determined		Size (nm)	PDI
PMOXA-graft(ss)-PCL 1	4.8	1.9±0.1	38.2±0.6	42±11	0.2
	13	5.8±0.2	40.8±1.6	48±12	0.3
	20	9.0±0.2	39.4±1.1	53±13	0.3
PMOXA-graft(ss)-PCL 2	4.8	1.7±0.1	35.7±1.3	33 ±10	0.3
	13	5.9±0.1	41.5±0.7	38±10	0.3
	20	9.9±0.3	41.5±1.0	45±9	0.5
PMOXA-graft(ss)-PCL 3	4.8	1.8±0.1	36.9±1.6	35±6	0.3
	13	5.9±0.1	41.1±0.9	32±7	0.4
	20	8.6±0.5	36±2.2	42±6	0.7

a: DLC (wt%) = (weight of loaded drug/weight of polymer) * 100%

b: DLE (%) = (weight of loaded drug/weight in feed) * 100%

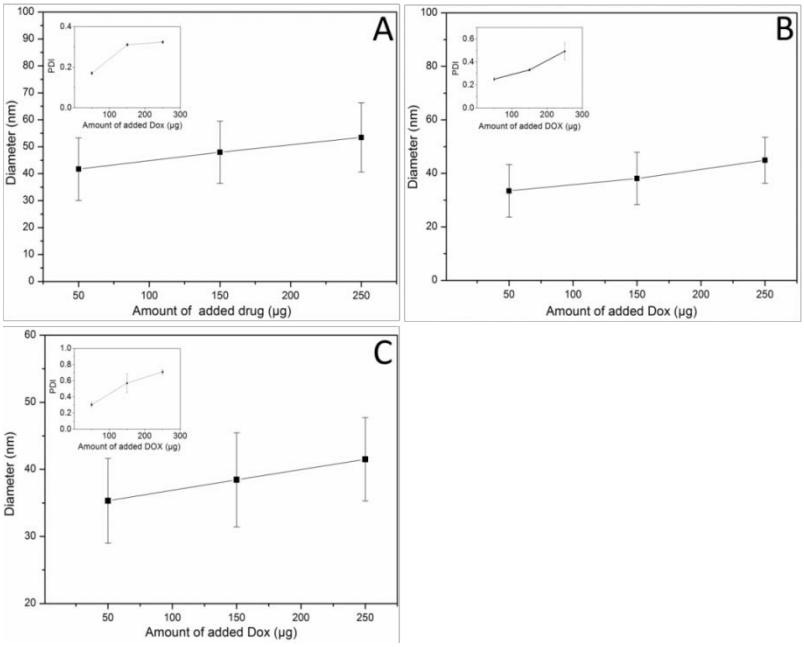

Figure 50. The changing trends of nanoparticle diameter and PDI (inset) with different increasing amount of DOX. (A): PMOXA-graft(ss)-PCL 1; (B): PMOXA-graft(ss)-PCL 2; (C): PMOXA-graft(ss)-PCL 3.

3.2.6. Intracellular DOX release and anti-proliferation activity of DOX-loaded PMOXA-graft(ss)-PCL nanoparticles.

CLSM was used to investigate the cellular uptake and intracellular release behavior of DOX-loaded PMOXA-graft(ss)-PCL nanoparticles in HeLa cells. DOX is known for its ability to intercalate with cellular DNA when released in cells causing an overlap of fluorescence signals of doxorubicin and the DNA-stain Hoechst.[204, 205] Results demonstrated that after 1 h incubation of cells with DOX loaded PMOXA-graft(ss)-PCL 2 nanoparticles (0.25 µg/mL DOX), the fluorescence signal of DOX was colocalizing with the nucleus (Figure 51). This indicates the fast internalization of DOX-loaded nanoparticles and rapid release of DOX inside cells. The fast release was attributed to the disulfide bond cleavage in the presence of the reducing agent-GSH in concentrations of 0.5-10 mM in the intracellular compartment of cells.[206] In addition, the fast increase of fluorescence intensity of DOX is in agreement with FCS data. The hydrophobic dye was released in several minutes under reducing conditions (Figure 49A). The fluorescence is determined only by the free DOX released from PMOXA-graft(ss)-PCL nanoparticles. CLSM images clearly demonstrate that DOX has been released from PMOXA-graft(ss)-PCL nanoparticles into the cytosol and the released DOX is colocalized with the cell nucleus after 1 h (Figure 51A). In comparison, free DOX (0.25 µg/mL DOX) also accumulated in the cell nucleus after 1 h (Figure 51B). The CLSM images of DOX loaded nanoparticles formed by PMOXA-graft(ss)-PCL uptake behavior after 2, 4 and 8 h (Figure 52, 53, 54) clearly demonstrated that the fluorescence intensity of DOX in the nucleus increased with incubation time.

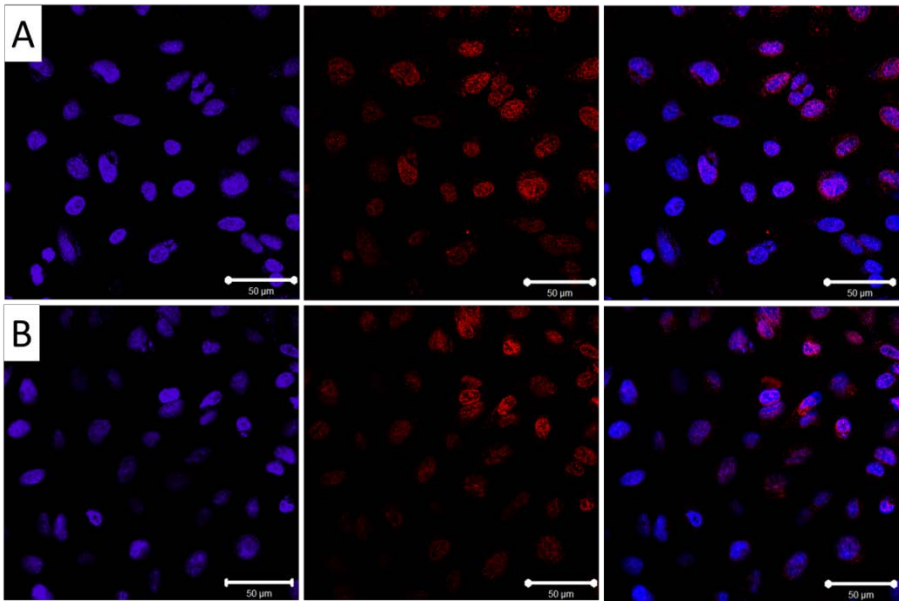

Figure 51. CLSM images of intracellular DOX release from the reduction responsive DOX loaded PMOXA-graft(ss)-PCL 2 nanoparticles in HeLa cells after 1 h. For each panel, images from left to right show cell nuclei stained by Hoechst 33342 (blue), DOX fluorescence in cells (red), and overlays of the two images. A: DOX loaded PMOXA-graft(ss)-PCL 2 nanoparticles (0.25 µg/mL DOX); (B) free DOX as control (0.25 µg/mL DOX).

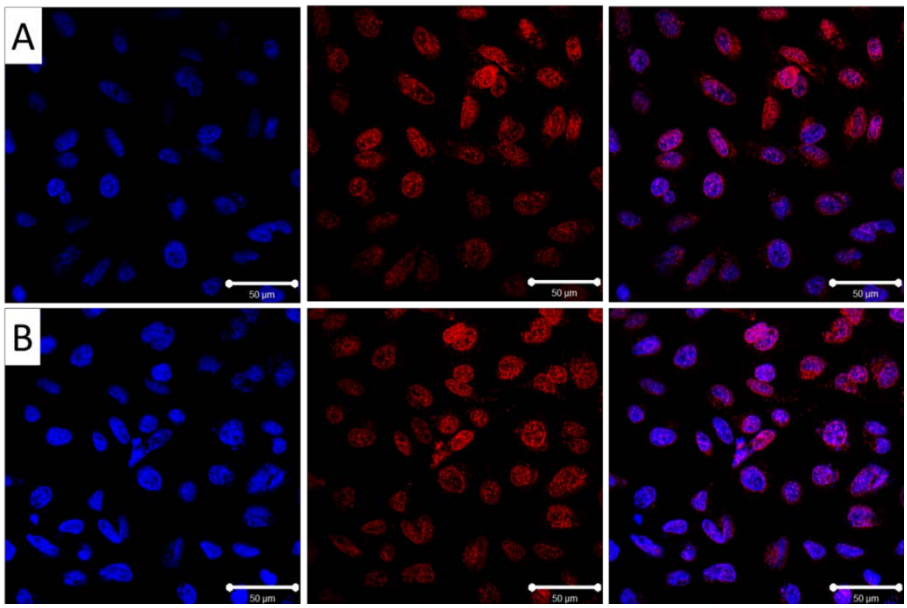

Figure 52. CLSM images of intracellular DOX release from the reduction responsive DOX loaded PMOXA-graft(ss)-PCL 2 nanoparticles in HeLa cells after 2 h incubation. For each panel, images from left to right show cell nuclei stained by Hoechst 33342 (blue), DOX fluorescence in cells (red) and overlays of the two images. A: DOX loaded PMOXA-graft(ss)-PCL 2 nanoparticles (0.25 µg/mL DOX); (B) free DOX as control (0.25 µg/mL DOX).

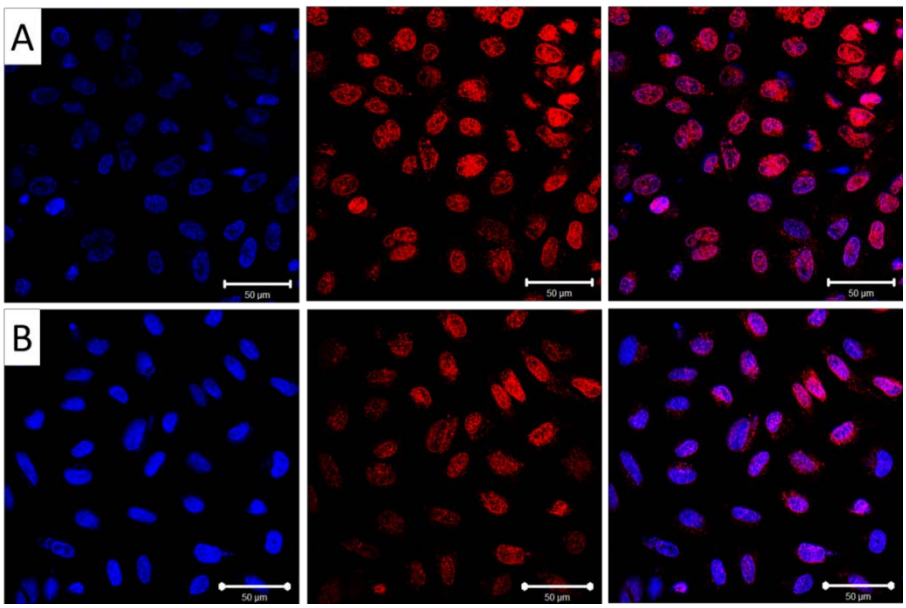

Figure 53. CLSM images of intracellular DOX release from the reduction responsive DOX loaded PMOXA-graft(ss)-PCL 2 nanoparticles in HeLa cells after 4 h incubation. For each panel, images from left to right show cell nuclei stained by Hoechst 33342 (blue), DOX fluorescence in cells (red) and overlays of the two images. A: DOX loaded PMOXA-graft(ss)-PCL 2 nanoparticles (0.25 µg/mL DOX); (B) free DOX as control (0.25 µg/mL DOX).

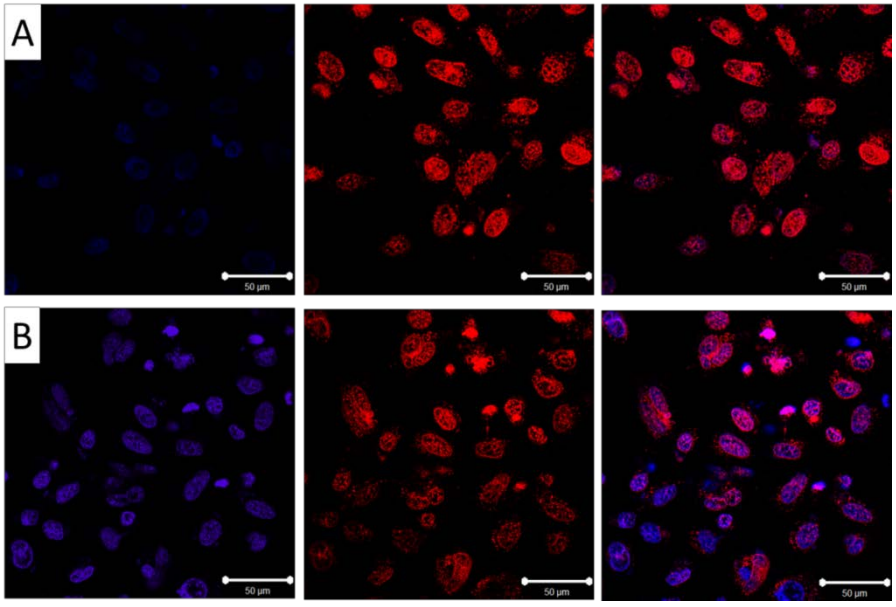

Figure 54. CLSM images of intracellular DOX release from the reduction responsive DOX loaded PMOXA-graft(ss)-PCL 2 nanoparticles in HeLa cells after 8 h incubation. For each panel, images from left to right show cell nuclei stained by Hoechst 33342 (blue), DOX fluorescence in cells (red) and overlays of the two images. A: DOX loaded PMOXA-graft(ss)-PCL 2 nanoparticles (0.25 µg/mL DOX); (B) free DOX as control (0.25 µg/mL DOX).

The three PMOXA-graft(ss)-PCL copolymers did not show toxicity to HeLa cells when measured by MTS. The cell viability remained high than 90% for copolymer concentrations ranging from 0.1 to 1 mg/mL after 48 h incubation (Figure 55). The good biocompatibility of this new copolymer indicates it as a promising candidate for drug delivery applications.

DOX-loaded PMOXA-graft(ss)-PCL nanoparticles exhibit a higher anti-proliferation effect in HeLa cells than DOX-loaded PMOXA-*b*-PCL after 48 h (DOX concentration ranging from 0.9, 2.7, 4.5 to 9 µg/mL) (Figure 56). Surprisingly, the cell viability of the lowest concentration (0.9 µg/mL) and highest concentration (9 µg/mL) of DOX loaded PMOXA-graft(ss)-PCL nanoparticles compared with DOX loaded PMOXA-*b*-PCL was not as higher than for concentrations of 2.7 µg/mL and 4.5 µg/mL, which indicated that the drug concentration also plays an essential role in increasing the anti-proliferation efficiency. For DOX concentrations of 4.5 µg/mL, the efficiency of anti-proliferation for HeLa cells for DOX-loaded PMOXA-graft(SS)-PCL was improved at least 40% comparing with DOX-loaded PMOXA-*b*-PCL nanoparticles. It should be noticed that the highest concentration of copolymer in the anti-proliferation effect for HeLa cells was 0.07 mg/mL, which is much lower than the one tested for cytotoxicity, respectively 1 mg/mL. As a result, the decreased viability of HeLa cells was caused by released DOX rather than the copolymer itself.

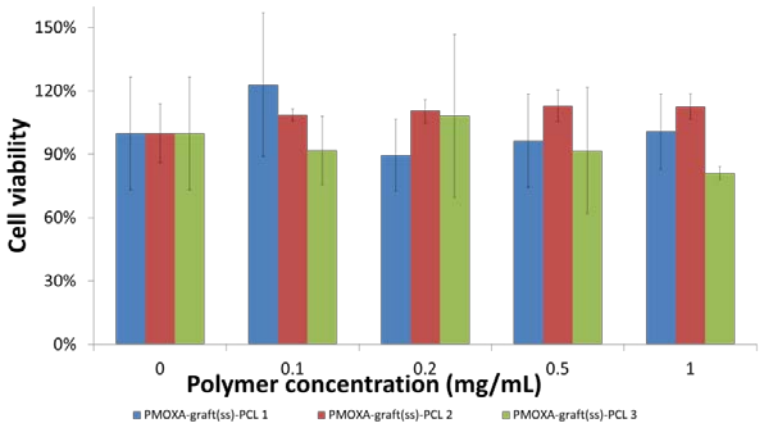

Figure 55. Viabilities of HeLa cells after 48 h incubation of PMOXA-graft(SS)-PCL nanoparticles. All the data are presented as the average ± standard deviation (n = 4).

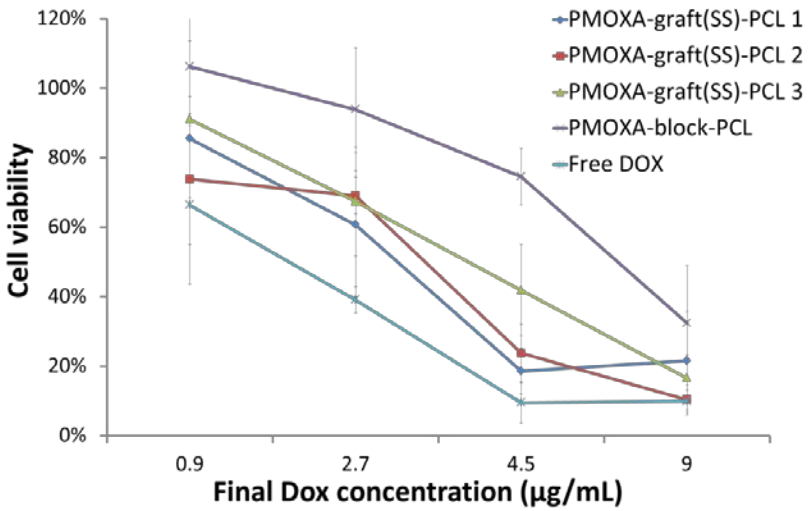

Figure 56. Viability of HeLa cells after 48 h incubation with DOX loaded PMOXA-graft(SS)-PCL nanoparticles, DOX loaded PMOXA-*b*-PCL nanoparticles and free DOX. DOX dosage was 0.9 µg/mL, 2.7 µg/mL, 4.5 µg/mL and 9 µg/mL. All the data are presented as the average ± standard deviation (n = 8).

3.3. Conclusion

A novel reduction responsive PMOXA-graft(ss)-PCL ABPs were synthesized through the thiol-disulfide exchange reaction between thiolated PMOXA (PMOXA-SH) and pyridyl disulfide functionalized poly(ε-caprolactone) (PCL-*co*-PPCL). This new type of biocompatible copolymer is not toxic itself, biocompatible, and biodegradable ABPs. Its self-assembled nanoparticle can encapsulate hydrophobic molecules, such as DOX, during the self-assembly process in aqueous solution with around 40% loading efficiency. In a suitable reducing condition, PMOXA-graft(ss)-PCL nanoparticles can release their encapsulated cargoes faster than PMOXA-*b*-PCL self-assemblies which show no reduction responsiveness. Our new reduction responsive PMOXA-graft(ss)-PCL is a promising candidate for targeted drug delivery in tumor cells that contain a much higher amount of reducing agents than the normal cells.

4. Design and synthesis of gene delivery nanocarriers based on reduction responsive amphiphilic poly(2-ethyl-2-oxazoline)-*block*-poly(ε-caprolactone)-*ss*-poly(L-lysine) (PEtOXA-*b*-PCL-*ss*-PLL) copolymers

Dalin Wu, Jason Duskey, Cornelia Palivan, Wolfgang Meier*

Some of the result about the polymer synthesis is being organized and wrote as the manuscript.

4.1. Introduction

Nucleic acids, including plasmid DNA, antisense oligodeoxyribonucleotides (ODN), and small interfering RNA (siRNA) have been receiving more and more attention as novel genetic drugs for treatment of single gene disorders, cancers, DNA vaccines, and regenerative medicine.[207] However, because nucleic acids are susceptible to hydrolytic and enzymatic degradation in the body and cannot pass through the cytoplasmic membrane, a safe and efficient delivery nanocarrier is necessary to deliver nucleic acids to maximally exert their therapeutic potential in vivo. Natural viruses are highly efficient delivery vehicles for nucleic acids, due to their ability to complex with nucleic acids through charge interaction to form polyplexes. This strategy enhances the stability of nucleic acids against hydrolytic and enzymatic degradation in the body. [76, 208, 209] However, non-viral delivery of nucleic acids involves two key stages: extracellular delivery and intracellular delivery[100] (Figure 57). Each step of delivery requires specific qualities of the nanocarriers. During the process of extracellular delivery, the first obstacle is to overcome the presence of nucleases which attack foreign nucleotides rapidly. In addition, biomacromolecules, such as serum proteins, can non-specifically interact with polyplexes inducing their dissociation or aggregation. Because of this, high stability and high resistance to protein absorption must be prerequisites for designing systemically injectable polyplexes. Even though stealth complexes can be obtained, the polyplexes should be less than 200 nm in order to take advantage of the EPR[1] effect to increase accumulation into tumor cells. Once delivered, nanocarriers are entrapped by the endosomes (pH 6.2-6.8) which is significantly lower than the extracellular matrix with a pH of 7.4. In order to ensure intracellular delivery to the nucleus the polyplex should escape the

endosome before it becomes a lysosome (pH of 4-5). Finally, the polyplexes DNA cargo must overcome the nuclear membrane to be functional. This requires the polyplexes to have the following properties : i) high stability during circulation in blood, ii) high resistance to biomolecules absorption, iii) size bellow 200 nm to utilize EPR[1] effect, iv) adsorption by the cellular membrane, for extracellular delivery, v) fast endosomal escape, vi) gene release from the polyplex, vii) nuclear internalization, and viii) minimal cytotoxicity of polycations, for intracellular delivery.[100]

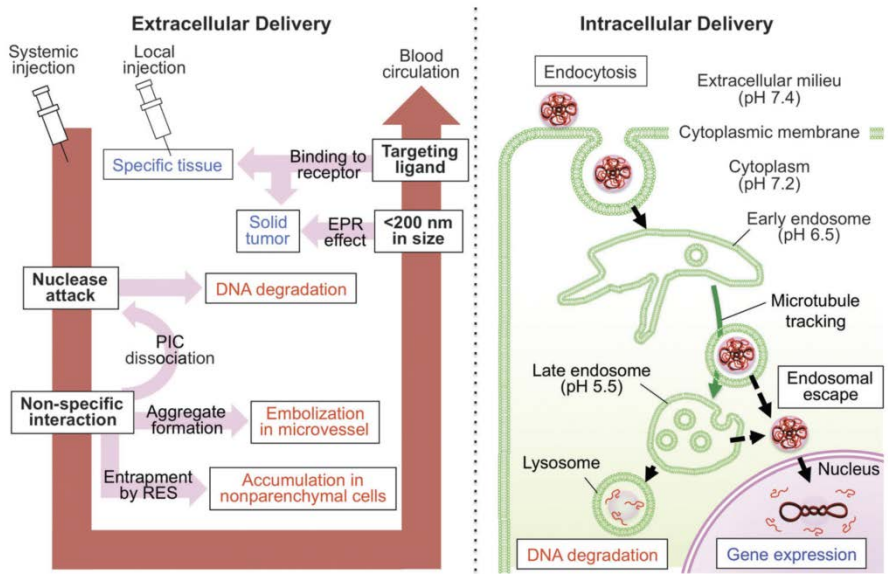

Figure 57. Schematic illustration of gene delivery from injection to cell nucleus and prerequisites for polyplexes to be successful non-viral vectors.[100]

In order to address the above mentioned requirements, we designed and synthesized a new type of amphiphilic triblock ABC copolymer poly(2-ethyl-2-oxazoline)-*block*-poly(ε-caprolactone)-ss-poly(L-lysine) (PEtOXA-*b*-PCL-ss-PLL) through the ring-opening polymerization of 2-ethyll-2-oxazoline, ε-caprolactone and ε-benzyloxycarbonyl-L-lysine N-carboxyanhydride. Because of its amphiphilicity, PEtOXA-*b*-PCL-ss-PLL can self-assemble into micelles in aqueous solution (Figure 58). It should be emphasized that hydrophilic PEtOXA was used instead of the hydrophilic PMOXA which was used in the section 3 was that PMOXA was not soluble in toluene during the initiation of ε-carprolactone in presence of catalyst stannous octoate. Stannous octoate can only express catalytic effect in the solution with low polarity, like toluene. However, PEtOXA, due to a more methylene group in repeating unit, it can be soluble in toluene and initiate the polymerization of ε-carprolactone.

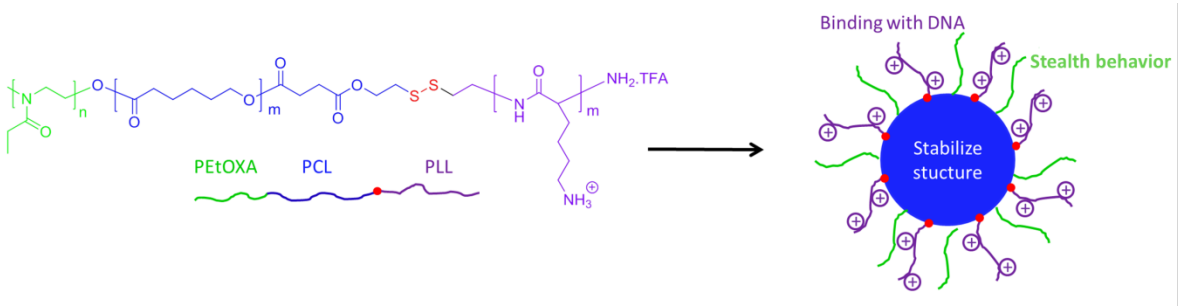

Figure 58. Schematic representation of the self-assembly of PEtOXA-*b*-PCL-ss-PLL in micelles in aqueous solution.

This specific copolymer structure was chosen because PEtOXA, as the hydrophilic block, can stretch over the surface of micelles endowing the micelles with "stealth behavior" and enabling prolonged circulation time in the blood. PCL block is a biocompatible and biodegradable hydrophobic polymer block can stabilize the nanostructures after complexation with DNA. Finally, PLL as the hydrophilic polymer block with pKa e of 9.85 ± 0.2[210] can bind with genes through the positive and negative interactions in physiological condition. The process of PEtOXA-*b*-PCL-ss-PLL micelles complex with gene to form the polyplex is illustrated in Figure 59.

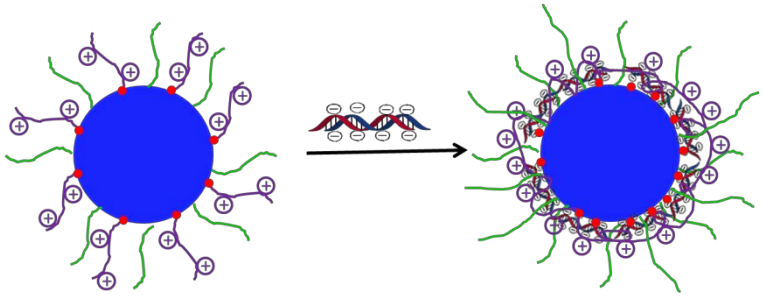

Figure 59. Schematic representation of process of polyplex formed by gene and PEtOXA-*b*-PCL-ss-PLL micelles.

In the structure of PEtOXA-*b*-PCL-ss-PLL, the disulfide bond that connects the PEtOXA-*b*-PCL and hydrophilic PLL can be reduced in the same way as GSH inside of the cancer cells. By reducing the disulfide bond of the polyplexes, the structures will fall apart releasing the DNA. This process could enhance the escape of DNA from the endosomes (Figure 60).

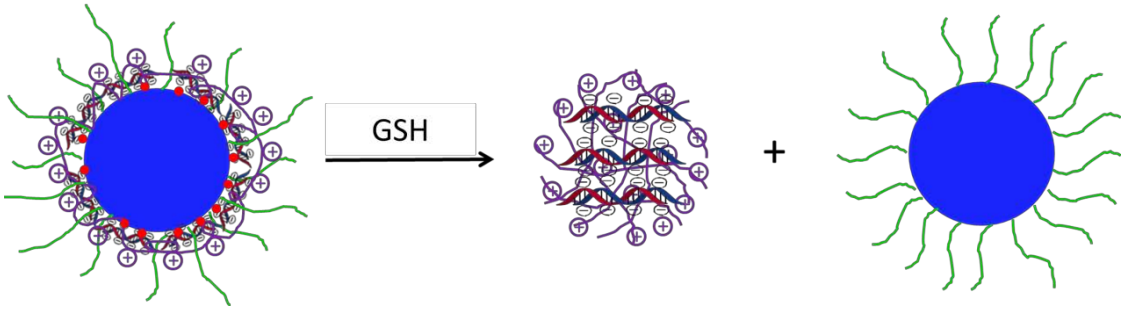

Figure 60. Schematic representation for the GSH triggered separation of gene and PEtOXA-*b*-PCL-ss-PLL micelle polyplexes.

As controls, two block copolymers, poly(2-ethyl-2-oxazoline)-ss-poly(L-lysine) (PEtOXA-ss-PLL) and poly(2-ethyl-2-oxazoline)-*block*-poly(L-lysine) (PEtOXA-*b*-PLL), were also synthesized. Neither of them have a PCL hydrophobic block. Also these, polymers contain only PEtOXA and polylysine blocks connected by reduction responsive disulfide and non-reduction sensitive carbon-carbon bond, responsively. Therefore, the overall influence of various blocks and reducing potential of the disulfide bond can be carefully investigated for DNA delivery.

4.2. Results and discussion

4.2.1. Synthesis and characterization of PEtOXA-*b*-PCL-ss-PLL, PEtOXA-ss-PLL and PEtOXA-*b*-PLL

4.2.1.1. Detailed PEtOXA-*b*-PCL-ss-PLL, PEtOXA-ss-PLL and PEtOXA-*b*-PLL synthesis procedure

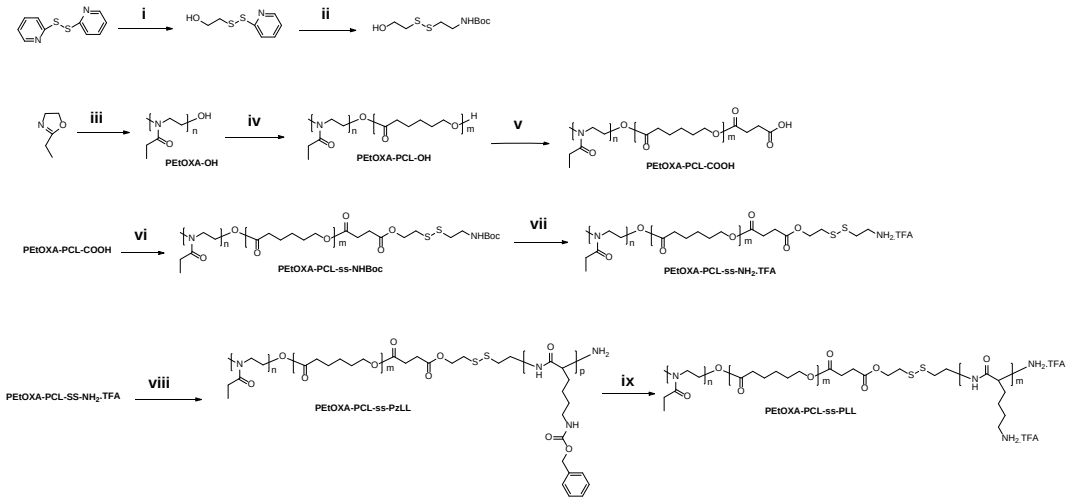

Scheme 10. Synthesis route of PEtOXA-*b*-PCL-ss-PLL.[a]

a: Reagents and conditions: (i) 2-Mercaptoethanol, acetic acid, MeOH, RT for 2 h under argon; (ii) N-(tert-butoxycarbonyl)-2-aminoethanethiol, MeOH/DCM, RT for 20 h under argon; (iii) methyl trifluoromethanesulfonate, acetonitrile, 80 °C for 24 h under argon: (iv) ε-caprolactone, Tin(II) 2-ethylhexanoate, toluene, 110 °C for 24 h under argon; (v) succinic anhydride, triethylamine, DMAP, chloroform, RT for 72 h under argon; (vi) 2-Boc-aminoethyl 2'-hydroxyethyl disulfide, DCC, DMAP, chloroform, RT for 72 h under argon; (vii) TFA, 0 °C for 1 h; (viii) ε-benzyloxycarbonyl-L-lysine N-carboxyanhydride, DIPEA, DMF, RT for 72 h under argon; (ix) TFA, HBr in acetic acid solution (33%), 0 °C for 1.5h.

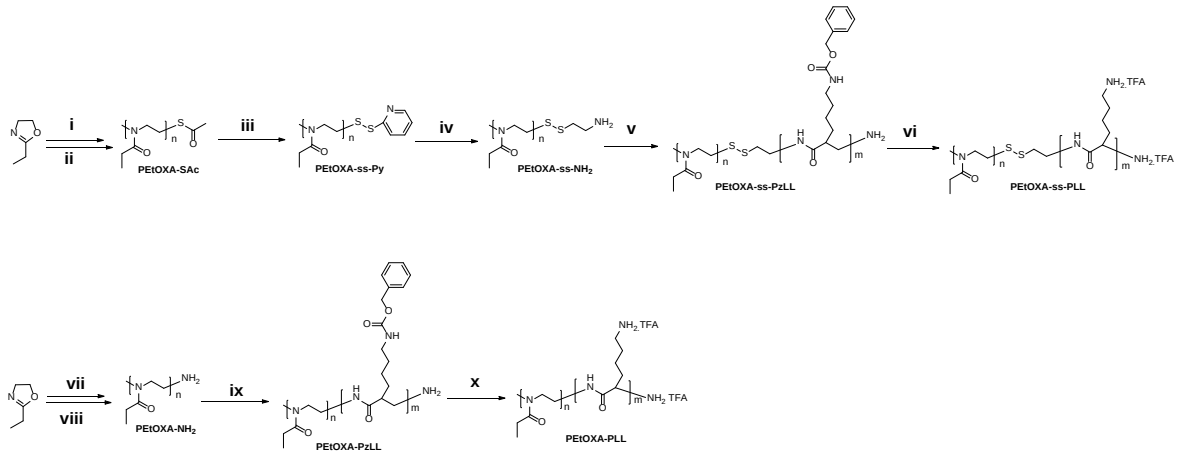

Scheme 11. Synthesis route of PEtOXA-ss-PLL and PEtOXA-*b*-PLL.[b]

b: Reagents and conditions: (i) Methyl trifluoromethanesulfonate, acetonitrile, 80 °C for 24 h under argon; (ii) potassium thioacetate, RT for 24 h under argon; (iii) diphenyl disulfide, PEtOXA-SAc, NH_3/MeOH (7N), RT for 48 h under argon; (iv) PEtOXA-ss-Ph, cysteamine, MeOH, RT for 48 h under argon; (v) PEtOXA-ss-NH2, ε-benzyloxycarbonyl-L-lysine N-carboxyanhydride, DMF, RT for 72 h under argon; (vi) PEtOXA-ss-PzLL, TFA, HBr in acetic acid (33%), 0 °C for 1.5 h; (vii) methyl trifluoromethanesulfonate, acetonitrile, 80 °C for 24 h under argon; (viii) NH_3/MeOH (7N), RT for 24 h under argon; (ix) PEtOXA-NH_2, ε-benzyloxycarbonyl-L-lysine N-carboxyanhydride, DMF, RT for 72 h under argon; (x) PEtOXA-*b*-PzLL, TFA, HBr in acetic acid solution (33%), 0 °C for 1.5 h.

4.2.1.2. Discussion about the synthesis procedure and result

Synthesis of tert-butyl N-(2[(2-hydroxyethyl)disulfanyl]ethyl)carbamate. Thiol-disulfide exchange reaction between diphenyl disulfide and 2-mercaptoethanol was used to synthesize 2-(2-(pyridin-2-yl)disulfanyl)ethanol. The same reaction type was further used to

synthesize 2-Boc-aminoethyl 2'-hydroxyethyl disulfide from 2-(2-(pyridin-2-yl)disulfanyl)ethanol and N-(tert-butoxycarbonyl)-2-aminoethanethiol at RT. The ^{1}H NMR and ^{13}C NMR proved the efficiency and the high purity of 2-(2-(pyridin-2-yl)disulfanyl)ethanol and N-(tert-butoxycarbonyl)-2-aminoethanethiol synthesis after the purification by column chromatography (Figure 61, Figure 62 and Figure 63).

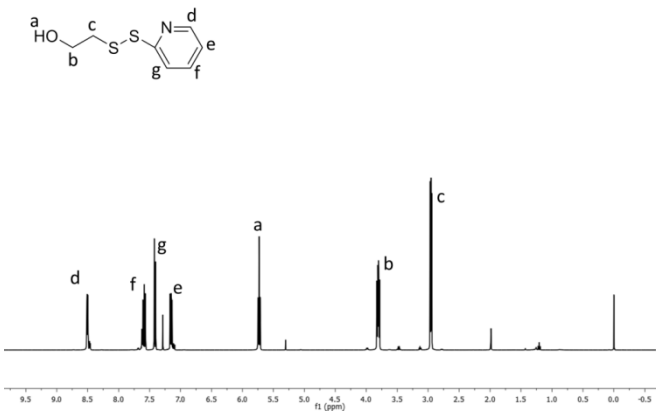

Figure 61. ^{1}H NMR spectrum of 2-(2-(pyridin-2-yl)disulfanyl)ethanol in $CDCl_3$.

Figure 62. ^{1}H NMR spectrum of 2-Boc-aminoethyl 2'-hydroxyethyl disulfide in $CDCl_3$.

Figure 63. ^{13}C NMR spectrum of 2-Boc-aminoethyl 2'-hydroxyethyl disulfide in $CDCl_3$.

Synthesis of poly(2-ethyl-2-oxazoline)-*block*-poly(ε-caprolactone)-OH (PEtOXA-*b*-PCL-OH). PEtOXA-OH was synthesized by the ROP of 2-ethyl-2-oxazoline initiated by methyl trifluoromethanesulfonate in acetonitrile. The ^{1}H NMR spectrum (Figure 64) proved the efficiency of the reaction and PDI values of 1.15 from the GPC measurements (Figure 65) underlines the living cationic ROP property of 2-ethyl-2-oxazoline.

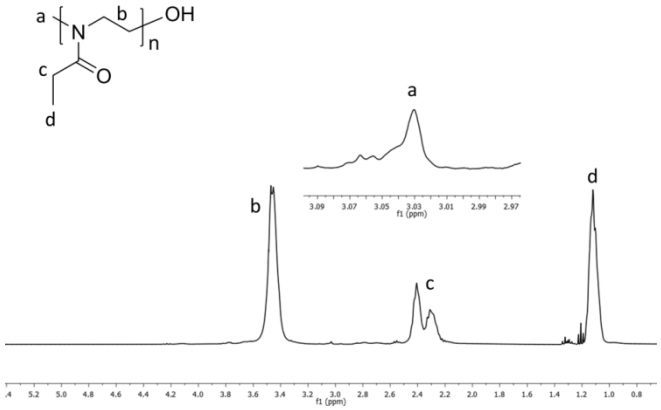

Figure 64. ^{1}H NMR spectrum of PEtOXA-OH in $CDCl_3$.

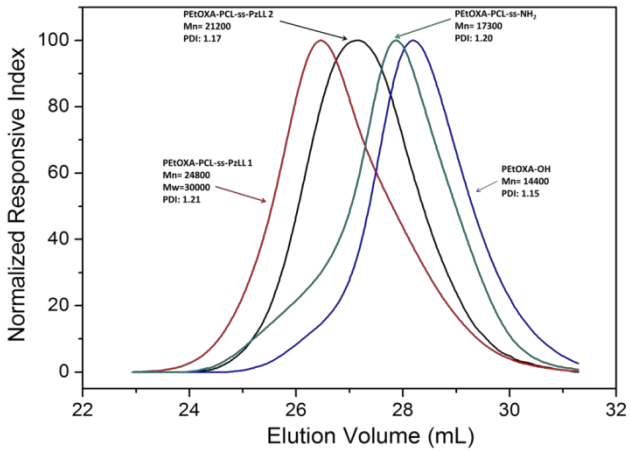

Figure 65. GPC curves of PEtOXA-OH, PEtOXA-*b*-PCL-ss-NH_2, PEtOXA-*b*-PCL-ss-PzLL1 and PEtOXA-*b*-PCL-ss-PzLL2.

Lyophilized PEtOXA-OH was first mixed with ε-caprolactone. Then, hot freshly distilled toluene was added to dissolve the PEtOXA-OH, because otherwise it cannot be dissolved. After the ROP of ε-caprolactone, the product was purified by precipitation in diethyl ether easily. The peaks at 1.10 ppm (characteristic for the protons on methyl groups of PEtOXA-OH) and 4.06 ppm (characteristic for the protons of methylene groups next to oxygen on PCL) from ^{1}H NMR spectrum proved the presence of PEtOXA-OH and PCL. The mono peak in the

GPC plot proved the covalent bonding between PEtOXA and PCL (Figure 66). The PDI of PEtOXA-*b*-PCL-OH was 1.20 indicating the living ROP of ε-caprolactone. In addition, in the GPC curve, there is no additional shoulder proving complete polymerization of PEtOXA-OH (Figure 65).

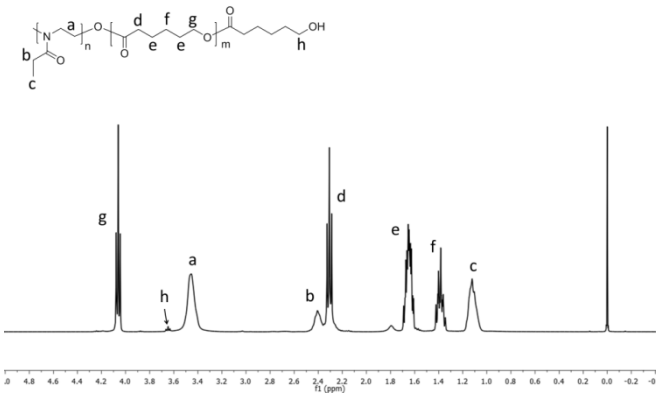

Figure 66. The ^{1}H NMR spectrum of PEtOXA-*b*-PCL-OH in $CDCl_3$.

Synthesis of poly(2-ethyl-2-oxazoline)-*block*-poly(ε-caprolactone)-ss-NH_2.TFA (PEtOXA-*b*-PCL-ss-NH_2.TFA). PEtOXA-*b*-PCL-OH was first reacted with succinic anhydride to synthesize carboxyl acid PEtOXA-*b*-PCL-COOH. The appearance of a new peak at 2.63 ppm characteristic for the protons on methylene next to carboxylic group in figure 67 demonstrated the successful carboxylation of PEtOXA-*b*-PCL. Further, PEtOXA-*b*-PCL-COOH was reacted with tert-butyl N-(2[(2-hydroxyethyl)disulfanyl]ethyl)carbamate in presence of DCC and DMAP. The appearance of new peaks at 1.44 ppm protons on Boc and 2.91 ppm, (protons on the methylene groups next to disulfide) in figure 68 shows the coupling of tert-butyl N-(2[(2-hydroxyethyl)disulfanyl]ethyl)carbamate on the PEtOXA-*b*-PCL. Finally, PEtOXA-*b*-PCL-NH_2-TFA macroinitiator was synthesized by deprotecting Boc in the presence of TFA. The disappearance of the peak at 1.44 ppm, characteristic for protons on the Boc protecting group in figure 69 demonstrated the complete deprotection of Boc.

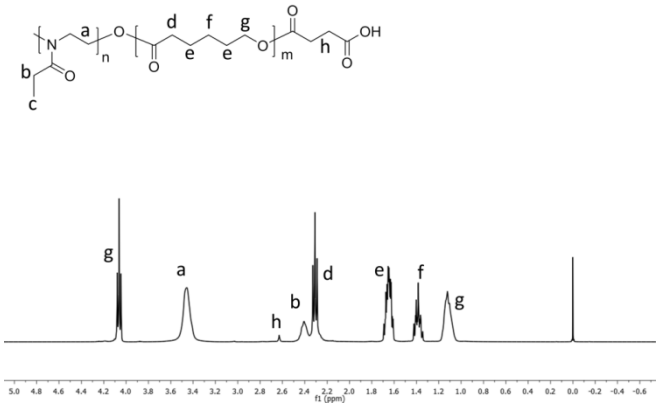

Figure 67. ^{1}H NMR spectrum of PEtOXA-*b*-PCL-COOH in $CDCl_3$.

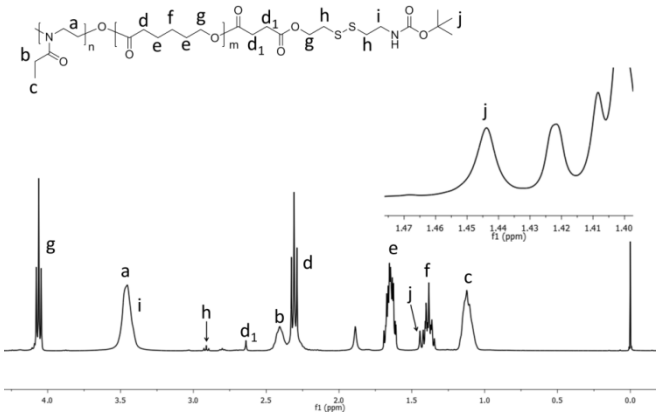

Figure 68. ^{1}H NMR spectrum of PEtOXA-*b*-PCL-ss-NHBoc in $CDCl_3$.

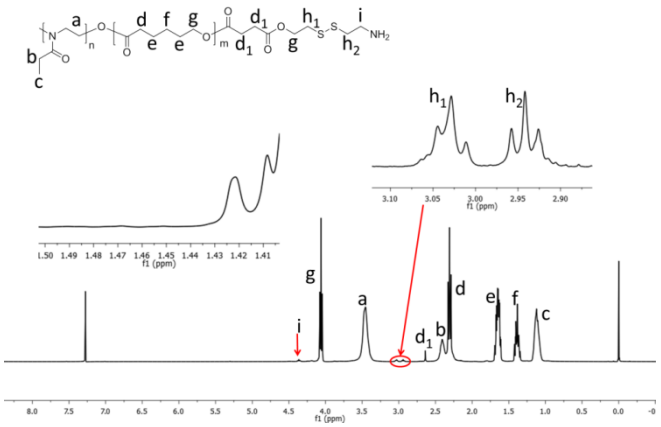

Figure 69. ^{1}H NMR spectrum of PEtOXA-*b*-PCL-ss-NH_2.TFA in $CDCl_3$

Synthesis of poly(2-ethyl-2-oxazoline)-*block*-poly(ε-caprolactone)-ss-poly(L-lysine) (PEtOXA-*b*-PCL-ss-PLL). PEtOXA-*b*-PCL-ss-NH_2.TFA initiated the ROP of ε-benzyloxycarbonyl-L-lysine N-carboxyanhydride in DMF with DIPEA. For that, DIPEA was added to neutralize the TFA and increase the reactivity of the primary amines. The new peaks at 7.26 ppm,

characteristic for the hydrogens on phenyl ring, and 4.99 ppm, for the protons on methylene next to phenyl ring, demonstrated the successful polymerization of poly(ε-benzyloxycarbonyl-L-lysine) (Figure 70). The GPC plot (Figure 65) shows only one narrow distributed retention peak, proving the successful coupling of poly(ε-benzyloxycarbonyl-L-lysine) and PEtOXA-*b*-PCL diblock copolymer. From the GPC (Figure 65), the M_ns of the two PEtOXA-*b*-PCL-ss-PzLLs were determined as 21.2 KDa and 24.8 KDa. Importantly, the PDIs of two PEtOXA-*b*-PCL-ss-PzLLs were 1.17 and 1.21, which demonstrates the living ROP of ε-benzyloxycarbonyl-L-lysine N-carboxyanhydride. PEtOXA-*b*-PCL-ss-PLL was synthesized by reacting PEtOXA-*b*-PCL-ss-PzLL with TFA and HBr in acetic acid solution (33%). The disappearance of the peaks at 7.26 ppm, (corresponding to hydrogens on phenyl ring, and 4.99 ppm, characteristic for protons on methylene next to phenyl ring, demonstrated the successful deprotection of phenyl rings on PzLL (Figure 71).

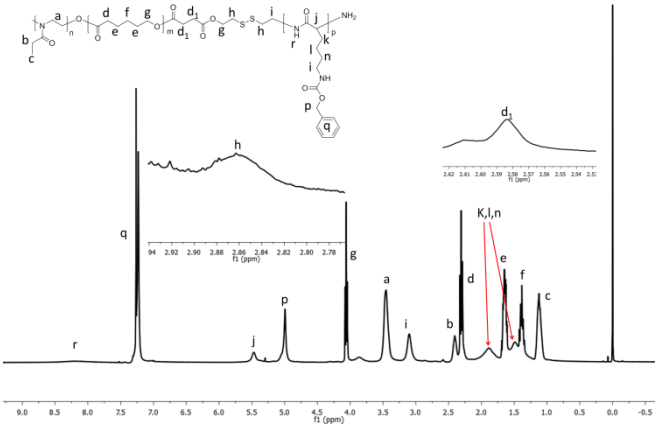

Figure 70. ^{1}H NMR spectrum of PEtOXA-*b*-PCL-ss-PzLL in $CDCl_3$.

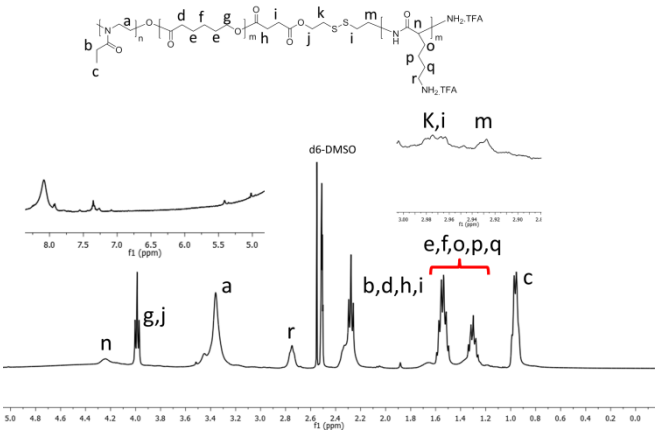

Figure 71. ^{1}H NMR spectrum of PEtOXA-*b*-PCL-ss-PzLL in d6-DMSO.

Synthesis of Poly(2-ethyl-2-oxazoline) disulfide amine (PEtOXA-ss-NH_2). The synthesis method of PEtOXA-SAc and PEtOXA-ss-Py was performed according to the previously published procedure. ^{1}H NMR spectra (Figure72) demonstrated the successful synthesis with high degree of purity. Further the thiol-disulfide exchanging reaction between PEtOXA-ss-Py and cysteamine was applied to synthesize PEtOXA-ss-NH_2. The disappearance of the peaks at 7.0 ppm and 8.5 ppm corresponding to the protons on the pyridine of PEtOXA-ss-Py and appearance of a new peak at 4.15 ppm, assigned to the protons on methylene next to amine of PEtOXA-ss-NH_2 in ^{1}H NMR spectra (Figure 73), suggests the successful synthesis of PEtOXA-ss-NH_2. In addition, the color of reaction mixture changed from colorless to yellow due to the appearance of a byproduct, pyridine-2-thione, that also proved the success of the thiol-disulfide exchanging reaction. The PDI of PEtOXA-ss-NH_2 is 1.22 (Figure 74).

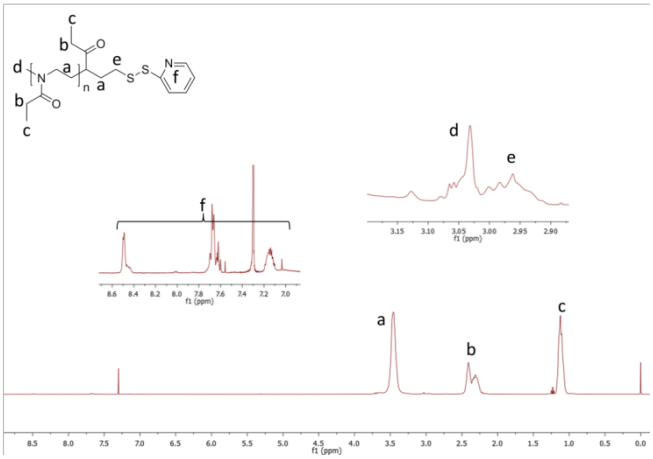

Figure 72. ^{1}H NMR spectrum of PEtOXA-ss-Py in $CDCl_3$.

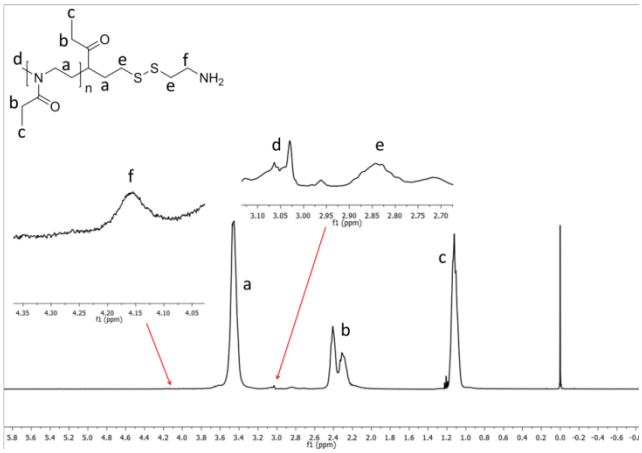

Figure 73. ^{1}H NMR spectrum of PEtOXA-ss-NH_2 in $CDCl_3$.

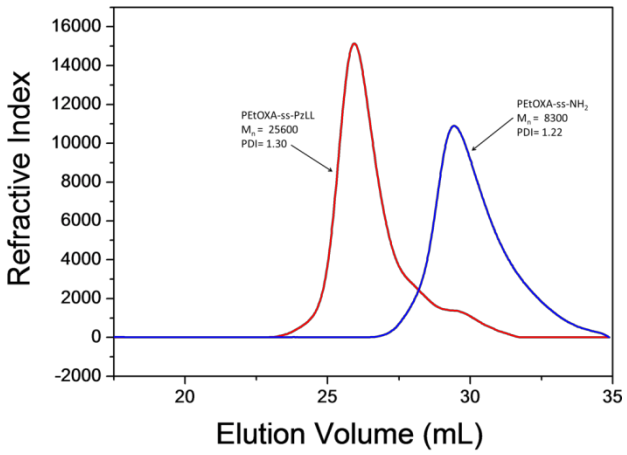

Figure 74. GPC curves of PEtOXA-ss-NH_2 and PEtOXA-ss-PzLL in DMF.

Synthesis of Poly(2-ethyl-2-oxazoline)-ss-poly(L-lysine) (PEtOXA-ss-PLL). PEtOXA-ss-PzLL was synthesized through the ROP of ε-benzyloxycarbonyl-L-lysine N-carboxyanhydride initiated by the macroinitiator PEtOXA-ss-NH_2 in a DMF solution. In the ^{1}H NMR spectrum, the new peaks at 7.26 ppm, characteristic for the protons from the phenyl ring, and 4.99 ppm (Figure 75), assigned to the protons on methylene groups next to phenyl ring, demonstrated the synthesis of poly(ε-benzyloxycarbonyl-L-lysine). One single retention peak in the GPC indicated the successful coupling reaction (Figure 74). PEtOXA-ss-PzLL had a low PDI around 1.30 and a molecular weight of 25.6 KDa.

The deprotection of ε-benzyloxycarbonyl was carried out in a mixture of TFA and HBr in acetic acid solution (33%) at 0 °C. The disappearance of signals at 7.26 ppm and 4.99 ppm in ^{1}H NMR spectrum demonstrated the successful deprotection of ε-benzyloxycarbonyl groups from PzLL (Figure 76).

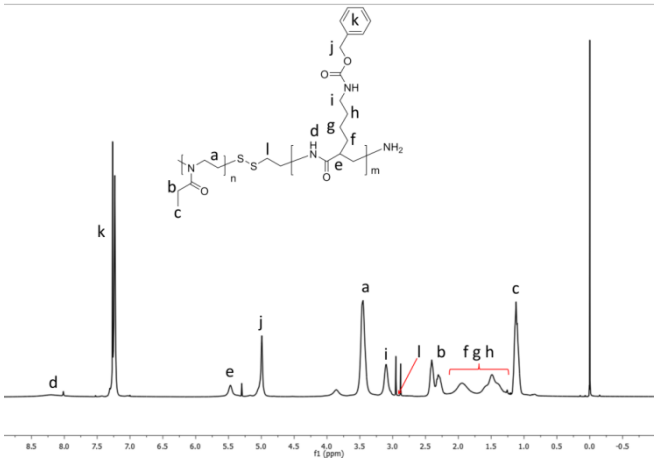

Figure 75. ^{1}H NMR spectrum of PEtOXA-ss-NH_2 in $CDCl_3$.

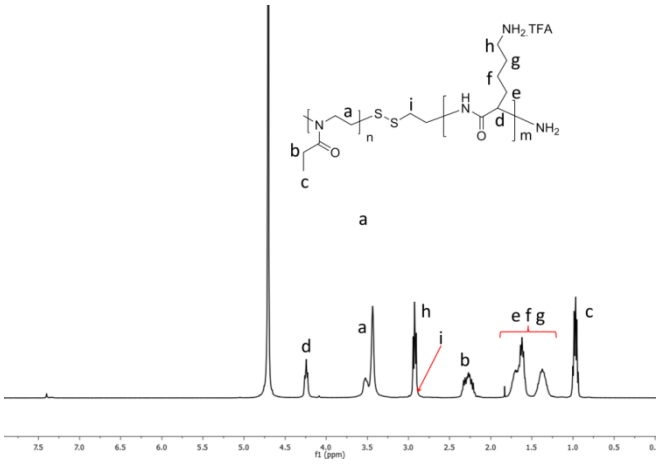

Figure 76. ^{1}H NMR spectrum of PEtOXA-ss-NH_2 in D_2O.

Synthesis of primary Amine Ended Poly(2-ethyl-2-oxazoline) (PEtOXA-NH_2). The synthesis of PEtOXA-NH_2 was performed according to the method previously published. The ^{1}H NMR spectrum (Figure 77) demonstrated the successful synthesis of PEtOXA-NH_2 with high purity. The polymer has a M_n of 6.7 KDa and a PDI of 1.30 (Figure 78).

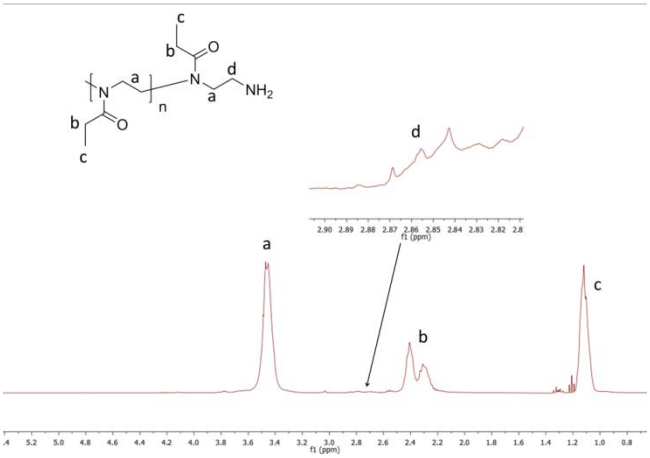

Figure 77. ^{1}H NMR spectrum of PEtOXA-NH_2 in $CDCl_3$.

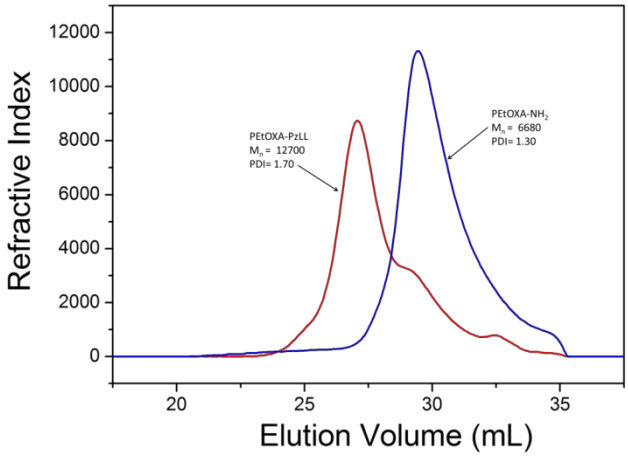

Figure 78. GPC curves of PEtOXA-NH_2 and PEtOXA-*b*-PzLL in DMF.

Synthesis of Poly(2-ethyl-2-oxazoline)-*block*-Poly(L-lysine) (PEtOXA-*b*-PLL). PEtOXA-*b*-PzLL was synthesized through the ROP of ε-benzyloxycarbonyl-L-lysine N-carboxyanhydride initiated by macroinitiator PEtOXA-NH_2 in a DMF solution. In the ^{1}H NMR spectrum, the new peaks at 7.23 ppm, characteristic for the protons of phenyl ring, and 4.99 ppm, assigned to the protons of the methylene groups next to phenyl ring, demonstrated the formation of of poly(ε-benzyloxycarbonyl-L-lysine) (Figure 79). A GPC plot shows only one retention peak corresponding to PEtOXA-*b*-PzLL shifted to the right side compared with the macroinitiator PEtOXA-NH_2 due to the increase of the M_n by polymerization (Figure 78). PEtOXA-*b*-PzLL has a PDI of 1.71 and a M_n of 21.7 KDa.

The deprotection of ε-benzyloxycarbonyl was carried out in a mixture of TFA and HBr in acetic acid solution (33%) at 0 °C. The disappearance of the peaks at 7.26 ppm, characteristic for the protons from the phenyl ring, and 4.99 ppm, assigned to the protons from (the methylene group near the phenyl ring), demonstrated the successful deprotection of ε-benzyloxycarbonyl groups from PzLL (Figure 80).

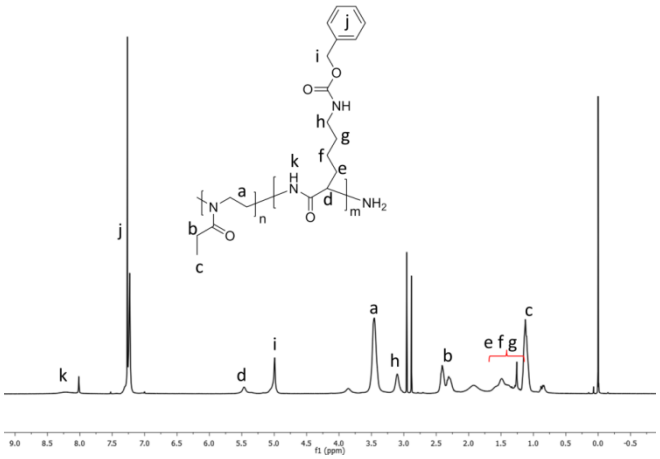

Figure 79. ^{1}H NMR spectrum of PEtOXA-*b*-PzLL in $CDCl_3$.

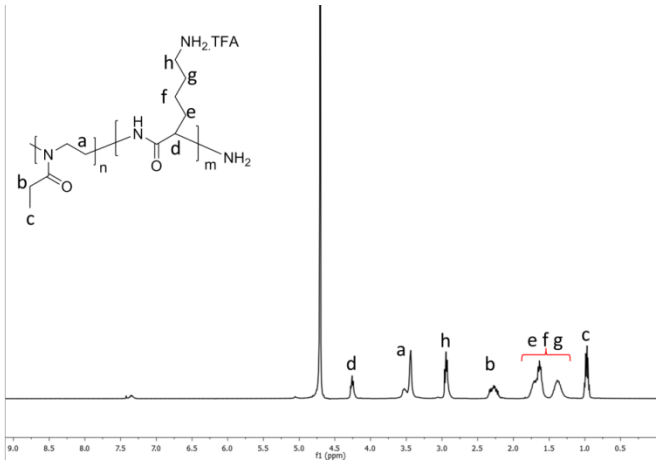

Figure 80. ^{1}H NMR spectrum of PEtOXA-*b*-PLL in D_2O.

4.2.2. Preparation and characterization of self-assemblies of PEtOXA-ss-PzLL and PEtOXA-*b*-PCL-ss-PLL

4.2.2.1. Reduction responsive property of PEtOXA-ss-PzLL.

GPC was used to characterize the reduction responsive property of $PEtOXA_{60}$-ss-$PzLL_{58}$. The $PEtOXA_{60}$-ss-$PzLL_{58}$ (5 mg) was dissolved in the DMF solution (1.2 mL) containing 10 mM DTT. After 2 h treatment, the sample was measured by GPC. Compared with $PEtOXA_{60}$-ss-$PzLL_{58}$ with or without DTT that shows one retention peak is seen until reduction occurs leading to two retention peaks corresponding to the lower M_n polymer fragments (Figure 81).

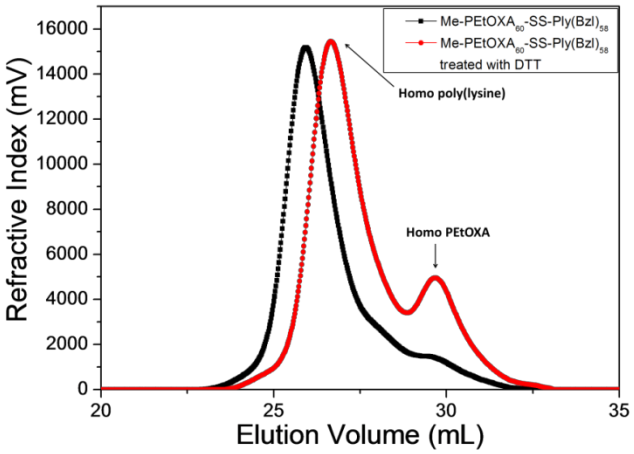

Figure 81. GPC curves of $PEtOXA_{60}$-ss-$PzLL_{58}$ and $PEtOXA_{60}$-ss-$PzLL_{58}$ treated with 10 mM DTT in DMF.

4.2.2.2. Reduction responsive property of PEtOXA-ss-PzLL self-assemblies.

Due the hydrophobic property of the phenyl ring group on the repeating unit of lysine, PEtOXA-ss-PzLL is amphiphilic. This means that PEtOXA-ss-PzLL can self-assemble in aqueous solution into nanostructures containing PzLL as the hydrophobic domain and PEtOXA as the hydrophilic block. The CMC values of $PEtOXA_{60}$-ss-$PzLL_{39}$ and $PEtOXA_{60}$-ss-$PzLL_{58}$ are 3.5*10-3 mg/mL and 0.4*10 - 3 mg/mL (Figure 82). In addition, according to the TEM images and DLS results, the self-assembled nanostructures of both $PEtOXA_{60}$-ss-$PzLL_{39}$ and $PEtOXA_{60}$-ss-$PzLL_{58}$ are with diameters of 58 ± 22 nm and 71 ± 20 nm (Figure 83). Because the hydrophobic block and hydrophilic block are connected by a disulfide bond, the self-assembled nanostructures will disassemble in the presence of the reduction agent, DTT. By treating the solution containing of $PEtOXA_{60}$-ss-$PzLL_{39}$ and $PEtOXA_{60}$-ss-$PzLL_{58}$ self-assembles with 10 mM DTT, the diameter of self-assembled nanostructures changed from 160 nm to 650 nm in 2 h, and to 1000 nm in 6 h (Figure 84). Finally, after 24 h, only hydrophobic polymer aggregates were present (Figure 85C).

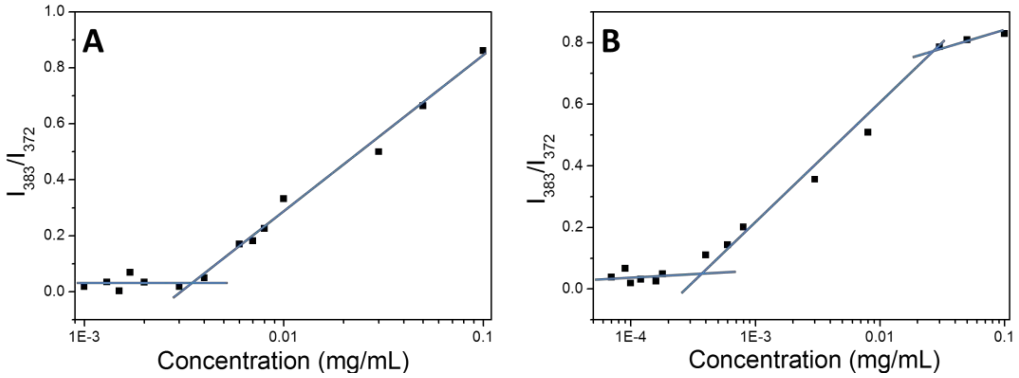

Figure 82. The fluorescence intensity ratio I_{383}/I_{372} of pyrene as a function of PEtOXA$_{60}$-ss-PzLLy copolymer concentration. The intersections are the values of CMC. A. PEtOXA$_{60}$-ss-PzLL$_{39}$; B. PEtOXA$_{60}$-ss-PzLL$_{58}$.

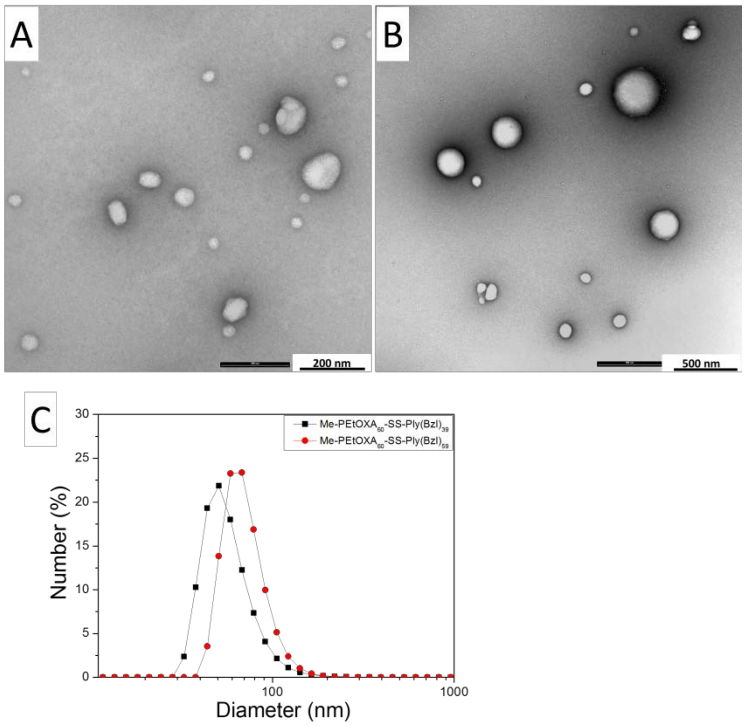

Figure 83. TEM images of self-assemblies of PEtOXA-ss-PzLL. (A). PEtOXA$_{60}$-ss-PzLL$_{39}$; (B). PEtOXA$_{60}$-ss-PzLL$_{58}$ (C). DLS results of self-assemblies of PEtOXA$_{60}$-ss-PzLL$_{39}$ and PEtOXA$_{60}$-ss-PzLL$_{58}$.

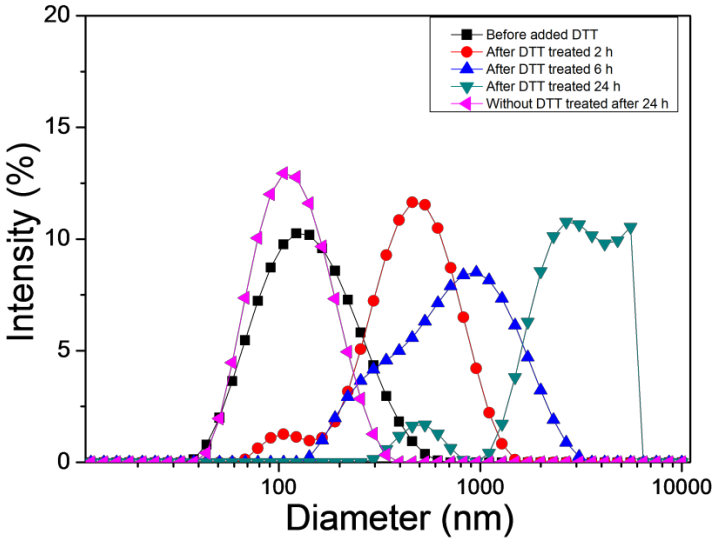

Figure 84. The self-assembled nanostructures size change after DTT was added with finial DTT concentration 10 mM.

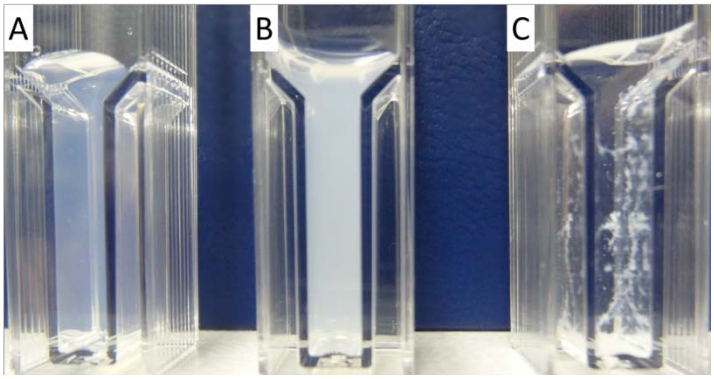

Figure 85. Digital images of nanoparticles treated with DTT with final concentration 10 mM. (A). 2 h after the addition of DTT; (B). 6 h after the addition of DTT; (C). 24 h after the addition of DTT.

4.2.2.3. Reduction responsive property of PEtOXA-*b*-PCL-ss-PzLL.

GPC was used to characterize the reduction responsive property $PEtOXA_{98}$-*b*-PCL_{100}-ss-$PzLL_{83}$. $PEtOXA_{98}$-*b*-PCL_{100}-ss-$PzLL_{83}$ (3 mg) was dissolved in a DMF solution (1.0 mL) containing 10 mM DTT. After 6 h, the sample was measured by GPC. $PEtOXA_{98}$-*b*-PCL_{100}-ss-$PzLL_{83}$ without being treated with DTT showed only one retention peak, while the polymer treated with DTT showed a retention peak corresponding to lower M_n than the polymer itself were indicating the $PEtOXA_{98}$-*b*-PCL_{100} (M_n = 21.1 KDa) and $PzLL_{83}$ (M_n = 25.4 KDa) blocks (Figure 86) cleaved in the presence of DTT.

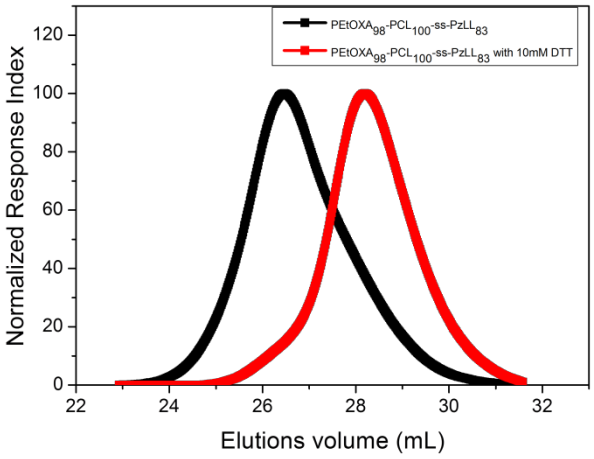

Figure 86. GPC curves of $PEtOXA_{98}$-*b*-PCL_{100}-ss-$PzLL_{83}$ treated with 10 mM DTT in DMF.

4.2.2.4. Reduction responsive property of PEtOXA-*b*-PCL-ss-PzLL self-assemblies.

Due to the amphiphilicity of PEtOXA-*b*-PCL-ss-PLLs, they can self-assemble in aqueous solution. TEM and DLS measurements demonstrated that PEtOXA-*b*-PCL-ss-PLL can self-assemble into nanostructures with diameter around 31 nm (Figure 87) by co-solvent method.

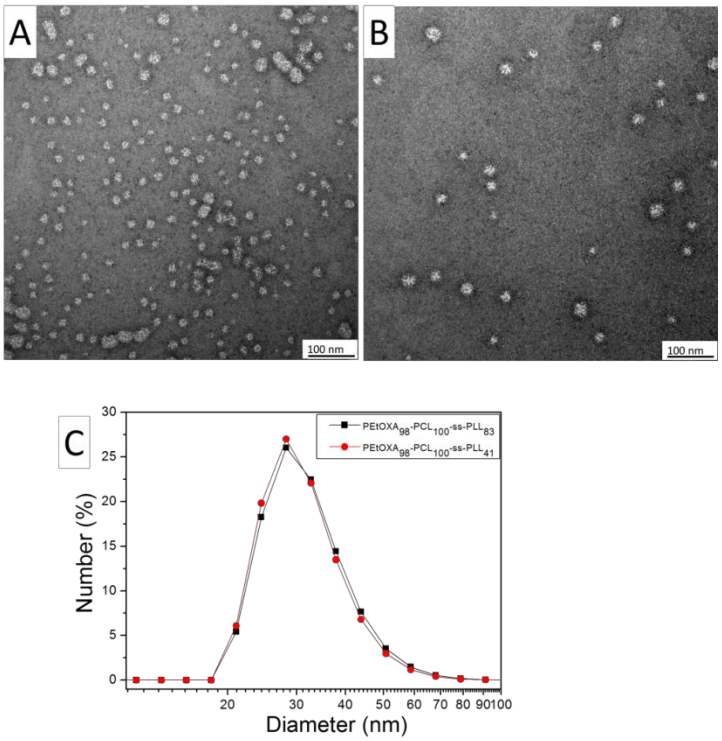

Figure 87. TEM images of self-assemblies of PEtOXA-ss-PzLL. (A). $PEtOXA_{98}$-*b*-PCL_{100}-ss-PLL_{83}; (B). $PEtOXA_{98}$-*b*-PCL_{100}-ss-PLL_{41}; (C). DLS results of self-assemblies of $PEtOXA_{98}$-*b*-PCL_{100}-ss-PLL_{83} and $PEtOXA_{98}$-*b*-PCL_{100}-ss-PLL_{83}.

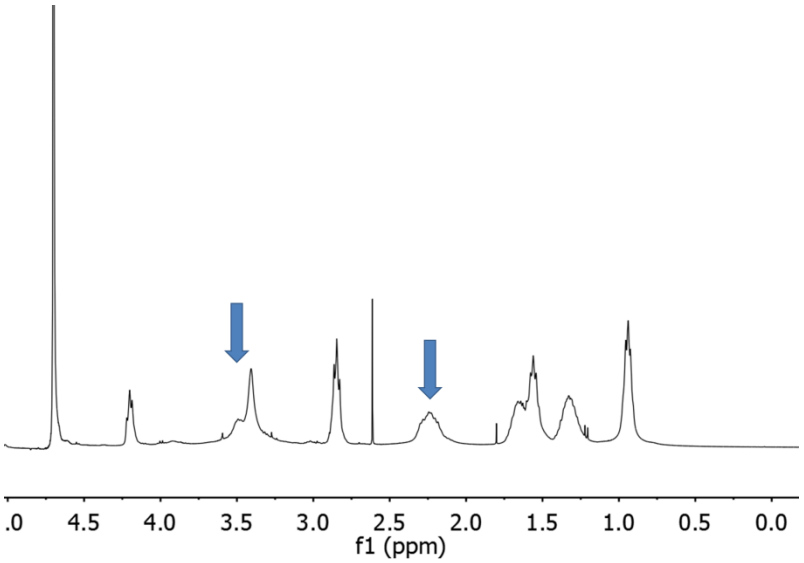

Figure 88. ^{1}H NMR spectrum of PEtOXA-PCL-ss-PLL in D_2O.

The clear proton singles corresponding to PEtOXA in D_2O demonstrate the PEtOXA is water soluble and surround over the hydrophobic PCL core (Figure 88). In addition, the zeta potential measurement showed the zeta potential values are 26 ± 1.4 mV and 13 ± 1.5 mV for PEtOXA$_{98}$-*b*-PCL$_{100}$-ss-PLL$_{83}$ and PEtOXA$_{98}$-*b*-PCL$_{100}$-ss-PLL$_{41}$, respectively (Table 6), proving the presence of positively charged PLL (Pk_a = 9.85 ± 0.20) on the outside surface of self-assembled nanostructures (Figure 89).[210]

The results of NMR, TEM, DLS, and zeta potential proved the self-assembled nanostructures were micelles with hydrophobic PCL as the core surrounded by the hydrophilic PEtOXA and PLL(Figure 89). In the presence of DTT the disulfide bond from PEtOXA$_{98}$-*b*-PCL$_{100}$-ss-PLL$_{41}$ will be reduced and two new polymer blocks will be obtained; one corresponding to the amphiphilic block copolymer PEtOXA$_{98}$-*b*-PCL$_{100}$, and another to homo PLL$_{41}$. Due to the amphiphilic property of PEtOXA$_{98}$-*b*-PCL$_{100}$, the polymer block can re-self-assemble after DTT treatment. As expected, treating 2 mg/mL PEtOXA$_{98}$-*b*-PCL$_{100}$-ss-PLL$_{41}$ self-assembled micelles solution with 10 mM DTT resulted in no change of the self-assembled diameter (Figure 90).

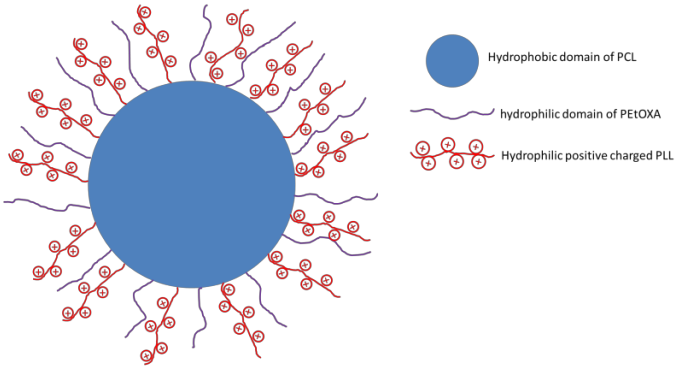

Figure 89. The representation of the PEtOXA-*b*-PCL-ss-PLL formed micelles structure.

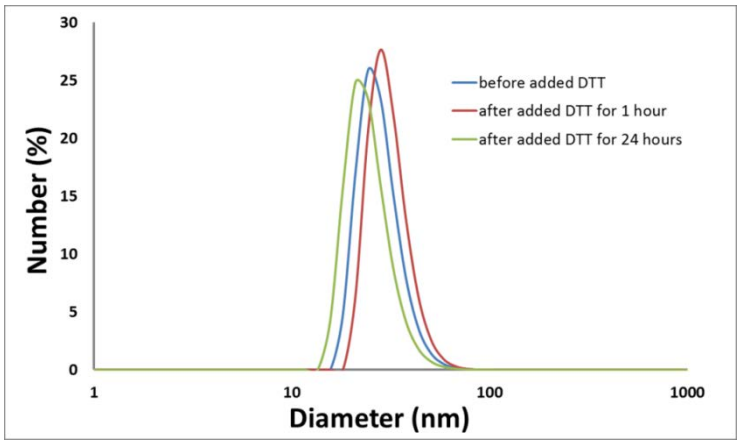

Figure 90. The micelles size change of $PEtOXA_{98}$-*b*-PCL_{100}-ss-PLL_{83} after treated by 10 mM DTT solution.

Table 6. The chemical parameter results of PEtOXA-ss-PzLL and PEtOXA-*b*-PCL-ss-PLL from the measurements of ^{1}H NMR, GPC, and self-assembly results from the measurements of DLS and zeta-potential.

Entry	Name	^{1}H NMR		GPC			DLS		Zeta Potential
		Block ratio	M_n (KDa)	M_n (KDa)	M_w (KDa)	PDI	Diameter (nm)	PDI	(mV)
1	PEtOXA$_x$-ss-PzLL$_y$	60: 39	16.2	18.5	25.7	1.40	58±22		
2	PEtOXA$_x$-ss-PzLL$_y$	60: 58	21.2	24.6	33.1	1.31	71±21		
3	PEtOXA$_x$-*b*-PCL$_y$-ss-PLL$_z$	98:100:83	44.0	24.8	30.0	1.21	32±8.6	0.39	26±1.4
4	PEtOXA$_x$-*b*-PCL$_y$-ss-PLL$_z$	98:100:41	33.0	21.2	24.7	1.17	31±8.5	0.5	13±1.5

4.2.3. The binding of plasmid DNA with PEtOXA-*b*-PCL-ss-PLL self-assembled micelles

Due to the presence of the positive charges on the surface of the self-assembled micelles, PEtOXA-*b*-PCL-ss-PLLs can form a complex with negative DNA in aqueous solution. The results of an electrophoresis band shift assay with the ratio of N/P of 7 between PEtOXA-*b*-PCL-ss-PLLs and DNA proved the DNA can bind with micelles (Figure 91). The free DNA migrated through the gel, however, in presence of the micelles of PEtOXA-*b*-PCL-ss-PLL, the DNA remained in the well indicating binding to the micelles.

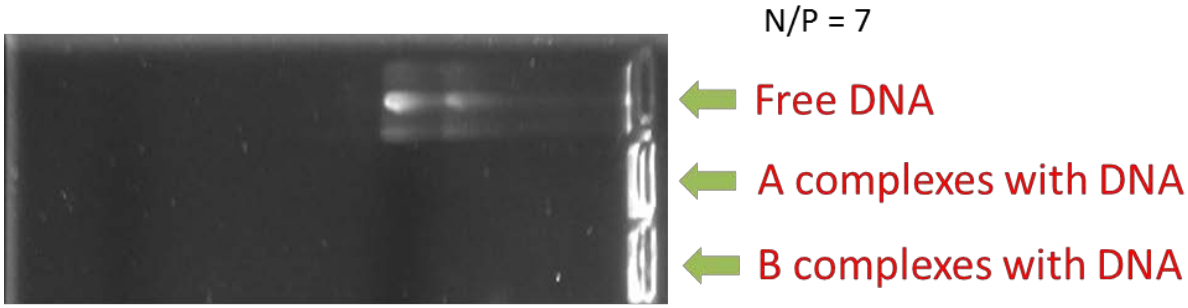

Figure 91. The electrophoresis results of free DNA and PEtOXA-*b*-PCL-ss-PLL micelles and DNA complexation.

4.3. Conclusions

Reduction responsive PEtOXA-*b*-PCL-ss-PLL triblock copolymers have been successfully synthesized through the ring opening polymerization of 2-ethyl-2-oxazoline, ε-caprolactone, and ε-benzyloxycarbonyl-L-lysine N-carboxyanhydride. The results of TEM, DLS, and zeta potential demonstrated that PEtOXA-*b*-PCL-ss-PLL triblock copolymers can self-assembled into micelles with diameter around 30 nm in aqueous solution with the hydrophobic PCL forming the core and hydrophilic PEtOXA and PLL forming the corona of the micelles. The reduction experiments showed that PEtOXA-*b*-PCL-ss-PLL triblock copolymers exhibit reduction responsiveness in the presence of a reducing agent (DTT). Finally, the self-assembled micelles complex negatively charged DNA in a pH 7.4 aqueous solution.

5. General conclusions and outlook

In this work, the synthesis, self-assembly, and application of three types of ABPs were presented. The main conclusions are:

- A library of PDMS-*b*-PMOXA was synthesized. The influence of various parameters, including initial concentration, self-assembly method, buffer, and molecular weight of each block on self-assembly nanostructures has been investigated in details. The 3D phase diagram has been prepared based on the self-assembly nanostructures and molecular weight of PDMS and f_{PMOXA}. In the copolymer system $PDMS_{65}$-*b*-$PMOXA_{10-38}$, we found the same diameter changing trend of self-assembled nanostructures with PBD-*b*-PEG system reported by S Förster et al.[147, 211] In addition, we found a "new" self-assembled nanostructure with similar size of polymersome (80 nm-100 nm) with "non-hollow" cavity. Due the resolution limitation of Cyro-TEM and SAXS, the clear inner structure is still unknown. For $PDMS_{39}$-*b*-$PMOXA_{6-22}$ and $PDMS_{16}$-b-$PMOXA_{2-10}$, surprisingly, we did not found the self-assembled polymersome. In addition, the M_n of copolymer are still lower than 10 KDa, stickily speaking, they are oligomers, so it is quite difficult to predict the changing trend in the case of copolymers with high M_n.
- The grafted shaped ABPs PMOXA-graft(ss)-PCL was synthesized by combining the cationic polymerization, coordination insertion polymerization, and thiol-disulfide exchange reaction methods. The synthesized PMOXA-graft(ss)-PCLs and their corresponding self-assembly nanoparticles show reduction responsiveness as proved by ^{1}H NMR, TEM, DLS, and FCS. In addition, the loaded molecules in the self-assembled nanoparticles can be released in the presence of reducing agents. Cell culture experiments showed that introduction of the disulfide group into the ABPs enhance the overall performance as smart nanocarriers in the drug delivery.
- The reduction responsive triblock ABPs PEtOXA-*b*-PCL-ss-PLLs were synthesized through cationic polymerization, coordination insertion polymerization, and ROP polymerization methods. The ^{1}H NMR and GPC results demonstrated right chemical structure. The DLS, TEM, and zeta-potential results showed that these ABPs can self-assemble into micelles in aqueous solutions with PCL forming the core and hydrophilic PLL and PEtOXA as the shell. The primary electrophoresis result

demonstrated that negatively charged DNA can bind on self-assembled micelles, which indicated that this reduction responsive triblock ABPs PEtOXA-*b*-PCL-ss-PLLs can be promising candidates for gene delivery. However, this system still cannot mimic the virus perfectly. The main reason that virus is a high efficacy gene carrier is that after it is uptake by cells, in the lower pH endosome, a protein segment will change from hydrophilic to hydrophobic, which can help the gene escape from endosome in a very short time.[100] For our PEtOXA-PCL-ss-PLL system, even though the PLL separates from the copolymer, the hydrophobic PCL still cannot be exposed outside and function as disturber in the endosome. Because PEtOXA-PCL still keeps the amphiphilic property. This process cannot accelerate the escape of gene from endosome; only accelerate the separation of gene from the copolymer complex.

Basing on the above results, the following directions are suggested to be further investigated:

- Use PDMS with PDIs 1.5-2.0, rather than 1.0-1.1, to synthesize the ABPs PDMS-*b*-PMOXA and investigate the influence of PDIs of PDMS on the self-assembled structures. It is because the fact that increasing the PDI of hydrophobic block can really influence the final self-assembly nanostructures in bulk and in solution.[212, 213] For example, Adi Eisenberg et al investigated the ABP system polystyrene-*block*-poly(acrylic acid) (PS-*b*-PAA), they found the diameters of self-assembled nanostructures decreased from 365±230 nm to 85±15 nm (apparent mass fraction of vesicles from 100% to 63%) with increasing the PDI of PAA from 1.37 to 2.13.[53]
- For the ABPs PEtOXA-*b*-PCL-ss-PLLs, a more detailed investigation of micelles as gene delivery carriers should be done, including cytotoxicity measurements of the polymers, characterization of nanostructures of PEtOXA-*b*-PCL-ss-PLLs after complexation with genes by TEM, DLS, and zeta potential, and the overall evaluation of the performance of PEtOXA-*b*-PCL-ss-PLLs as gene delivery nanocarrier.
- Basing on the PEtOXA-*b*-PCL-ss-PLLs platform, it may be interesting to synthesize dual responsive triblock ABPs, for example adding a pH responsive linker between PEtOXA and PCL, which is also a possible way to enhance the overall performance of ABPs as the gene delivery nanocarriers.

6. Experimental part

6.1. Materials

2-Mercaptoethanol (≥99%, Aldrich), 2-(Boc-amino)ethanethiol (97%, Aldrich), 2-methyl-2-oxazoline (98%, Aldrich),), 2-ethyl-2-oxazoline (≥99%, Aldrich), Tin(II) 2-ethylhexanoate (92.5-100.0%, Aldrich), triethylamine (≥99%, Aldrich), phenyl disulfide (99%, Aldrich), succinic anhydride (≥99%, Aldrich), trifluoromethanesulfonic anhydride (≥99%, Aldrich), hexamethylcyclotrisiloxane (D3) (98%, Aldrich), calcium hydroxide (95%, Aldrich), platinum(0)-1,3-divinyl-1,1,3,3-tetramethyldisiloxane complex (Pt(dvs)) solution in xylene (Pt ~2 %, Aldrich), 2-allyloxyethanol (98%, Aldrich), ε-benzyloxycarbonyl-L-lysine ((≥99%, Aldrich), chlorodimethylsilane (98%, Aldrich), n-butyllithium solution (2.5 M in cyclohexane, Aldrich), activated carbon (Fluka), molecular sieve 4 Å (Chemie Uetikon AG, Switzerland), 5-doxylstearic acid (5-DSA) and 16-doxylstearic acid (16-DSA), N,N-Diisopropylethylamine (99.5%, Aldrich), methyl trifluoromethanesulfonate (≥ 98%, Sigma), ε-caprolactone (≥ 99%, Sigma), potassium thioacetate (98%, Sigma), triphenylphosphine (99%, Sigma), Tin(II) 2-ethylhexanoate (~95%, Sigma), Pd/C (10 wt. %, Sigma), 2-pyridylthio cysteamine hydrochloride (≥ 97%, Activate Scientific), N,N'-dicyclohexylcarbodiimide (99%, sigma), 4-dimethylaminopyridine (≥ 99%, sigma), Dox.HCl (98%, Beijing Zhongshuo Pharmaceutical Technology Development Co., Ltd.), trifluoroacetic acid (99%, Sigma), acetic acid (≥ 99.8%, Fluka), hydrobromic acid solution (33 wt. % in acetic acid, Sigma), anhydrous meOH (≥99.5%, Sigma), anhydrous DMF (99.8%, Sigma), anhydrous EtOH (≥99.5%, Sigma), diethyl ether (≥99.9%, Sigma), ethyl acetate (≥99.8%, Sigma), dichloromethane (≥99.9%, Sigma), toluene (≥99.9%, Sigma), PBS buffer (pH=7.2, life technologies). Dichloromethane, acetonitrile, toluene, triethylamine and chloroform with 100-200 ppm amylenes as stabilizers were freshly refluxed with calcium hydroxide under argon. Tetrahydrofuran (THF) and cyclohexane were refluxed with sodium and benzophenone under argon. Triton X-100 (Fluka) was used as a 1% solution in distilled water. Other chemicals and solvents were used directly without any purification.

6.2. Copolymer synthesis procedures

6.2.1. Synthesis of PDMS-*b*-PMOXA diblock copolymer

Monocarbinol Poly(dimethylsiloxane) (PDMS-OH). Fresh dried hexamethylcyclotrisiloxane (D_3) (69.12 g, 310.71 mmol) was distilled into a dried three necks round flask under vacuum. Fresh dried and distilled cyclohexane (110 mL) and n-buty lithium solution (9.52 mL, 23.91 mmol) were added successively at the room temperature under argon atmosphere. After 4.5 hours, fresh dried and distilled THF (12 mL) was added under argon atmosphere. After 40 hours, dimethylchlorosilane (8.5 mL, 76.57 mmol) was added to quench the reaction. The white LiCl salt was filtrated in 4 hours, and then the solvent and unreacted D_3 were distilled under high pressure in order to yield the 1. 1 (5.2 g, 2 mmol) was dissolved in fresh distilled toluene first, then 2-allyloxyethanol (0.25g, 2.1 mmol) and Pt(dvs) (2.28 µL) were added successively. The mixture was stirred overnight at 110 °C under inert atmosphere. After removal of the toluene, dichloromethane and the activated carbon were added and the final product was filtrated to yield the PDMS-OH as colorless oil. ^{1}H NMR (400 MHz, δ, $CDCl_3$): 0 ppm (m, -Si(CH_3)$_2$), 0.54 ppm (m, -SiCH_2), 0.88 ppm (t, -CH_3), 1.31 (m, -CH_2-CH_2-), 1.62 (m, -SiCH$_2$-CH_2-CH$_2$O-), 3.44 ppm (t, -CH_2-O-), 3.54 ppm (t, -O-CH_2-), 3.72 ppm (t, -CH_2-OH).

PDMS-OTf and PDMS-*b*-PMOXA. PDMS-OH (10.71g, 2.142 mmol) was put into a three-neck, round-bottomed flask and dried under stirring over night at 120 °C in high vacuum. Dry toluene was added under argon atmosphere and the solution was dried for 24 hours by reflux in a Soxleth apparatus containing a molecular sieve 4 Å. After cooling to room temperature, fresh dried and distilled triethylamine was added. The solution was cooled to 0 °C and trifluoromethanesulfonic anhydride in 20 mL of dry toluene was added slowly over 30 minutes. The mixture was reacted for another 3 hours at 0 °C. Then the mixture was separated from triflate salt by filtration through a glass frit. After evaporating the toluene, fresh dried and distilled chloroform (65 mL), acetonitrile (28 mL) and 2-methyl-2-oxazoline (4.19 g, 49.27 mmol) were added successively. The reaction mixture was stirred for 60 h at 40 °C. Finally, the solution was cooled to room temperature, triethylamine (20 mL) and H_2O (20 mL) were added to quench the reaction. The polymer was dissolved in ethanol, subsequently the ethanol solution was transferred into a solvent-resistant, stirred ultrafiltration device (Millipore, USA) equipped with a 3000 MWCO regenerated cellulose

membrane (Millipore, USA) and extensively washed with ethanol and H_2O mixture for six times to yield transparent, rubber-like PDMS-*b*-PMOXA-OH diblock copolymer.

PDMS-OTf: ^{1}H NMR (400 MHz, δ, $CDCl_3$): 0 ppm (m, -Si(C*H*$_3$)$_2$), 0.54 ppm (m, -SiC*H*$_2$), 0.88 ppm (t, -C*H*$_3$), 1.31 (m, CH$_3$-C*H*$_2$-C*H*$_2$-), 1.62 (m, -Si-CH$_2$-C*H*$_2$-CH$_2$-O-), 3.45 ppm (t, -C*H*$_2$-O-), 3.75 ppm (t, -O-C*H*$_2$-), 4.62 ppm (t, -C*H*$_2$-OTrf).

PDMS-*b*-PMOXA: ^{1}H NMR (400 MHz, δ, $CDCl_3$): 0 ppm (m, -Si(C*H*$_3$)$_2$), 0.54 ppm (m, -SiC*H*$_2$), 0.88 ppm (t, -C*H*$_3$), 1.31 ppm (m, -C*H*$_2$-C*H*$_2$-), 1.62 ppm (m, -SiCH$_2$-C*H*$_2$-CH$_2$O-), 2.08-2.21 ppm (m, C*H*$_3$-C=O), 3.40-3.60 ppm (m, -C*H*$_2$-O-C*H*$_2$-C*H*$_2$-N-C*H*$_2$-C*H*$_2$-), 3.75 ppm (t, -C*H*$_2$-OH).

6.2.2. PMOXA-graft(ss)-PCL copolymer synthesis

6.2.2. Synthesis of PMOXA-graft(ss)-PCL graft copolymer

Poly(2-methyl-2-oxazoline) thioacetate (PMOXA-SAc). Methyl trifluoromethanesulfonate (120 mg, 0.73 mmol) and 2-methyl-2-oxazoline (5 g, 58.8 mmol) were dissolved in distilled acetonitrile (30 mL) and the polymerization was carried out at 80 °C for 18 h under argon atmosphere. The polymerization was terminated by the addition of potassium thioacetate (0.6 g, 3.74 mmol) at RT and the mixture was further stirred for another 24 h under argon. The excess of potassium thioacetate was filtered away and the produc,t PMOXA-SAc, was purified by precipitation in cold diethyl ether. The obtained precipitatant was dissolved in ddH_2O and dialyzed against ddH_2O for another 48 h to yield 4.6 g colorless PMOXA-SAc with a yield of 92%. ^{1}H NMR (d6-DMSO): δ = 1.98 ppm (C*H*$_3$-(C=O)), 2.34-2.37 ppm (S(O=C)-C*H*$_3$), 2.94 ppm (-C*H*$_2$-S-), 2.99 ppm (C*H*$_3$-N-), 3.35-3.47 ppm (-C*H*$_2$-C*H*$_2$-N).

Thiolated poly(2-methyl-2-oxazoline) (PMOXA-SH). PMOXA-SAc (200 mg, 0.03 mmol) was dissolved in anhydrous MeOH (10 mL), and triphenylphosphine (56 mg, 0.22 mmol) was added. The solution was stirred for another 48 h at RT under argon atmosphere. Afterwards, the reaction mixture was precipitated twice in cold diethyl ether, and 170 mg of light pink PMOXA-SH was obtained with a yield of 85%. ^{1}H NMR (d6-DMSO): δ = 1.98 ppm (C*H*$_3$-(C=O)), 2.94 ppm (-C*H*$_2$-S-), 2.99 ppm (C*H*$_3$-N-), 3.34-3.74 ppm (-C*H*$_2$-C*H*$_2$-N).

Poly(ε-caprolactone)-co-poly(α-benzyl carboxylate-ε-caprolactone) (PCL-*co*-PBCL). Anhydrous EtOH (20.5 µL) was mixed with freshly distilled toluene (25 mL), followed by addition of ε-caprolactone (4.12 g, 36.1 mmol) and α-benzyl carboxylate-ε-caprolactone (0.85 g, 3.4 mmol) which was synthesized according to previously published procedure.[199] Subsequently, Tin(II) 2-ethylhexanoate (4 µL) was added to the above reaction mixture.

Finally, the reaction was carried out at 110 °C under argon atmosphere for 24 h. After the polymerization, the polymer was precipitated twice in diethyl ether to obtain 4.1 g of colorless poly(ε-caprolactone)-co-poly(α-benzyl carboxylate-ε-caprolactone) (PCL-*co*-PBCL) with a yield of 82%. ^{1}H NMR ($CDCl_3$): δ = 1.19 ppm (CH_3-CH_2-O-), 1.31 ppm ((C=O)-CH_2-CH_2-CH_2-CH_2-CH_2-O-), 1.56 ppm ((C=O)-CH_2-CH_2-CH_2-CH_2-CH_2-O-), 1.87 ppm (C_6H_6-CH_2-(COO)-CH-CH_2-), 2.22 ppm ((C=O)-CH_2-CH_2-CH_2-CH_2-CH_2-O-), 3.33 ppm (C_6H_6-CH_2-(COO)-CH-CH_2-), 3.97 ppm ((C=O)-CH_2-CH_2-CH_2-CH_2-CH_2-O-), 5.23 ppm (C_6H_6-CH_2-), 7.26 ppm (C_6H_6-CH_2-).

Poly(ε-caprolactone)-co-poly(α-carboxylic acid-ε-caprolactone) (PCL-*co*-PCCL). PCL-*co*-PBCL (2 g, 0.11 mmol) was first dissolved in deoxygenated ethyl acetate (20 mL), and then Pd/C (600 mg) was added. Finally, the solution was stirred for 42 h at RT under hydrogen atmosphere. After the reaction was complete, the sample was centrifuged in order to remove the catalyst Pd/C, and was precipitated twice in cold diethyl ether to purify the polymer. 1.70 g of colorless PCL-*b*-PCCL was obtained with a yield of 85%. ^{1}H NMR ($CDCl_3$): δ = 1.27 ppm (CH_3-CH_2-O-), 1.41 ppm ((C=O)-CH_2-CH_2-CH_2-CH_2-CH_2-O-), 1.67 ppm ((C=O)-CH_2-CH_2-CH_2-CH_2-CH_2-O-), 1.95 ppm (HOOC-CH-CH_2-), 2.34 ppm ((C=O)-CH_2-CH_2-CH_2-CH_2-CH_2-O-), 3.37 ppm (HOOC-CH-CH_2-), 4.07 ppm ((C=O)-CH_2-CH_2-CH_2-CH_2-CH_2-O-).

Poly(ε-caprolactone)-*co*-poly(α-pyridyldisulfide-ε-caprolactone) (PCL-*co*-PPCL). PCL-*co*-PCCL (500 mg, 0.028 mmol), 2-pyridylthiol cysteamine hydrochloride (60 mg, 0.27 mmol) and triethylamine (104 µL) were dissolved in freshly distilled dichloromethane (20 mL), and then N,N'-dicyclohexylcarbodiimide (100 mg, 0.48 mmol) and 4-dimethylaminopyridine (10 mg, 0.082 mmol) were added. The reaction was carried out at RT under argon atmosphere for 60 h. The mixture was precipitated in cold diethyl ether twice, yielding 300 mg of colorless PCL-*co*-PPCL with a yield of 60%. ^{1}H NMR ($CDCl_3$): δ = 1.26 ppm (CH_3-CH_2-O-), 1.34 ppm ((C=O)-CH_2-CH_2-CH_2-CH_2-CH_2-O-), 1.65 ppm ((C=O)-CH_2-CH_2-CH_2-CH_2-CH_2-O-), 1.98 ppm (-NH-(C=O)-CH-CH_2-), 2.30 ppm ((C=O)-CH_2-CH_2-CH_2-CH_2-CH_2-O-), 2.93 ppm (-SS-CH_2-CH_2-), 3.54 ppm (-NH-(C=O)-CH-CH_2-), 3.65 ppm (-SS-CH_2-CH_2-), 4.05 ppm ((C=O)-CH_2-CH_2-CH_2-CH_2-CH_2-O-), 7.0-8.6 ppm (-SS-C_6H_4N).

Poly(2-methyl-2-oxazoline)-graft(ss)-poly(ε-caprolactone) (PMOXA-graft(ss)-PCL). PCL-*co*-PPCL (120 mg, 0.0067 mmol) and PMOXA-SH (290 mg, 0.038 mmol) were dissolved in dimethylformamide (10 mL), and acetic acid (200 µL) was added all at once. The solution was stirred at RT under argon atmosphere for 72 h. The copolymer was purified by precipitation in cold MeOH and produced 100 mg of a white solid product with a yield of 38%. ^{1}H NMR

($CDCl_3$): δ = 1.26 ppm (CH_3-CH_2-O-), 1.38 ppm ((C=O)-CH_2-CH_2-CH_2-CH_2-CH_2-O-), 1.64 ppm ((C=O)-CH_2-CH_2-CH_2-CH_2-CH_2-O-), 2.11 ppm (-(C=O)-CH_3), 2.30 ppm ((C=O)-CH_2-CH_2-CH_2-CH_2-CH_2-O-), 2.84 ppm (-CH_2-SS-CH_2-), 3.05 ppm (CH_3-N(C=O)-), 3.46 ppm (-N-CH_2-CH_2-N-), 4.06 ppm ((C=O)-CH_2-CH_2-CH_2-CH_2-CH_2-O-).

6.2.3. Synthesis of PEtOXA-PCL-ss-PLL amphiphilic triblock copolymer

Tert-butyl N-(2[(2-hydroxyethyl)disulfanyl]ethyl)carbamate. 2-(2-(pyridin-2-yl)disulfanyl)ethanol was synthesized according to the method previously published.[214] 2-(2-(pyridin-2-yl)disulfanyl)ethanol (0.6 g, 3.2 mmol) was first dissolved in a mixture of MeOH (8 mL) and DCM (8 mL). Then N-(tert-butoxycarbonyl)-2-aminoethanethiol (1.62 mL, 9.6 mmol) was added and the reaction mixture was deoxygenated by vacuum argon cycles, the reaction was carried out at RT for 20 h under argon. The reaction was quenched by adding 0.05 g/mL I_2/MeOH and a color change from colorless to brown was observed. For purification, the reaction mixture was washed with brine twice, and the organic phase was collected and dried with Na_2SO_4. Finally, the product was purified by column chromatography with silica as the solid phase using a mixture of hexane and ethyl acetate (V/V = 2/1) as the running phase. 0.7 g colorless oil product was obtained with a yield of 87.5%. ^{1}H NMR ($CDCl_3$): δ = 4.97 ppm (br, 1H), 3.89 ppm (t, 2H), 3.46 ppm (q, 2H), 2.88 ppm (t, 2H), 2.81 ppm (t, 2H), 1.45 ppm (s, 2H). ^{13}C NMR ($CDCl_3$): δ = 156 ppm, 80 ppm, 60 ppm, 42 ppm, 39 ppm, 38 ppm, 28 ppm.

Poly(2-ethyl-2-oxazoline)-OH. Methyl trifluoromethanesulfonate (109 µL, 0.99 mmol) was dissolved in anhydrous acetonitrile (100 ml), and then 2-ethyl-2-oxazoline (10 mL) was added. After deoxygenating, the polymerization was initiated and further carried out at 80 °C for 24 h under argon. After polymerization, the reaction mixture was cooled down to RT and a KOH/MeOH solution (0.5 M) (10 mL) was added in order to quench the reaction. 9 g of a colorless solid polymer was obtained by precipitation from diethyl ether with a yield of 90%. ^{1}H NMR ($CDCl_3$): δ = 3.45 ppm (br, N-CH_2-CH_2-), 2.2-2.41 ppm (br, O=C(N)-CH_2-CH_3), 1.12 ppm (O=C(N)-CH_2-CH_3).

Poly(2-ethyl-2-oxazoline)-*block*-poly(ε-caprolactone)-OH. Lyophilized PEtOXA-OH (3.18 g) was first mixed with freshly distilled ε-caprolactone (4.53 mL, 41.2 mmol), then, freshly distilled toluene (80 °C) (200 mL) was added to dissolve the PEtOXA-OH and ε-caprolactone. Finally, stannous octoate (30 µL, 0.09 mmol) was added to the polymerization medium. After deoxygenation, the polymerization was carried out at 110 °C for 24 h under argon. 6 g of a colorless solid was obtained by precipitation from diethyl ether twice in a 78% yield. ^{1}H NMR

($CDCl_3$): δ = 4.06 ppm (t, CH_2-(O) C=O), 3.65 ppm (t, CH_2-OH), 3.45 ppm (br, N-CH_2-CH_2-), 2.2.-2.41 ppm (br, O=C(N)-CH_2-CH_3), 2.31 ppm (t, O=C(O)-CH_2-CH_2-CH_2-CH_2-), 1.66 ppm (br, O=C(O)-CH_2-CH_2-CH_2-CH_2-), 1.38 ppm (m, OC(O)-CH_2-CH_2-CH_2-CH_2-), 1.12 ppm (O=C(N)-CH_2-CH_3).

Poly(2-ethyl-2-oxazoline)-*block*-poly(ε-caprolactone)-COOH (PEtOXA-*b*-PCL-COOH). PEtOXA-*b*-PCL-OH (2 g) was first dissolved in anhydrous chloroform (25 mL). Then succinic anhydride (84 mg, 0.84 mmol), triethylamine (150 µL, 1.08 mmol) and DMAP (6 mg, 0.05 mmol) were added. After deoxygenation, the reaction was carried out at RT for 72 h under argon. Finally, 1.82 g of polymer was obtained by precipitation in diethyl ether with a yield of 91%. ^{1}H NMR ($CDCl_3$): δ = 4.06 ppm (t, CH_2-(O)C=O), 3.46 ppm (br, N-CH_2-CH_2-), 2.63 ppm (-CH_2-CH_2-COOH), 2.2.-2.41 ppm (br, O=C(N)-CH_2-CH_3), 2.33 ppm (t, O=C(O)-CH_2-CH_2-CH_2-CH_2-), 1.66 ppm (br, O=C(O)-CH_2-CH_2-CH_2-CH_2-), 1.38 ppm (m, O=C(O)-CH_2-CH_2-CH_2-CH_2-), 1.12 ppm (O=C(N)-CH_2-CH_3).

Poly(2-ethyl-2-oxazoline)-*block*-poly(ε-caprolactone)-ss-NHBoc (PEtOXA-*b*-PCL-ss-NHBoc). PEtOXA-*b*-PCL-COOH (1.05 g) was first dissolved in anhydrous chloroform. Then, tert-butyl N-(2[(2-hydroxyethyl)disulfanyl]ethyl)carbamate (85 mg, 0.34 mmol), DCC (130 mg, 0.63 mmol) and DMAP (2 mg, 0.016 mmol) were added. After deoxygenation, the reaction was carried out at RT for 72 h under argon. Finally, 865 mg PEtOXA-*b*-PCL-ss-NHBoc was obtained by precipitation in diethyl ether with a yield of 86.5%. ^{1}H NMR ($CDCl_3$): δ = 4.04 ppm (t, CH_2-(O)C=O), 3.45 ppm (br, N-CH_2-CH_2-), 2.91 ppm (-CH_2-SS-CH_2-), 2.64 ppm (O=C(O)-CH_2-CH_2-(O)C=O), 2.2.-2.41 ppm (br, O=C(N)-CH_2-CH_3), 2.31 ppm (t, O=C(O)-CH_2-CH_2-CH_2-CH_2-), 1.66 ppm (br, O=C(O)-CH_2-CH_2-CH_2-CH_2-), 1.44 ppm (s, (CH_3)-C-), 1.38 ppm (m, O=C(O)-CH_2-CH_2-CH_2-CH_2-), 1.12 ppm (O=C(N)-CH_2-CH_3).

Poly(2-ethyl-2-oxazoline)-*block*-poly(ε-caprolactone)-ss-NH_2.TFA (PEtOXA-*b*-PCL-ss-NH_2.TFA). PEtOXA-*b*-PCL-ss-NHBoc was dissolved in TFA (10 mL), and then the solution was stirred for 1.5 h at 0 °C. 821 mg of a colorless solid was obtained by precipitation from diethyl ether with a yield of 95%. ^{1}H NMR ($CDCl_3$): δ = 4.36 ppm (t, NH_2-CH_2-), 4.04 ppm (t, CH_2-(O)C=O), 3.45 ppm (br, N-CH_2-CH_2-), 2.94, 3.03 ppm (-CH_2-SS-CH_2-), 2.64 ppm (O=C(O)-CH_2-CH_2-(O)C=O), 2.2-2.41 ppm (br, O=C(N)-CH_2-CH_3), 2.31 ppm (t, O=C(O)-CH_2-CH_2-CH_2-CH_2), 1.66 ppm (br, O=C(O)-CH_2-CH_2-CH_2-CH_2-), 1.38 ppm (m, O=C(O)-CH_2-CH_2-CH_2-CH_2-), 1.12 ppm (O=C(N)-CH_2-CH_3).

Poly(2-ethyl-2-oxazoline)-*block*-poly(ε-caprolactone)-ss-poly(ε-benzyloxycarbonyl-L-lysine) (PEtOXA-*b*-PCL-ss-PzLL). PEtOXA-*b*-PCL-ss-NH_2.TFA (98 mg) was first dissolved in anhydrous DMF (4.5 mL). Then DIPEA (10 µL) and ε-benzyloxycarbonyl-L-lysine N-carboxyanhydride (138 mg) were added.[215] After deoxygenation, the reaction was carried out at RT for 72 h under argon. 180 mg of a colorless solid was obtained by precipitation in diethyl ether with a yield of 83%. ^{1}H NMR ($CDCl_3$): δ = 8.24 ppm (br, N*H*-C=O), 7.26 ppm (m, -C_6H_5), 4.99 ppm (br, C_6H_5-CH_2-), 4.06 ppm (t, CH_2-(O)C=O), 3.46 ppm (br, N-CH_2-CH_2-), 3.10 ppm (br, C_6H_5-CH_2-O-C(=O)-NH_2-CH_2-), 2.86 ppm (-CH_2-SS-CH_2-), 2.58 ppm (O=C(O)-CH_2-CH_2-(O)C=O), 2.2-2.43 ppm (br, O=C(N)-CH_2-CH_3), 2.31 ppm (t, O=C(O)-CH_2-CH_2-CH_2-CH_2-), 1.39-1.88 ppm (br, NH-C(=O)-CH-CH_2-CH_2-CH_2-), 1.63 ppm (br, O=C(O)-CH_2-CH_2-CH_2-CH_2-), 1.39 ppm (m, O=C(O)-CH_2-CH_2-CH_2-CH_2-), 1.12 ppm (m, O=C(N)-CH_2-CH_3).

Poly(2-ethyl-2-oxazoline)-*block*-poly(ε-caprolactone)-ss-poly(L-lysine) (PEtOXA-*b*-PCL-ss-PLL). PEtOXA-*b*-PCL-ss-PzLL (240 mg) was dissolved in TFA (15 mL), then a HBr in acetic acid solution (33%) (5mL) was added drop wise at 0 °C. The solution was further stirred for another 1 h at 0 °C. The product was precipitated in diethyl ether and then dissolved in DMSO. The DMSO solution was dialyzed against ddH_2O for 48 h, changing the ddH_2O three times. After lyophilizing, a white powder (180 mg) was obtained with a yield of 85%. ^{1}H NMR (d_6-DMSO): 4.25 ppm (br, NH-(C=O)-C*H*-), 4 ppm (m, CH_2-O-C=O), 3.45 ppm (br, N-CH_2-CH_2-), 2.96 ppm (m, -CH_2-SS-CH_2-), 2.75 ppm (-CH_2-NH_2), 2.26 ppm (br, O=C(N)-CH_2-CH_3 and -O-(C=O)-CH_2-CH_2-CH_2-CH_2-), 1.30-1.54 ppm (-O-(C=O)-CH_2-CH_2-CH_2-CH_2- and –CH_2-CH_2-CH_2-CH_2-NH_2), 0.95 ppm (m, O=C(N)-CH_2-CH_3).

6.2.4. Synthesis of PEtOXA-ss-PLL and PEtOXA-PLL control copolymers.

Poly(2-ethyl-2-oxazoline) disulfide amine (PEtOXA-ss-NH_2). PEtOXA-SAc and PEtOXA-ss-Py were synthesized according to the method described in the literature.[198] PEtOXA-ss-Py (1 g) was first dissolved in MeOH (20 mL), and then cysteamine (279 mg, 3.62 mmol) was added. After deoxygenation, the reaction was carried out at RT for 48 h under argon. Finally, 0.96 g of a colorless solid polymer was obtained by precipitation in diethyl ether twice with a yield of 96%. ^{1}H NMR ($CDCl_3$): δ = 4.16 ppm (s, -CH_2-NH_2), 3.45 ppm (br, N-CH_2-CH_2-), 3.03 ppm (CH_3-CH_2-CH_2-), 2.84 ppm (-CH_2-SS-CH_2-), 2.31-2.41 ppm (br, O=C(N)-CH_2-CH_3), 1.12 ppm (O=C(N)-CH_2-CH_3).

Poly(2-ethyl-2-oxazoline)-ss-poly(ε-benzyloxycarbonyl-L-lysine) (PEtOXA-ss-PzLL). PEtOXA-ss-NH_2 (102 mg) was first dissolved in anhydrous DMF (3 mL), and then ε-benzyloxycarbonyl-

L-lysine N-carboxyanhydride (205 mg, 0.67 mmol) was added. After deoxygenation, the polymerization was carried out at RT for 48 h under argon. 253 mg of a colorless polymer was obtained by precipitation from diethyl ether with a yield of 82.4%. ^{1}H NMR ($CDCl_3$): δ = 8.22 ppm (br, N*H*-C=O), 7.23 ppm (m, -C_6H_5), 5.47 ppm (br, O=C-N*H*-), 4.99 ppm (br, C_6H_5-CH_2-), 3.45 ppm (br, N-CH_2-CH_2-), 3.10 ppm (br, C_6H_5-CH_2-O-C(=O)-NH_2-CH_2-), 2.86 ppm (-CH_2-SS-CH_2-), 2.29.-2.41 ppm (br, O=C(N)-CH_2-CH_3), 1.26-2.10 ppm (br, NH-C(=O)-CH-CH_2-CH_2-CH_2-), 1.12 ppm (O=C(N)-CH_2-CH_3).

Poly(2-ethyl-2-oxazoline)-ss-poly(L-lysine) (PEtOXA-ss-PLL). PEtOXA-ss-PzLL (419 mg) was dissolved in TFA (15 mL), then HBr in acetic acid solution (33%) (4 mL) at 0 °C was added dropwise. The solution was stirred for another 1 h at 0 °C. The product was precipitated in diethyl ether and then dissolved in DMSO. The DMSO solution was further dialyzed against ddH_2O for 48 h changing ddH_2O three times. After lyophilizing, a white powder (300 mg) was obtained with a yield of 80%. ^{1}H NMR (D_2O): δ = 4.24 ppm (t, NH-C(=O)-C*H*-), 3.27-3.64 ppm (br, N-CH_2-CH_2-), 2.93 ppm (t, NH_2-CH_2-), 2.27 ppm (m, O=C(N)-CH_2-CH_3), 1.25-1.82 ppm (NH_2-CH_2-CH_2-CH_2-CH_2-), 0.97 ppm (m, O=C(N)-CH_2-CH_3).

Poly(2-ethyl-2-oxazoline)-*block*-poly(ε-benzyloxycarbonyl-L-lysine) (PEtOXA-*b*-PzLL). PEtOXA-NH_2 (150 mg) was synthesized according with the previously published procedure,[216] was dissolved in anhydrous DMF (10 mL), and further ε-benzyloxycarbonyl-L-lysine N-carboxyanhydride (126 mg, 0.41 mmol) was added in the solution mixture After deoxygenation, the reaction was carried out at RT for 50 h under argon. Finally, 242 mg colorless polymer was obtained after precipitation in diethyl ether twice with a yield of 94%. ^{1}H NMR ($CDCl_3$): δ = 8.21 ppm (br, N*H*-C=O), 7.23 ppm (m, -C_6H_5), 5.46 ppm (br, O=C-N*H*-), 4.99 ppm (br, C_6H_5-CH_2-), 3.45 ppm (br, N-CH_2-CH_2-), 3.10 ppm (br, C_6H_5-CH_2-O-C(=O)-NH_2-CH_2-), 2.20-2.48 ppm (br, O=C(N)-CH_2-CH_3), 1.26-2.08 ppm (br, NH-C(=O)-CH-CH_2-CH_2-CH_2-), 1.12 ppm (O=C(N)-CH_2-CH_3).

Poly(2-ethyl-2-oxazoline)-*block*-poly(L-lysine) (PEtOXA-*b*-PLL). PEtOXA-*b*-PzLL (355.7 mg) was dissolved in TFA (17 mL), then HBr in acetic acid solution (33%) (4 mL) at 0 °C was added dropwise. The solution was stirred for another 1 h at 0 °C. The product was purified by precipitation in diethyl ether and then dissolved in DMSO. The DMSO solution was then dialyzed against ddH_2O for 48 h changing ddH_2O three times. After lyophilizing, 240 mg white powder was obtained with a yield of 68%. ^{1}H NMR (D_2O): δ = 4.26 ppm (t, NH-C(=O)-

C*H*-), 3.32-3.60 ppm (br, N-CH_2-CH_2-), 2.96 ppm (t, NH_2-CH_2-), 2.29 ppm (m, O=C(N)-CH_2-CH_3), 1.22-1.78 ppm (NH_2-CH_2-CH_2-CH_2-CH_2-), 0.97 ppm (m, O=C(N)-CH_2-CH_3).

6.3. Characterization techniques

^{1}H NMR spectra were recorded on a Bruker DPX-400 MHz spectrometer in $CDCl_3$ without tetramethysilane standard, $CDCl_3$ with tetramethysilane standard, d6-DMSO and D_2O, and analyzed using MestReNova software.

The molecular weight and PDIs of polymers were determined using a Viscotek GPC max system equipped with four Agilent PL gel columns (10µm guard; mixed C; 10 µm, 100 Å; 5 µm, 103 Å). THF and DMF were used as eluent at a flow rate of 1 mL min^{-1} at 40 °C. Signals were recorded with a refractive-index detector and calibrated against polystyrene standards (Agilent).

Transmission electron microscopy (TEM) was used to analyze the supramolecular assemblies of block copolymers. Sample solutions were negatively stained with 2% uranyl acetate solution and deposited on a carbon-coated copper grid. The samples were examined on a Philips Morgagni 268D TEM operated at 80 kV. Particle sizes were calculated from TEM images by averaging the diameters (mean ± S.D.) from at least 50 particles.

Cryo-electron microscopy was used to visualize the self-assembled structures in their native environment. Polymer suspensions in buffer (20 mM Hepes, pH 7.4, 50 mM NaCl) at concentrations of 5 mg/mL were deposited on glow-discharged holey carbon grids (Quantufoil, Germany) and blotted before quick-freezing in liquid ethane by using a Vitrobot plunging freezing device (FEI company, USA). The grids were stored in liquid nitrogen before transferring them to a cryo-holder (Gatan, USA).). Imaging was performed with a Philips CM200 FEG TEM at an accelerating voltage of 200 kV in low-dose mode with a defocus of -6 µm for imaging and a defocus of -3 µm for membrane thickness determination. Membrane thicknesses represent a mean value of at least 150 single distance measurements along the membrane thickness of five different images.[217]

Light scattering (LS) was used to characterize the assembled structures in solution. Dynamic light scattering (DLS) and static light scattering (SLS) experiments were performed on an ALV goniometer (ALV GmbH, Germany), equipped with an ALV He-Ne laser (λ = 632.8 nm). Light scattering measurements were performed in 10 mm cylindrical quartz cells at angles of 30 –

150° at 293 K. The obtained data were processed using ALV static & dynamic fit and plot software (version 4.31 10/01). SLS data were processed according to the Guinier-model, and DLS data by using a Williams-Watts function.

The critical micelle concentration (CMC) was determined for the $PDMS_{65}$-*b*-$PMOXA_{14}$ and $PDMS_{65}$-*b*-$PMOXA_{32}$ by surface tension with concentration from 3*10-4 to 1*10-2. Surface tension was measured on a Sigma 703D (KSV Inst.) tensiometer with a platinum wilhelmy plate precleaned with isopropyl alcohol and water, followed by flame annealing. Solution was prepared 24 h prior to measurement by diluting the stock solution to different concentration. The CMC values were calculated from the interception point of the two tangent straight lines.

The critical micelles concentration (CMC) values of three PMOXA-graft(SS)-PCL samples were determined by using pyrene as the fluorescence probe. The concentration of graft copolymers was varied from $1*10^{-5}$ mg/mL to 0.5 mg/mL, while preserving the same concentration of pyrene at 0.8 µM. After mixing the graft copolymer solution with pyrene, the solution was kept in the dark at 37 °C for 12 h before measuring. Fluorescence spectra were recorded using fluorescence spectroscopy at an excitation wavelength of 330 nm. Fluorescence emission at 372 and 383 nm were monitored. The CMC was estimated as the cross-point when extrapolating the intensity ratio I_{383} / I_{372} at low and high concentration regions.

Small angle X-ray scattering (SAXS) was performed on a Bruker AXS Nanostar with an Incoatec Cu - IµS Microfocus X-ray source (λ = 0.154 nm) and a virtually noise-free, real-time 2D Hi-Star detector with photon counting ability. The measurements were done with 45 kV and 650 µA and the integration time was 9 h. About 20 µl of sample with the concentration of 5 $mg \cdot ml^{-1}$ was loaded into a glass capillary (d = 1 mm, thickness of the wall = 0.01 mm). The closed capillary set up into the Nanostar, vacuum was applied and the measurement was started. The data were azimuthally averaged with SAXS v.4.1.36 Bruker software and fitted with Nanofit.

Electron paramagnetic resonance (EPR) measurements were performed on a Bruker CW EPR Elexsys-500 spectrometer equipped with a variable temperature unit. The spectra were recorded at temperatures varying between 150 and 320 K with the following parameters: 100 KHz magnetic field modulation, microwave power 2 mW, number of scans up to 20, modulation amplitude in the range of 0.4 G. The nitrogen hyperfine coupling (a_N) was

determined directly from the spectra for motionally narrowed lineshapes with an error limit of 5%. $2a_N$ values correspond to the distance (in gauss) between the low-field and high-field lines of the motionally averaged spectra (triplets) recorded at temperatures above 270 K, whereas 2Azz values are measured as a distance between the last minimum and the first maximum (extreme separation) in the rigid limit spectra recorded from frozen solutions. The microviscosity in the proximity of the nitroxide free-radical probe was determined from the correlation time τc, which is related to the rate of rotational reorientation of the probe:

$$\tau_c = 6.5e^{-10} * \Delta H_0 * \left\{ \sqrt{\frac{I_0}{I_{+1}}} + \sqrt{\frac{I_0}{I_{-1}} - 2} \right\}$$

where ΔH_0 is the linewidth of the mI = 0 transition, and I_0, I+1, I-1 are the peak to peak heights of the mI = 0, +1 and -1 transitions, respectively.[160]

Fourier transform infrared spectroscopy (FTIR) (PerkinElmer Spectrum 100 FTIR Spectrometer) was used to characterize the presence of specific chemical groups. Polymer samples were measured with 256 scans and 2 cm^{-1} resolution. The spectra were measured from 400 to 4000 cm^{-1}.

The particle size was characterized by dynamic light scattering (DLS) at a fixed angle of θ = 173° using a Zetasizer Nano (Malvern, Worcestershire, UK) with a laser beam wavelength of 633 nm.

Fluorescence emission spectroscopy was performed on a Perkin Elmer, LS55.

Fluorescence correlation spectroscopy (FCS) and confocal laser scanning microscopy (CLSM) were performed on a commercial Zeiss LSM 510 META/ConfCor 2. For FCS, a HeNe laser (633 nm), a 40x water-immersion objective (Zeiss C/Apochromat 63X, NA 1.2) and the appropriate filter sets were used. For CLSM, a laser diode (405 nm), argon laser (488 nm), helium/neon laser (633 nm) and a 63× water-immersion objective (Zeiss C/Apochromat 63X, NA 1.2) were used. The cells were imaged in multitrack mode, whereas the channel for Doxorubicin was fixed to the same settings over all images. The images were processed using LSM Image Browser (Zeiss).

6.4. Reduction-triggered destabilization of PMOXA-graft(ss)-PCL nanoparticles

The size of the nanoparticles in response to 10 mM DTT in PBS was traced by DLS measurements. Briefly, 1 mL of a PMOXA-graft(ss)-PCL nanoparticle solution (1 mg/mL) in

PBS was transferred into a DLS measurement cell, to which concentrated DTT PBS buffer solution was added to adjust the final concentration of DTT to 10 mM. At different time intervals, the size of the nanoparticles was measured by DLS.

6.5. Reduction-triggered release of dye from nanoparticles formed by PMOXA-graft(ss)-PCL

BODIPY 630-loaded PMOXA-graft(ss)-PCL nanoparticles were prepared as described above using 1 µM of dye-solution in PBS. Aliquots of 20 µl nanoparticle solution were added to 200 µl pre-warmed (37 °C) PBS (controls) or 11 mM DTT in PBS and incubated under shaking (500 RPM) at 37 °C in an Eppendorf Thermomixer Comfort. 5 µl of these mixtures were transferred for subsequent FCS measurements at each time point (20 x 5s FCS curves each). Resulting FCS curves were fitted with a two-component system, whereas one diffusion parameter was fixed to free dye diffusion (about 60 µs). FCS curves that could not be fitted correctly by the program were excluded from the average (less than 1% of all curves). Percentage of free dye is presented as average ± s.e.m. for three independent measurements using two independent samples for each copolymer. Hydrodynamic diameters (D_H) were calculated using Einstein-Stokes equation; diffusion constants obtained for the nanoparticles and free Atto655 in PBS as a calibration for the confocal volume. D_H for nanoparticles was only given when smaller than 350 nm (aggregates are represented with D_H 350 nm) and a particle fraction of at least 10%.

6.6. Loading of anti-cancer drug DOX in nanoparticles formed by PMOXA-graft(ss)-PCL

DOX-loaded PMOXA-graft(ss)-PCL nanoparticles were obtained by drop wise addition of 1 mL PBS into the mixture 0.2 mL PMOXA-graft(ss)-PCL or PMOXA-*b*-PCL solution in DMF (5 mg/mL) and 10 µl, 30 µl and 50 µl DOX in the solution DMSO (5 mg/mL) under stirring at RT, followed by dialysis against PBS with MWCO 3500 dialysis tube at RT in the dark with changing three times PBS buffer solution in 24 h. The amount of DOX was determined using fluorescence measurement with excitation at 480 nm and emission at 560 nm. For determination of the drug loading content, the samples were first lyophilized, then DOX loaded PMOXA-graft(SS)-PCL or PMOXA-*b*-PCL nanoparticles were dissolved in 1 mL DMSO/DMF mixture (V_{DMSO} /V_{DMF} = 2 : 1) and analyzed with fluorescence spectroscopy. The

DOX standard calibration curve in DMSO/DMF mixture solvent (V_{DMSO} /V_{DMF} = 2 : 1) was obtained also by fluorescence spectroscopy.

Drug loading content (DLC) and drug loading efficiency (DLE) were calculated according to the following formulas:

DLC (wt%) = (weight of loaded drug / weight of polymer) * 100%

DLE (%) = (weight of loaded drug / weight in feed) * 100%

6.7. Cell culture

HeLa cells were grown in 75 cm^2 cell culture flasks (BD Bioscience) at 37 °C under a 5% CO_2 atmosphere in the cell culture medium (normal cell grow conditions). When cells reached a confluency of about 80%, they were split in a 1 : 10 ratio. To prepare the cell culture medium 50 ml fetal bovine serum (BioConcept AG), 10 ml 10'000 U/ml penicillin and 10'000 µg/ml streptomycin (Gibco) were filled up to 500 ml with fresh Dulbecco's modified eagle's medium (DMEM) (Sigma). The medium was sterile filtered through a 0.2 µm vacuum filter (Millipore). The cells were subcultured by trypsinization.

6.8. Preparation for live cell imaging

For live images 50'000 HeLa cells were seeded into each 8-well microscope chamber slides (Nunc) for 24 h in a normal cell culture conditions. Before adding the samples to the cells, old medium was removed; new medium was added to such an amount that in the end the total volume with sample resulted to be 100 µl. After 1 h, 2 h, 4 h or 8 h incubation under normal cell growing conditions cells were washed with PBS and 400 µl DMEM was added. To stain nucleus and cell membrane, cells were incubated with 0.2 µg/ml Hoechst 33342 (Invitrogen) for 25 min and 2.5 µg/ml CellMask Deep Red (Invitrogen) for 5 min. Subsequently, cells were washed with PBS and wells were filled up with 400 µl PBS.

6.9. MTS assay

Into each vial of a 96-well plate (Falcon) 10'000 cells were seeded, filled up to 100 µl with cell culture medium and incubated for 24 h under normal cell grow conditions. Prior to addition of the sample, the old medium was removed, DOX loaded PMOXA-graft(ss)-PCL nanoparticles, DOX loaded PMOXA-*b*-PCL nanoparticles, free DOX or PBS were added to a volume of 20 µl and filled up to 100 µl with cell growing medium. The samples had a final DOX concentration of 0.9 µg/ml, 2.7 µg/ml, 4.5 µg/ml and 9 µg/ml, or blank PMOXA-

graft(ss)-PCL nanoparticles. As a control, 20 µl PBS was added and filled up to 100 µl with cell growing medium and the blank measurement was prepared the same but without cells. The cells were then incubated for 48 h at normal cell growing conditions. Subsequently, 10 µl of MTS (Promega) was added to each well and incubated for another 4 h. The absorbance at 490 nm was measured with a plate reader Spectramax M5e (Molecular Device). To calculate the cell viability the average value from the blank was subtracted from the measured samples values and normalized to the average of value only cells. Data are presented as average ± SD (*n* = 8).

6.10. DNA complex with PEtOXA-PCL-ss-PLL and gel retardation assay

Dissolved 2mg PEtOXA-PCL-ss-PLL in 100 µL DMSO, and then dropwised 500 µL PBS into DMSO with continually being stirred slowly. The solution was transferred into dialysis tube with 3.5 KDa cut-off to dialyze against PBS for two days with changing PBS solution for three times, and finally adjusted PEtOXA-PCL-ss-PLL final concentration to be 2 mg/mL. Mix pDNA with PEtOXA-PCL-ss-PLL solution together with N/P equaling to 7 to prepare DNA and PEtOXA-PCL-ss-PLL complexion solution. The mixture was kept at room temperature for another 30 minutes to make sure the complexion formation. For tracking a loading buffer (15% Ficoll 400 in TBE) containing bromophenol blue (0.1%) was added to each sample. All samples were loaded on a 0.8% agarose gel with 0.05 mg/mL ethidium bromide (EtBr) and electrophoresed with TBA buffer at 80 V for 45 min. Finally, the gel was imaged with a Gel Documentation System to visualize the pDNA migration.

7. References

(1) Szwarc, M.; Levy, M.; Milkovich, R. *Journal of the American Chemical Society* 1956, 78, (11), 2656.

(2) Quirk, R. P.; Lee, B. *Polymer International* 1992, 27, (4), 359.

(3) Feldthusen, J.; Iván, B.; Müller, A. H. E. *Macromolecules* 1998, 31, (3), 578.

(4) Baskaran, D.; Müller, A. H. E. *Progress in Polymer Science* 2007, 32, (2), 173.

(5) Baskaran, D. *Progress in Polymer Science* 2003, 28, (4), 521.

(6) Goethals, E. J.; Du Prez, F. *Progress in Polymer Science* 2007, 32, (2), 220.

(7) Bae, Y. C.; Faust, R. *Macromolecules* 1998, 31, (8), 2480.

(8) Chen, W.; Zou, Y.; Jia, J.; Meng, F.; Cheng, R.; Deng, C.; Feijen, J.; Zhong, Z. *Macromolecules* 2013, 46, (3), 699.

(9) Tempelaar, S.; Mespouille, L.; Coulembier, O.; Dubois, P.; Dove, A. P. *Chemical Society Reviews* 2013, 42, (3), 1312.

(10) Le Garrec, D.; Gori, S.; Luo, L.; Lessard, D.; Smith, D. C.; Yessine, M. A.; Ranger, M.; Leroux, J. C. *Journal of Controlled Release* 2004, 99, (1), 83.

(11) Albertsson, A.-C.; Varma, I. K. *Biomacromolecules* 2003, 4, (6), 1466.

(12) Xiong, M.-H.; Wu, J.; Wang, Y.-C.; Li, L.-S.; Liu, X.-B.; Zhang, G.-Z.; Yan, L.-F.; Wang, J. *Macromolecules* 2009, 42, (4), 893.

(13) Kim, Y.; Jnaneshwara, G. K.; Verkade, J. G. *Inorganic Chemistry* 2003, 42, (5), 1437.

(14) Varma, I. K.; Albertsson, A.-C.; Rajkhowa, R.; Srivastava, R. K. *Progress in Polymer Science* 2005, 30, (10), 949.

(15) Suriano, F.; Coulembier, O.; Hedrick, J. L.; Dubois, P. *Polymer Chemistry* 2011, 2, (3), 528.

(16) Stridsberg, K.; Ryner, M.; Albertsson, A.-C., Controlled Ring-Opening Polymerization: Polymers with designed Macromolecular Architecture. In *Degradable Aliphatic Polyesters*, Springer Berlin Heidelberg: 2002; Vol. 157, pp 41.

(17) Hoogenboom, R. *Angewandte Chemie International Edition* 2009, 48, (43), 7978.

(18) Sedlacek, O.; Monnery, B. D.; Filippov, S. K.; Hoogenboom, R.; Hruby, M. *Macromolecular Rapid Communications* 2012, 33, (19), 1648.

(19) Viegas, T. X.; Bentley, M. D.; Harris, J. M.; Fang, Z.; Yoon, K.; Dizman, B.; Weimer, R.; Mero, A.; Pasut, G.; Veronese, F. M. *Bioconjugate Chemistry* 2011, 22, (5), 976.

(20) Hadjichristidis, N.; Iatrou, H.; Pitsikalis, M.; Sakellariou, G. *Chemical Reviews* 2009, 109, (11), 5528.

(21) Cheng, J.; Deming, T., Synthesis of Polypeptides by Ring-Opening Polymerization of α-Amino Acid N-Carboxyanhydrides. In *Peptide-Based Materials*, Deming, T., Ed. Springer Berlin Heidelberg: 2012; Vol. 310, pp 1.

(22) Cha, J. N.; Stucky, G. D.; Morse, D. E.; Deming, T. J. *Nature* 2000, 403, (6767), 289.

(23) Nowak, A. P.; Breedveld, V.; Pakstis, L.; Ozbas, B.; Pine, D. J.; Pochan, D.; Deming, T. J. *Nature* 2002, 417, (6887), 424.

(24) Matyjaszewski, K., Controlled/Living Radical Polymerization: State of the Art in 2002. In *Advances in Controlled/Living Radical Polymerization*, American Chemical Society: 2003; Vol. 854, pp 2.

(25) Zetterlund, P. B.; Kagawa, Y.; Okubo, M. *Chemical Reviews* 2008, 108, (9), 3747.

(26) Braunecker, W. A.; Matyjaszewski, K. *Progress in Polymer Science* 2007, 32, (1), 93.

(27) Matyjaszewski, K.; Spanswick, J. *Materials Today* 2005, 8, (3), 26.

(28) Stenzel, M. H.; Davis, T. P. *Journal of Polymer Science Part A: Polymer Chemistry* 2002, 40, (24), 4498.

(29) He, T.; Li, D.; Sheng, X.; Zhao, B. *Macromolecules* 2004, 37, (9), 3128.

(30) Semsarilar, M.; Ladmiral, V.; Perrier, S. b. *Macromolecules* 2010, 43, (3), 1438.

(31) Hadjichristidis, N.; Iatrou, H.; Pitsikalis, M.; Mays, J. *Progress in Polymer Science* 2006, 31, (12), 1068.

(32) Coessens, V.; Pintauer, T.; Matyjaszewski, K. *Progress in Polymer Science* 2001, 26, (3), 337.

(33) Yokozawa, T.; Ogawa, M.; Sekino, A.; Sugi, R.; Yokoyama, A. *Journal of the American Chemical Society* 2002, 124, (51), 15158.

(34) Elias, H.-G., Polycondensations. In *Macromolecules*, Springer US: 1984; pp 583.

(35) Dan, K.; Ghosh, S. *Polymer Chemistry* 2014, 5, (12), 3901.

(36) Dan, K.; Ghosh, S. *Angewandte Chemie International Edition* 2013, 52, (28), 7300.

(37) Satoh, K.; Poelma, J. E.; Campos, L. M.; Stahl, B.; Hawker, C. J. *Polymer Chemistry* 2012, 3, (7), 1890.

(38) Li, Y.; Liu, T.; Zhang, G.; Ge, Z.; Liu, S. *Macromolecular Rapid Communications* 2014, 35, (4), 466.

(39) Jin, Q.; Cai, T.; Wang, Y.; Wang, H.; Ji, J. *ACS Macro Letters* 2014, 679.

(40) Weber, C.; Babiuch, K.; Rogers, S.; Perevyazko, I. Y.; Hoogenboom, R.; Schubert, U. S. *Polymer Chemistry* 2012, 3, (10), 2976.

(41) Rao, J.; Khan, A. *Journal of the American Chemical Society* 2013, 135, (38), 14056.

(42) Rauwald, U.; Scherman, O. A. *Angewandte Chemie International Edition* 2008, 47, (21), 3950.

(43) Dunn, A. S.; Melville, H. W. *Nature* 1952, 169, (4304), 699.

(44) Hadjichristidis, N.; Pitsikalis, M.; Iatrou, H., Synthesis of Block Copolymers. In *Block Copolymers I*, Abetz, V., Ed. Springer Berlin Heidelberg: 2005; Vol. 189, pp 1.

(45) Yao, Y.; Xue, M.; Chen, J.; Zhang, M.; Huang, F. *Journal of the American Chemical Society* 2012, 134, (38), 15712.

(46) Mai, Y.; Zhang, F.; Feng, X. *Nanoscale* 2014, 6, (1), 106.

(47) Mai, Y.; Eisenberg, A. *Chemical Society Reviews* 2012, 41, (18), 5969.

(48) Leibler, L. *Macromolecules* 1980, 13, (6), 1602.

(49) Bates, F. S.; Fredrickson, G. H. *Print edition* 1999, 52, (2), 32.

(50) Antonietti, M.; Förster, S. *Advanced Materials* 2003, 15, (16), 1323.

(51) Dan, N.; Safran, S. A. *Advances in Colloid and Interface Science* 2006, 123–126, (0), 323.

(52) Choucair, A.; Lavigueur, C.; Eisenberg, A. *Langmuir* 2004, 20, (10), 3894.

(53) Terreau, O.; Luo, L.; Eisenberg, A. *Langmuir* 2003, 19, (14), 5601.

(54) Cooke, D. M.; Shi, A.-C. *Macromolecules* 2006, 39, (19), 6661.

(55) Rakhmatullina, E.; Braun, T.; Chami, M.; Malinova, V.; Meier, W. *Langmuir* 2007, 23, (24), 12371.

(56) Pearson, R. T.; Warren, N. J.; Lewis, A. L.; Armes, S. P.; Battaglia, G. *Macromolecules* 2013, 46, (4), 1400.

(57) Fernyhough, C.; Ryan, A. J.; Battaglia, G. *Soft Matter* 2009, 5, (8), 1674.

(58) Borisov, O. V.; Zhulina, E. B. *Macromolecules* 2002, 35, (11), 4472.

(59) Choucair, A.; Eisenberg, A. *European Physical Journal E* 2003, 10, (1), 37.

(60) Zhang, W.; Shi, L.; An, Y.; Gao, L.; Wu, K.; Ma, R.; He, B. *Physical Chemistry Chemical Physics* 2004, 6, (1), 109.

(61) Wu, D.; Spulber, M.; Itel, F.; Chami, M.; Pfohl, T.; Palivan, C. G.; Meier, W. *Macromolecules* 2014, 47, (15), 5060.

(62) Cameron, N. S.; Corbierre, M. K.; Eisenberg, A. *Canadian Journal of Chemistry* 1999, 77, (8), 1311.

(63) Shen, H.; Eisenberg, A. *Angewandte Chemie International Edition* 2000, 39, (18), 3310.

(64) Israelachvili, J. N., 19 - Thermodynamic Principles of Self-Assembly. In *Intermolecular and Surface Forces (Third Edition)*, Israelachvili, J. N., Ed. Academic Press: Boston, 2011; pp 503.

(65) Blanazs, A.; Armes, S. P.; Ryan, A. J. *Macromolecular Rapid Communications* 2009, 30, (4-5), 267.

(66) Kita-Tokarczyk, K.; Grumelard, J.; Haefele, T.; Meier, W. *Polymer* 2005, 46, (11), 3540.

(67) Lee, J. C. M.; Santore, M.; Bates, F. S.; Discher, D. E. *Macromolecules* 2001, 35, (2), 323.

(68) Lundberg, P.; Lynd, N. A.; Zhang, Y.; Zeng, X.; Krogstad, D. V.; Paffen, T.; Malkoch, M.; Nystrom, A. M.; Hawker, C. J. *Soft Matter* 2013, 9, (1), 82.

(69) Li, J.; Wang, T.; Wu, D.; Zhang, X.; Yan, J.; Du, S.; Guo, Y.; Wang, J.; Zhang, A. *Biomacromolecules* 2008, 9, (10), 2670.

(70) Fleige, E.; Quadir, M. A.; Haag, R. *Advanced Drug Delivery Reviews* 2012, 64, (9), 866.

(71) Mura, S.; Nicolas, J.; Couvreur, P. *Nat Mater* 2013, 12, (11), 991.

(72) Kelley, E. G.; Albert, J. N. L.; Sullivan, M. O.; Epps, I. I. I. T. H. *Chemical Society Reviews* 2013.

(73) Schacher, F. H.; Rupar, P. A.; Manners, I. *Angewandte Chemie International Edition* 2012, 51, (32), 7898.

(74) Zou, H.; Yuan, W. *Journal of Materials Chemistry B* 2015, 3, (2), 260.

(75) Yuan, L.; Liu, J.; Wen, J.; Zhao, H. *Langmuir* 2012, 28, (30), 11232.

(76) Cheng, R.; Feng, F.; Meng, F.; Deng, C.; Feijen, J.; Zhong, Z. *Journal of Controlled Release* 2011, 152, (1), 2.

(77) Sun, H.; Guo, B.; Li, X.; Cheng, R.; Meng, F.; Liu, H.; Zhong, Z. *Biomacromolecules* 2010, 11, (4), 848.

(78) Ren, T.; Wu, W.; Jia, M.; Dong, H.; Li, Y.; Ou, Z. *ACS Applied Materials & Interfaces* 2013, 5, (21), 10721.

(79) Duncan, T. V.; Ghoroghchian, P. P.; Rubtsov, I. V.; Hammer, D. A.; Therien, M. J. *Journal of the American Chemical Society* 2008, 130, (30), 9773.

(80) Berret, J.-F.; Schonbeck, N.; Gazeau, F.; El Kharrat, D.; Sandre, O.; Vacher, A.; Airiau, M. *Journal of the American Chemical Society* 2006, 128, (5), 1755.

(81) Balasubramanian, V.; Onaca, O.; Ezhevskaya, M.; Van Doorslaer, S.; Sivasankaran, B.; Palivan, C. G. *Soft Matter* 2011, 7, (12), 5595.

(82) Christian, D. A.; Cai, S.; Bowen, D. M.; Kim, Y.; Pajerowski, J. D.; Discher, D. E. *European Journal of Pharmaceutics and Biopharmaceutics* 2009, 71, (3), 463.

(83) Lee, J. S.; Feijen, J. *Journal of Controlled Release* 2012, 161, (2), 473.

(84) Onaca, O.; Enea, R.; Hughes, D. W.; Meier, W. *Macromol Biosci* 2009, 9, (2), 129.

(85) Pawar, P. V.; Gohil, S. V.; Jain, J. P.; Kumar, N. *Polymer Chemistry* 2013, 4, (11), 3160.

(86) Meng, F.; Zhong, Z. *The Journal of Physical Chemistry Letters* 2011, 2, (13), 1533.

(87) Tanner, P.; Balasubramanian, V.; Palivan, C. G. *Nano Letters* 2013, 13, (6), 2875.

(88) Graff, A.; Sauer, M.; Van Gelder, P.; Meier, W. *Proceedings of the National Academy of Sciences* 2002, 99, (8), 5064.

(89) Langowska, K.; Palivan, C. G.; Meier, W. *Chemical Communications* 2013, 49, (2), 128.

(90) Egli, S.; Nussbaumer, M. G.; Balasubramanian, V.; Chami, M.; Bruns, N.; Palivan, C.; Meier, W. *Journal of the American Chemical Society* 2011, 133, (12), 4476.

(91) Han, P.; Li, S.; Cao, W.; Li, Y.; Sun, Z.; Wang, Z.; Xu, H. *Journal of Materials Chemistry B* 2013, 1, (6), 740.

(92) Chen, W.; Du, J. *Sci. Rep.* 2013, 3.

(93) Amstad, E.; Kim, S.-H.; Weitz, D. A. *Angewandte Chemie International Edition* 2012, 51, (50), 12499.

(94) Zhou, K.; Wang, Y.; Huang, X.; Luby-Phelps, K.; Sumer, B. D.; Gao, J. *Angewandte Chemie International Edition* 2011, 50, (27), 6109.

(95) Tanner, P.; Baumann, P.; Enea, R.; Onaca, O.; Palivan, C.; Meier, W. *Accounts of Chemical Research* 2011, 44, (10), 1039.

(96) Chausson, M.; Fluchère, A.-S.; Landreau, E.; Aguni, Y.; Chevalier, Y.; Hamaide, T.; Abdul-Malak, N.; Bonnet, I. *International Journal of Pharmaceutics* 2008, 362, (1–2), 153.

(97) Brannon-Peppas, L.; Blanchette, J. O. *Advanced Drug Delivery Reviews* 2004, 56, (11), 1649.

(98) Nardin, C.; Thoeni, S.; Widmer, J.; Winterhalter, M.; Meier, W. *Chemical Communications* 2000, (15), 1433.

(99) de Vries, A.; Custers, E.; Lub, J.; van den Bosch, S.; Nicolay, K.; Grüll, H. *Biomaterials* 2010, 31, (25), 6537.

(100) Miyata, K.; Nishiyama, N.; Kataoka, K. *Chemical Society Reviews* 2012, 41, (7), 2562.

(101) Fang, J.; Nakamura, H.; Maeda, H. *Advanced Drug Delivery Reviews* 2011, 63, (3), 136.

(102) Sun, Q.; Radosz, M.; Shen, Y. *Journal of Controlled Release* 2012, 164, (2), 156.

(103) Huo, M.; Yuan, J.; Tao, L.; Wei, Y. *Polymer Chemistry* 2014, 5, (5), 1519.

(104) Schumers, J.-M.; Fustin, C.-A.; Gohy, J.-F. *Macromolecular Rapid Communications* 2010, 31, (18), 1588.

(105) Meng, F.; Zhong, Z.; Feijen, J. *Biomacromolecules* 2009, 10, (2), 197.

(106) Harnoy, A. J.; Rosenbaum, I.; Tirosh, E.; Ebenstein, Y.; Shaharabani, R.; Beck, R.; Amir, R. J. *Journal of the American Chemical Society* 2014.

(107) Boyle, M. J.; Richards, J. S.; Gilson, P. R.; Chai, W.; Beeson, J. G., *Interactions with heparin-like molecules during erythrocyte invasion by Plasmodium falciparum merozoites*. 2010; Vol. 115, p 4559.

(108) Cowman, A. F.; Crabb, B. S. *Cell* 2006, 124, (4), 755.

(109) Wang, Y.; Zhou, K.; Huang, G.; Hensley, C.; Huang, X.; Ma, X.; Zhao, T.; Sumer, B. D.; DeBerardinis, R. J.; Gao, J. *Nat Mater* 2013, advance online publication.

(110) Zhang, X.; Zeng, X.; Liang, X.; Yang, Y.; Li, X.; Chen, H.; Huang, L.; Mei, L.; Feng, S.-S. *Biomaterials* 2014, 35, (33), 9144.

(111) Shi, C.; Guo, X.; Qu, Q.; Tang, Z.; Wang, Y.; Zhou, S. *Biomaterials* 2014, 35, (30), 8711.

(112) Liu, Q.; Chen, J.; Du, J. *Biomacromolecules* 2014, 15, (8), 3072.

(113) Huang, P.; Song, H.; Wang, W.; Sun, Y.; Zhou, J.; Wang, X.; Liu, J.; Liu, J.; Kong, D.; Dong, A. *Biomacromolecules* 2014, 15, (8), 3128.

(114) Ko, N. R.; Oh, J. K. *Biomacromolecules* 2014, 15, (8), 3180.

(115) Xu, P.; Yu, H.; Zhang, Z.; Meng, Q.; Sun, H.; Chen, X.; Yin, Q.; Li, Y. *Biomaterials* 2014, 35, (26), 7574.

(116) Wang, H.-X.; Yang, X.-Z.; Sun, C.-Y.; Mao, C.-Q.; Zhu, Y.-H.; Wang, J. *Biomaterials* 2014, 35, (26), 7622.

(117) Dorresteijn, R.; Billecke, N.; Schwendy, M.; Pütz, S.; Bonn, M.; Parekh, S. H.; Klapper, M.; Müllen, K. *Advanced Functional Materials* 2014, 24, (26), 4026.

(118) van Eldijk, M. B.; Smits, F. C. M.; Vermue, N.; Debets, M. F.; Schoffelen, S.; van Hest, J. C. M. *Biomacromolecules* 2014, 15, (7), 2751.

(119) Chen, W.; Zhong, P.; Meng, F.; Cheng, R.; Deng, C.; Feijen, J.; Zhong, Z. *Journal of Controlled Release* 2013, 169, (3), 171.

(120) Hu, X.; Li, H.; Luo, S.; Liu, T.; Jiang, Y.; Liu, S. *Polymer Chemistry* 2013, 4, (3), 695.

(121) Yan, Q.; Wang, J.; Yin, Y.; Yuan, J. *Angewandte Chemie International Edition* 2013, 52, (19), 5070.

(122) Miura, Y.; Takenaka, T.; Toh, K.; Wu, S.; Nishihara, H.; Kano, M. R.; Ino, Y.; Nomoto, T.; Matsumoto, Y.; Koyama, H.; Cabral, H.; Nishiyama, N.; Kataoka, K. *ACS Nano* 2013, 7, (10), 8583.

(123) Wang, Q.; Bao, Y.; Ahire, J.; Chao, Y. *Advanced Healthcare Materials* 2013, 2, (3), 459.

(124) Onaca, O.; Hughes, D. W.; Balasubramanian, V.; Grzelakowski, M.; Meier, W.; Palivan, C. G. *Macromolecular Bioscience* 2010, 10, (5), 531.

(125) Spulber, M.; Najer, A.; Winkelbach, K.; Glaied, O.; Waser, M.; Pieles, U.; Meier, W.; Bruns, N. *Journal of the American Chemical Society* 2013, 135, (24), 9204.

(126) Palivan, C. G.; Fischer-Onaca, O.; Delcea, M.; Itel, F.; Meier, W. *Chemical Society Reviews* 2012, 41, (7), 2800.

(127) Peters, R. J. R. W.; Marguet, M.; Marais, S.; Fraaije, M. W.; van Hest, J. C. M.; Lecommandoux, S. *Angewandte Chemie International Edition* 2014, 53, (1), 146.

(128) Palivan, C. G.; Fischer-Onaca, O.; Delcea, M.; Itel, F.; Meier, W. *Chem Soc Rev* 2012, 41, (7), 2800.

(129) Meier, W.; Nardin, C.; Winterhalter, M. *Angew Chem Int Ed Engl* 2000, 39, (24), 4599.

(130) Kim, K. T.; Cornelissen, J. J. L. M.; Nolte, R. J. M.; van Hest, J. C. M. *Advanced Materials* 2009, 21, (27), 2787.

(131) Adams, D. J.; Butler, M. F.; Weaver, A. C. *Langmuir* 2006, 22, (10), 4534.

(132) Pourtau, L.; Oliveira, H.; Thevenot, J.; Wan, Y.; Brisson, A. R.; Sandre, O.; Miraux, S.; Thiaudiere, E.; Lecommandoux, S. *Advanced Healthcare Materials* 2013, 2, (11), 1420.

(133) Brinkhuis, R. P.; Rutjes, F. P. J. T.; van Hest, J. C. M. *Polymer Chemistry* 2011, 2, (7), 1449.

(134) Discher, D. E.; Ahmed, F. *Annual Review of Biomedical Engineering* 2006, 8, (1), 323.

(135) Dobrunz, D.; Toma, A. C.; Tanner, P.; Pfohl, T.; Palivan, C. G. *Langmuir* 2012, 28, (45), 15889.

(136) Yilgor, I.; Yilgor, E. *Polymer Bulletin* 1998, 40, (4-5), 525.

(137) Bellas, V.; Iatrou, H.; Hadjichristidis, N. *Macromolecules* 2000, 33, (19), 6993.

(138) Kobayashi, S.; Masuda, E.; Shoda, S.; Shimano, Y. *Macromolecules* 1989, 22, (7), 2878.

(139) Chang, X.; Dong, C.-M. *Biomacromolecules* 2013, 14, (9), 3329.

(140) Chan, N.; Khorsand, B.; Aleksanian, S.; Oh, J. K. *Chemical Communications* 2013, 49, (68), 7534.

(141) Lim Soo, P.; Eisenberg, A. *Journal of Polymer Science Part B: Polymer Physics* 2004, 42, (6), 923.

(142) Adams, N.; Schubert, U. S. *Advanced Drug Delivery Reviews* 2007, 59, (15), 1504.

(143) Braun, J.; Bruns, N.; Pfohl, T.; Meier, W. *Macromolecular Chemistry and Physics* 2011, 212, (12), 1245.

(144) de Bruyn Ouboter, D.; Schuster, T. B.; Mantion, A.; Meier, W. *The Journal of Physical Chemistry C* 2011, 115, (30), 14583.

(145) Babinot, J.; Renard, E.; Le Droumaguet, B.; Guigner, J.-M.; Mura, S.; Nicolas, J.; Couvreur, P.; Langlois, V. *Macromolecular Rapid Communications* 2013, 34, (4), 362.

(146) Stauch, O.; Schubert, R.; Savin, G.; Burchard, W. *Biomacromolecules* 2002, 3, (3), 565.

(147) Forster, S.; Zisenis, M.; Wenz, E.; Antonietti, M. *Journal of Chemical Physics* 1996, 104, (24), 9956.

(148) van Hest, J. C. M.; Delnoye, D. A. P.; Baars, M. W. P. L.; van Genderen, M. H. P.; Meijer, E. W. *Science* 1995, 268, (5217), 1592.

(149) Discher, D. E.; Eisenberg, A. *Science* 2002, 297, (5583), 967.

(150) Kita-Tokarczyk, K.; Meier, W. *CHIMIA International Journal for Chemistry* 2008, 62, (10), 820.

(151) Choucair, A.; Eisenberg, A. *Eur. Phys. J. E* 2003, 10, (1), 37.

(152) Ma, L.; Eisenberg, A. *Langmuir* 2009, 25, (24), 13730.

(153) CHANDAR, P.; SOMASUNDARAN; #160; P.; WATERMAN; C., K.; TURRO; J., N., *Variation in nitroxide probe chain flexibility within sodium dodecyl sulfate hemimicelles*. American Chemical Society: Washington, DC, ETATS-UNIS, 1987; Vol. 91.

(154) Ristori, S.; Ottaviani, M. F.; Lenti, D.; Martini, G. *Langmuir* 1991, 7, (9), 1958.

(155) Ristori, S.; Maggiulli, C.; Appell, J.; Marchionni, G.; Martini, G. *The Journal of Physical Chemistry B* 1997, 101, (20), 4155.

(156) Kamogawa, K.; Tajima, K. *The Journal of Physical Chemistry* 1993, 97, (37), 9506.

(157) Zhou, L.; Schlick, S. *Polymer* 2000, 41, (12), 4679.

(158) Wasserman, A. M. *Russian Chemical Reviews* 1994, 63, (5), 373.

(159) Deo, N.; Somasundaran, P.; Subramanyan, K.; Ananthapadmanabhan, K. P. *Journal of Colloid and Interface Science* 2002, 256, (1), 100.

(160) Beghein, N.; Rouxhet, L.; Dinguizli, M.; Brewster, M. E.; Arien, A.; Preat, V.; Habib, J. L.; Gallez, B. *J Control Release* 2007, 117, (2), 196.

(161) Arnold, T.; Linke, D. *BioTechniques* 2007, 43, (4), 427.

(162) Nallani, M.; Benito, S.; Onaca, O.; Graff, A.; Lindemann, M.; Winterhalter, M.; Meier, W.; Schwaneberg, U. *Journal of Biotechnology* 2006, 123, (1), 50.

(163) Nakagawa, K. *Lipids* 2007, 42, (5), 457.

(164) Peer, D.; Karp, J. M.; Hong, S.; Farokhzad, O. C.; Margalit, R.; Langer, R. *Nat Nano* 2007, 2, (12), 751.

(165) Ashley, C. E.; Carnes, E. C.; Phillips, G. K.; Padilla, D.; Durfee, P. N.; Brown, P. A.; Hanna, T. N.; Liu, J.; Phillips, B.; Carter, M. B.; Carroll, N. J.; Jiang, X.; Dunphy, D. R.; Willman, C. L.; Petsev, D. N.; Evans, D. G.; Parikh, A. N.; Chackerian, B.; Wharton, W.; Peabody, D. S.; Brinker, C. J. *Nat Mater* 2011, 10, (5), 389.

(166) Upadhyay, K. K.; Bhatt, A. N.; Mishra, A. K.; Dwarakanath, B. S.; Jain, S.; Schatz, C.; Le Meins, J.-F.; Farooque, A.; Chandraiah, G.; Jain, A. K.; Misra, A.; Lecommandoux, S. *Biomaterials* 2010, 31, (10), 2882.

(167) Horcajada, P.; Chalati, T.; Serre, C.; Gillet, B.; Sebrie, C.; Baati, T.; Eubank, J. F.; Heurtaux, D.; Clayette, P.; Kreuz, C.; Chang, J.-S.; Hwang, Y. K.; Marsaud, V.; Bories, P.-N.; Cynober, L.; Gil, S.; Ferey, G.; Couvreur, P.; Gref, R. *Nat Mater* 2010, 9, (2), 172.

(168) Xu, C.; Wang, B.; Sun, S. *Journal of the American Chemical Society* 2009, 131, (12), 4216.

(169) Bruns, N.; Pustelny, K.; Bergeron, L. M.; Whitehead, T. A.; Clark, D. S. *Angewandte Chemie International Edition* 2009, 48, (31), 5666.

(170) Langowska, K.; Kowal, J.; Palivan, C. G.; Meier, W. *Journal of Materials Chemistry B* 2014, 2, (29), 4684.

(171) Tang, F.; Li, L.; Chen, D. *Advanced Materials* 2012, 24, (12), 1504.

(172) Du, D.; Wang, L.; Shao, Y.; Wang, J.; Engelhard, M. H.; Lin, Y. *Analytical Chemistry* 2011, 83, (3), 746.

(173) Duncan, B.; Kim, C.; Rotello, V. M. *Journal of Controlled Release* 2010, 148, (1), 122.

(174) Meng, H.-M.; Zhang, X.; Lv, Y.; Zhao, Z.; Wang, N.-N.; Fu, T.; Fan, H.; Liang, H.; Qiu, L.; Zhu, G.; Tan, W. *ACS Nano* 2014, 8, (6), 6171.

(175) Wang, L.; Chierico, L.; Little, D.; Patikarnmonthon, N.; Yang, Z.; Azzouz, M.; Madsen, J.; Armes, S. P.; Battaglia, G. *Angewandte Chemie International Edition* 2012, 51, (44), 11122.

(176) Onaca, O.; Enea, R.; Hughes, D. W.; Meier, W. *Macromolecular Bioscience* 2009, 9, (2), 129.

(177) Sanson, C.; Schatz, C.; Le Meins, J.-F.; Soum, A.; Thévenot, J.; Garanger, E.; Lecommandoux, S. *Journal of Controlled Release* 2010, 147, (3), 428.

(178) Jia, L.; Cui, D.; Bignon, J.; Di Cicco, A.; Wdzieczak-Bakala, J.; Liu, J.; Li, M.-H. *Biomacromolecules* 2014, 15, (6), 2206.

(179) Kim, H. J.; Miyata, K.; Nomoto, T.; Zheng, M.; Kim, A.; Liu, X.; Cabral, H.; Christie, R. J.; Nishiyama, N.; Kataoka, K. *Biomaterials* 2014, 35, (15), 4548.

(180) Hu, J.; Zhang, G.; Liu, S. *Chemical Society Reviews* 2012, 41, (18), 5933.

(181) Osada, K.; Kataoka, K., Drug and Gene Delivery Based on Supramolecular Assembly of PEG-Polypeptide Hybrid Block Copolymers
Peptide Hybrid Polymers. Klok, H.-A.; Schlaad, H., Eds. Springer Berlin / Heidelberg: 2006; Vol. 202, pp 113.

(182) Chang, L.; Deng, L.; Wang, W.; Lv, Z.; Hu, F.; Dong, A.; Zhang, J. *Biomacromolecules* 2012.

(183) Guo, S.; Huang, Y.; Wei, T.; Zhang, W.; Wang, W.; Lin, D.; Zhang, X.; Kumar, A.; Du, Q.; Xing, J.; Deng, L.; Liang, Z.; Wang, P. C.; Dong, A.; Liang, X.-J. *Biomaterials* 2011, 32, (3), 879.

(184) Cunningham, A.; Oh, J. K. *Macromolecular Rapid Communications* 2013, 34, (2), 163.

(185) Pidhatika, B.; Rodenstein, M.; Chen, Y.; Rakhmatullina, E.; Mühlebach, A.; Acikgöz, C.; Textor, M.; Konradi, R. *Biointerphases* 2012, 7, (1), 1.

(186) Zalipsky, S.; Hansen, C. B.; Oaks, J. M.; Allen, T. M. *J Pharm Sci-Us* 1996, 85, (2), 133.

(187) Seebach, D.; Beck, A. K.; Bierbaum, D. J. *Chem Biodivers* 2004, 1, (8), 1111.

(188) Miller, S. M.; Simon, R. J.; Ng, S.; Zuckermann, R. N.; Kerr, J. M.; Moos, W. H. *Drug Development Research* 1995, 35, (1), 20.

(189) Konradi, R.; Pidhatika, B.; Mühlebach, A.; Textor, M. *Langmuir* 2008, 24, (3), 613.

(190) Petit, A.; Müller, B.; Meijboom, R.; Bruin, P.; van de Manakker, F.; Versluijs-Helder, M.; de Leede, L. G. J.; Doornbos, A.; Landin, M.; Hennink, W. E.; Vermonden, T. *Biomacromolecules* 2013, 14, (9), 3172.

(191) Cabane, E.; Malinova, V.; Menon, S.; Palivan, C. G.; Meier, W. *Soft Matter* 2011, 7, (19), 9167.

(192) Liao, L.; Liu, J.; Dreaden, E. C.; Morton, S. W.; Shopsowitz, K. E.; Hammond, P. T.; Johnson, J. A. *Journal of the American Chemical Society* 2014.

(193) Wei, H.; Zhuo, R.-X.; Zhang, X.-Z. *Progress in Polymer Science* 2013, 38, (3–4), 503.

(194) Wei, H.; Volpatti, L. R.; Sellers, D. L.; Maris, D. O.; Andrews, I. W.; Hemphill, A. S.; Chan, L. W.; Chu, D. S. H.; Horner, P. J.; Pun, S. H. *Angewandte Chemie International Edition* 2013, 52, (20), 5377.

(195) Engler, A. C.; Chan, J. M. W.; Fukushima, K.; Coady, D. J.; Yang, Y. Y.; Hedrick, J. L. *ACS Macro Letters* 2013, 2, (4), 332.

(196) Townsend, D. M.; Tew, K. D.; Tapiero, H. *Biomedicine & Pharmacotherapy* 2003, 57, (3-4), 145.

(197) Lee, M. H.; Yang, Z.; Lim, C. W.; Lee, Y. H.; Dongbang, S.; Kang, C.; Kim, J. S. *Chemical Reviews* 2013.

(198) Hsiue, G.-H.; Chiang, H.-Z.; Wang, C.-H.; Juang, T.-M. *Bioconjugate Chemistry* 2006, 17, (3), 781.

(199) Mahmud, A.; Xiong, X.-B.; Lavasanifar, A. *Macromolecules* 2006, 39, (26), 9419.

(200) Cui, C.; Xue, Y.-N.; Wu, M.; Zhang, Y.; Yu, P.; Liu, L.; Zhuo, R.-X.; Huang, S.-W. *Biomaterials* 2013, 34, (15), 3858.

(201) Sun, T.-M.; Du, J.-Z.; Yan, L.-F.; Mao, H.-Q.; Wang, J. *Biomaterials* 2008, 29, (32), 4348.

(202) Zhang, Q.; Vakili, M. R.; Li, X.-F.; Lavasanifar, A.; Le, X. C. *Biomaterials* 2014, 35, (25), 7088.

(203) Yu, S.; Ding, J.; He, C.; Cao, Y.; Xu, W.; Chen, X. *Advanced Healthcare Materials* 2014, 3, (5), 752.

(204) Tacar, O.; Sriamornsak, P.; Dass, C. R. *Journal of Pharmacy and Pharmacology* 2013, 65, (2), 157.

(205) Oh, J. K.; Siegwart, D. J.; Lee, H.-i.; Sherwood, G.; Peteanu, L.; Hollinger, J. O.; Kataoka, K.; Matyjaszewski, K. *Journal of the American Chemical Society* 2007, 129, (18), 5939.

(206) Meng, F.; Hennink, W. E.; Zhong, Z. *Biomaterials* 2009, 30, (12), 2180.

(207) Wong, A. D.; DeWit, M. A.; Gillies, E. R. *Advanced Drug Delivery Reviews* 2012, 64, (11), 1031.

(208) Endres, T.; Zheng, M.; Kılıç, A.; Turowska, A.; Beck-Broichsitter, M.; Renz, H.; Merkel, O. M.; Kissel, T. *Molecular Pharmaceutics* 2014, 11, (4), 1273.

(209) Osada, K.; Christie, R. J.; Kataoka, K. *Journal of The Royal Society Interface* 2009, 6, (Suppl 3), S325.

(210) Dos, A.; Schimming, V.; Tosoni, S.; Limbach, H.-H. *The Journal of Physical Chemistry B* 2008, 112, (49), 15604.

(211) Bermudez, H.; Brannan, A. K.; Hammer, D. A.; Bates, F. S.; Discher, D. E. *Macromolecules* 2002, 35, (21), 8203.

(212) Lynd, N. A.; Hillmyer, M. A. *Macromolecules* 2005, 38, (21), 8803.

(213) Lynd, N. A.; Meuler, A. J.; Hillmyer, M. A. *Progress in Polymer Science* 2008, 33, (9), 875.

(214) Jones, L. R.; Goun, E. A.; Shinde, R.; Rothbard, J. B.; Contag, C. H.; Wender, P. A. *Journal of the American Chemical Society* 2006, 128, (20), 6526.

(215) Daly, W. H.; Poché, D. *Tetrahedron Letters* 1988, 29, (46), 5859.

(216) Tsutsumiuchi, K.; Aoi, K.; Okada, M. *Macromolecules* 1997, 30, (14), 4013.

(217) Sakata, K.; Tahara, Y.; Morikawa, K.; Fujiyoshi, Y.; Kimura, Y. *Ultramicroscopy* 1992, 45, (2), 253.

8. Curriculum Vitae and list of publication.

Personal Information

Name: Dalin Wu

Date of Birth: 23.02.1984

E-Mail: dalin.wu@unibas.ch

Education

09/2010-present: **University of Basel, Department of Chemistry, Switzerland**

- PhD in Chemistry, supervised by Prof. Wolfgang Meier

09/2007-07/2010: **Zhengzhou University, School of Material Science and Engineering, China**

- Master in Materials Science, supervised by Prof. Afang Zhang

07/2008-01/2009: **ETH Zürich, Department of Materials, Switzerland**

- Guest Master Student in Polymer Chemistry

09/2003-07/2007: **Zhengzhou University, School of Material Science and Engineering, China**

- Bachelor in Polymer Science and Engineering

Publications

- **Dalin Wu**, Mariana Spulber, Fabian Itel, Cornelia G. Palivan*, Wolfgang Meier*, Effect of molecular parameters on the architecture and membrane properties of 3D assemblies of amphiphilic copolymers, ***Macromolecules***, 2014, 47, 5060–5069.
- **Dalin Wu**, Martin Nussbaumer, Adrian Najer, Cornelia G. Palivan*, Wolfgang Meier*, Amphiphilic graft PMOXA-graft(ss)-PCL copolymer synthesis and application in the nanocarrier. (to be submitted to polymer chemistry)
- Dominik Witzigmann [§], **Dalin Wu** [§], Susanne Schenk, Vimalkumar Balasubramanian, Wolfgang Meier*, Jörg Huwyler*, PMOXA-Pasp(DET) - A Versatile Polymer Peptide Hybrid System for Biocompatible pDNA Delivery in vitro. (to be submitted to ACS Applied Materials & Interfaces). §: both authors contribute equally to this work.
- Fabian Itel, Mohamed Chami, Adrian Najer, Samuel Lörcher, **Dalin Wu**, Ionel A. Dinu, and Wolfgang Meier, Molecular Organization and Dynamics in Polymersome Membranes: A Lateral Diffusion Study, ***Macromolecules***, 2014, 47, 7588-7596.
- Le-Ha Dieu; **Dalin Wu**; Cornelia Palivan; Vimalkumar Balasubramanian; Joerg Huwyler*, Polymersomes Conjugated to 83-14 Monoclonal Antibodies: in Vitro Targeting of Brain Capillary Endothelial Cells, ***European Journal of Pharmaceutics and Biopharmaceutics***, 88 (2014) 316–324.

- Adrian Najer, **Dalin Wu**, Andrej Bieri, Françoise Brand, Cornelia G. Palivan, Hans-Peter Beck, Wolfgang Meier*, Nanomimics of host cell membranes block invasion and expose invasive, (accepted by ACS Nano)
- Liu, Juan; Spulber, Mariana; **Wu, Dalin**; Talom, Renee; Palivan, Cornelia*; Meier, Wolfgang*, Poly (N-isopropylacrylamide-co-tris-nitrilotriacetic acid acrylamide) for a combined study of molecular recognition and distance constraints in protein binding and interactions, ***J. Am. Chem. Soc.***, **2014**, *136* (36), pp 12607–12614.
- JustynaŁ Kowal, Julia K. Kowal, **Dalin Wu**, Henning Stahlberg, Cornelia G. Palivan, Wolfgang P. Meier*, Functional surface engineering by nucleotide-modulated potassium channel insertion into polymer membranes attached to solid supports, ***Biomaterials***, 2014, 35, 7286-7294.
- Marine Camblin, Pascal Detampel, Helene Kettiger, **Dalin Wu**, Vimalkumar Balasubramanian, Jörg Huwyler*, Polymersomes containing quantum dots for cellular imaging, ***International Journal of Nanomedicine***, 2014:9 2287–2298.
- A. Najer, **Dalin. Wu**, D. Vasquez, C. G. Palivan*, W. Meier*, Polymer nanocompartments in broad-spectrum medical applications. *Nanomedicine,* 2013**, 8**, 425-447***.***
- **Dalin Wu**, Patric Baumann, Cornelia G. Palivan*, Wolfgang Meier*, The synthesis of diblock copolymer poly(2-methyl-2-oxazoline)-*block*-poly(beta-benzyl-L-aspartate) (PMOXA-*b*-PBLA) and its application in hydrophobic drug delivery (in preparation).
- Jiatao Yan, Wen Li, Kun Liu, **Dalin Wu**, Feng Chen, Peiyi Wu, Afang Zhang*. Thermoresponsive Supramolecular Dendronized Polymers***. Chem. Asian J***., 2011, 6, 3260-3269.
- Wen Li, **Dalin Wu**, A. Dieter Schlüter and Afang Zhang*, Synthesis of an Oligo(ethylene glycol)-Based Third-Generation Thermoresponsive Dendronized Polymer. ***Journal of Polymer Science: Part A: Polymer Chemistry,*** 2009, 47, 6630–6640***.***
- Jingguo Li, Tao Wang, **Dalin Wu**, Xiuqiang Zhang, Jiatao Yan, Song Du, Yifei Guo, Jintao Wang, and Afang Zhang*, Stimuli-Responsive Zwitterionic Block Copolypeptides: Poly(N-isopropylacrylamide)-block-poly(lysine-co-glutamic acid). ***Biomacromolecules,*** 2008, 9, 2670-2676.

Posters

- **Dalin Wu**, Adrian Najer, Martin Nussbaumer, Cornelia Palivan and Wolfgang Meier, Amphiphilic graft block copolymer PMOXA-graft(ss)-PCL synthesis and its potential application in drug targeting delivery, BIO-FRIENDLY POLYMERS (BPPA14), Budapest (Hungary), May 2014.
- **Dalin Wu**, Adrian Najer, Martin Nussbaumer, Cornelia Palivan and Wolfgang Meier, Amphiphilic graft block copolymer PMOXA-graft(ss)-PCL synthesis and its potential application in drug targeting delivery, Swiss Soft Day, Zurich (Switzerland), January 2014.

- **Dalin Wu**, Mariana Spulber, Cornelia Palivan and Wolfgang Meier, Self-assembling behavior of PDMS-*b*-PMOXA diblock polymers: structure influence, 3rd International Symposium-Fronties in Polymer Science, Melia Sitges (Spain), March 2013.
- **Dalin Wu** and Wolfgang Meier, The self-assembly phase diagram of PDMS-PMOXA diblock copolymer, Swiss Soft Day, Geneva (Switzerland), June 2012.
- **Dalin Wu**, Cornelia G. Palivan and Wolfgang Meier, Synthesis, Self-assembly and Application of Diblock Copolymer PMOXA-PBLA, Swiss Soft Day, PSI (Switzerland), May 2012.
- **Dalin Wu** and Wolfgang Meier, PDMS-PMOXA diblock copolymer synthesis and its self-assembly behavior in water, European Science Foundation (ESF), Strasbourg (France), December 2011.